POLITECNICO DI MILANO

Facoltà di Ingegneria Industriale

Corso di Laurea in
Ingegneria Aeronautica

Design of M-346 Aircraft's Vertical Tail in CFC by means of Progressive Failure Analysis

In collaboration with AleniaAermacchi

Relatore: Gian Luca GHIRINGHELLI
Tutor Aziendale: Andrea RUSSO

Tesi di Laurea di:
Daniele Emilio PERLINI

Anno Accademico 2013/2014

"Stay Hungry, Stay Foolish"
Steve Jobs

Ai miei genitori

ABSTRACT

The thesis describes the innovative procedure adopted for the design of M-346 aircraft's vertical tail, in carbon fiber composite (CFC), by mean of Progressive Failure Analysis. This will be performed by the numerical code MSC/NASTRAN 2012.1 (SOL 400) with the aid of the pre-post-processor PATRAN 2012.2.

The aim is to investigate the potentiality of PFA, which are: perform the prediction of composite structure behavior; increase the performance; reduce the structural weight.

The first phase of the project consist in a bibliographic research to define one or more internal configurations of the fin, followed by a finite element modeling. Subsequently, the structures will be dimensioned through a static analysis, according to the criterion of First Ply Failure (method commonly used for the design of composite components). Finally, applying the Progressive Failure Analysis will be possible to verify the structures and possibly proceed with further optimization.

The reliability of the results is supported by a preliminary and detailed investigation of the PFA features, carried out on a simple example in order to fully understand the functioning of this innovative method of analysis.

SOMMARIO

La tesi descrive l'innovativo procedimento adottato per il dimensionamento del Vertical Tail del velivolo M-346, in materiale composito, facendo uso della Progressive Failure Analysis (PFA). Tale analisi verrà eseguita per mezzo del codice numerico MSC/NASTRAN 2012.1 (SOL 400) con l'ausilio del pre-post-processore PATRAN 2012.2.

L'obbiettivo primario riguarda l'indagine delle potenzialità del metodo PFA: migliorare la prevedibilità dei fenomeni legati alla natura dei materiali compositi nonché ridurre il peso e migliorare le prestazioni della struttura analizzata.

La prima fase del progetto consiste in una ricerca bibliografica per definire una possibile configurazione interna della deriva, seguita da una modellazione ad elementi finiti. Successivamente la struttura verrà dimensionata, tramite un'analisi statica, secondo il criterio della First Ply Failure (metodo comunemente utilizzato per la progettazione di componenti in materiale composito). Infine, applicando la Progressive Failure Analysis, sarà possibile verificare la struttura ed eventualmente procedere con un'ulteriore ottimizzazione.

L'affidabilità dei risultati è supportata da un esame preliminare e dettagliato delle caratteristiche della PFA, effettuato su un semplice esempio per apprendere appieno il funzionamento di questo innovativo metodo di analisi.

Contents

1 Introduction 7
1.1 AleniaAermacchi M-346 . . . 8
1.2 Project's specification . . . 9
1.3 List of abbreviations . . . 10

2 Overview of Progressive Failure Analysis 11
2.1 Nonlinear Analysis . . . 12
2.2 Strain/Stress Recovery . . . 13
2.3 Failure Analysis . . . 13
2.4 Material Degradation . . . 13

3 Bibliographic Research 15
3.1 Problem Statement . . . 15
3.2 Numerical Results and Discussion . . . 16
3.3 Concluding Remarks . . . 19

4 Open Hole Tension Laminate 21
4.1 Results of Interest . . . 21
  4.1.1 First Ply Failure . . . 21
  4.1.2 Total Damage . . . 22
  4.1.3 Final Failure . . . 25
4.2 Mesh Size Influence . . . 25
4.3 Time Step Size Influence . . . 28
4.4 Residual Stiffness Fraction . . . 30
4.5 Force Control vs. Displacement Control . . . 31
4.6 Computational Cost . . . 32
  4.6.1 Subcases . . . 33
4.7 Other Results . . . 35

5 Planning 41

6 Vertical Tail FEM 43
6.1 FEM Idealization . . . 43
  6.1.1 Element Selection . . . 43
  6.1.2 Mesh Density . . . 44
6.2 FEM Loading . . . 44
  6.2.1 Test Load Case . . . 45
  6.2.2 Loading Scheme . . . 45
  6.2.3 Internal Forces Comparison . . . 48
6.3 FEM Constraints . . . 49
6.4 Nodal Displacements . . . 51
6.5 Verification Procedure . . . 51

7 Vertical Tail Current Design 53
7.1 Parameters of Interest . . . 56

8 New Possible Design 59

9 Materials 61
9.1 Metallic Materials . . . 61
  9.1.1 Aluminium Alloy 7050 T7451 . . . 61
  9.1.2 Calculation Methods for Metals . . . 62
9.2 Composite Materials . . . 62
  9.2.1 Hexcel 8552/IM7 Unidirectional Tape . . . 63
  9.2.2 Calculation Methods for Laminates . . . 64
  9.2.3 Laminate Design . . . 65
  9.2.4 Lamination Sequences . . . 66
9.3 Honeycomb . . . 67

9.3.1 Non Metallic Honeycomb HRH10 - Nomex 67
9.3.2 Calculation Methods for Honeycomb 68
9.3.3 Correction Factors for Honeycomb Cores 68

10 Spar Model FPF 71
10.1 General Description 71
10.2 Preliminary Design 72
10.2.1 Composite Parts 72
10.2.2 Metallic Parts 73
10.3 Vertical Tail FEM Check Validation 73
10.3.1 Pre-Analysis Check 73
10.3.2 Static Analysis Check 74
10.4 Static Analysis 79
10.4.1 Thickness Distribution 79
10.4.2 Composite Components Verification 82
10.4.3 Metallic Components Verification 84
10.5 Buckling Analysis 86
10.5.1 General Description 86
10.5.2 Buckling of the Panels 87
10.5.3 Improvement of the Model 87
10.6 SOL 400 89
10.6.1 FPF Check 89
10.6.2 Evaluation of the Margin from the FC 91
10.7 Conclusions 94

11 Spar Model PFA 97
11.1 General Description 97
11.2 Static Analysis and SOL 400 98
11.2.1 FI Verification 98
11.2.2 FC Verification 99
11.3 Buckling Analysis 102
11.4 Conclusion 102

12 Sandwich Model FPF 105
12.1 General Description 105
12.2 Static Analysis and SOL 400 106
12.2.1 FI Verification 106
12.2.2 FC Verification 107
12.2.3 Honeycomb Verification 109
12.3 Buckling Analysis 111
12.4 Conclusion 112

13 Sandwich Model PFA 115
13.1 General Description 115
13.2 Static Analysis and SOL 400 116
13.2.1 FI Verification 116
13.2.2 FC Verification 117
13.2.3 Honeycomb Verification 119
13.3 Buckling Analysis 121
13.4 Conclusion 122

14 Models Comparison 125

15 Conclusion 129

16 Appendix 131
16.1 SOL 400 - NASTRAN Cards 131
16.1.1 MATF 131
16.1.2 NLSTEP 132

List of Figures

1 First Ply Failure design 7
2 Progressive Failure Analysis design 8
3 AleniaAermacchi M-346 Aircraft 8
4 M-346 features 9
5 Typical progressive failure analysis methodology 11
6 Post-failure degradation behavior in composite laminates 14
7 Finite element model of the open hole tension specimen 16
8 Comparison of different PFA models for the cross-ply laminate (0.02) 17
9 Comparison of different PFA models for the cross-ply laminate (0.01) 17
10 Maximum solution increment size influence on the progressive failure predictions 18
11 Comparison of different PFA models for the quasi-isotropic laminate 18
12 Open-hole-tension specimen FPF: Time Step 20% 22
13 Open-hole-tension specimen TD: maximum (all layer) 23
14 Open-hole-tension specimen TD: minimum (all layer) 24
15 Different mesh size 25
16 Different Finite Element Models 27
17 FEM influence on the progressive failure predictions 28
18 Time step influence on the progressive failure predictions 29
19 Time step influence on the failure 30
20 Residual Stiffness Fraction influence on the progressive failure predictions 31
21 Force Control vs. Displacement Control 32
22 Computational cost 33
23 Subcase 5-22-5: computational cost 34
24 Subcase 1-22-5: computational cost 34
25 Standard analysis: load displacement curve 35
26 Elements considered 36
27 Total Damage: 90° 37
28 Total Damage: 0° 37
29 Ply strain 38
30 Ply stress: 90° 39
31 Ply stress: 0° 39
32 Planning 41
33 VT loading by mean of saddle and pad-ups 44
34 Fin and rudder loading points (csys A/C) 45
35 VT saddles and pad-ups 46
36 Fin and rudder test loads (Test LC UL) 47
37 VT test/theoretical SHEAR comparison 48
38 VT test/theoretical TORQUE comparison 48
39 VT test/theoretical BENDING comparison 49
40 Connection to fuselage 49
41 Hinges 50
42 Transducers application points 51
43 Fin box assembly 53
44 Root rib to rear fuselage connection 53
45 Root rib to VT rudder mount connection 54
46 Rudder connection 54
47 Skin thickness distribution 55
48 Fin honeycomb core components 55
49 Current model deformed: maximum deflection 100% 56
50 Current model: trasducers displacements 57
51 Boeing F15 Silent Eagle 59
52 Boeing EA-18G Growler 59
53 Eurofighter Typhoon 60
54 Typical compression strain allowable values as a function of the impact energy 64
55 Skins, spars caps and stringers lamination sequences 66
56 Ribs and spars webs lamination sequences 66

57 Honeycomb: L and W direction 68
58 Correction factors for thickness 68
59 Correction factors for temperature 69
60 Spar model FPF cutaways 71
61 Assembly 72
62 Connection to fuselage 73
63 Spar model: bolt applied load 76
64 Deformation modes 77
65 Rigid body modes 78
66 Spar model FPF thickness distribution: skin 79
67 Spar model FPF thickness distribution: ribs and spars 80
68 Spar model FPF thickness distribution: stringers 80
69 Root machined parts: thickness distribution 81
70 Hinges: thickness distribution 81
71 Spar model FPF skin: max FI (SOL 106) 82
72 Spar model FPF ribs and spars: max FI (SOL 106) 83
73 Spar model FPF stringers: max FI (SOL 106) 83
74 Root machined parts: Von Mises Stress (SOL 101) 84
75 Hinges: Von Mises Stress (SOL 101) 85
76 COCOMAT 86
77 Buckling constant K_c 87
78 Stiffening of the rear free edges 88
79 Spar model FPF: buckling 88
80 Spar model FPF skin: max FI (SOL 400) 89
81 Spar model FPF ribs and spars: max FI (SOL 400) 90
82 Spar model FPF stringers: max FI (SOL 400) 90
83 Spar model FPF: load displacement curve 91
84 Spar model FPF skin: TD min 91
85 Spar model FPF ribs and spars: TD min 92
86 Spar model FPF stringers: TD min 92
87 Spar model FPF: propagation of damage 93
88 Spar model FPF deformed: maximum deflection 57.1% 94
89 Spar model FPF: nodes displacement 95
90 Spar model FPF vs. spar model PFA: cutaways 97
91 Spar model FPF vs. spar model PFA: thickness 97
92 Spar model PFA: max FI (SOL 106 vs. SOL 400) 98
93 Spar model PFA skin: TD min 99
94 Spar model PFA ribs and spars: TD min 99
95 Spar model PFA stringers: TD min 100
96 Spar model PFA: propagation of damage 101
97 Spar model PFA: buckling 102
98 Spar models: load displacement curves 103
99 Spar model PFA deformed: maximum deflection 64.1% 103
100 Spar model PFA: nodes displacement 104
101 Sandwich model FPF cutaways 105
102 Sandwich model FPF thickness distribution 105
103 Sandwich model FPF: max FI (SOL 106 vs. SOL 400) 106
104 Sandwich model FPF: load displacement curve 107
105 Sandwich model FPF skin: TD min 107
106 Sandwich model FPF ribs and spars: TD min 108
107 Sandwich model FPF: propagation of damage 108
108 Sandwich model FPF: full depth honeycomb 109
109 Sandwich model FPF: stress in T-direction 109
110 Sandwich model FPF: stress in L-direction 110
111 Sandwich model FPF: stress in W-direction 110
112 Sandwich model FPF: buckling 111
113 Sandwich model FPF deformed: maximum deflection 65.2% 112
114 Sandwich model FPF: nodes displacement 113

115 Sandwich model PFA cutaways . . . 115
116 Sandwich model FPF vs. sandwich model PFA: thickness . . . 115
117 Sandwich model PFA: max FI (SOL 106 vs. SOL 400) . . . 116
118 Sandwich models: load displacement curves . . . 117
119 Sandwich model PFA skin: TD min . . . 117
120 Sandwich model PFA ribs and spars: TD min . . . 118
121 Sandwich model PFA: propagation of damage . . . 118
122 Sandwich model PFA: full depth honeycomb . . . 119
123 Sandwich model PFA: stress in T-direction . . . 119
124 Sandwich model PFA: stress in L-direction . . . 119
125 Sandwich model PFA: stress in W-direction . . . 120
126 Spar model PFA: buckling . . . 121
127 Sandwich model PFA deformed: maximum deflection 73.2% . . . 122
128 Sandwich model PFA: nodes displacement . . . 123
129 PFA models comparison: load displacement curves . . . 125
130 Leading edge comparison . . . 126
131 Trailing edge comparison . . . 127

List of Tables

1 M-346 technical data . . . 9
2 Abbreviations . . . 10
3 Material degradation for maximum strain criteria . . . 14
4 T800/3900-2 graphite-epoxy properties . . . 15
5 T800/3900-2 graphite-epoxy allowable values . . . 15
6 Comparison between test peak failure loads and different PFA models . . . 19
7 Comparison between T800H/3900-2 and 8552/IM7 . . . 21
8 Mesh size influence on the progressive failure predictions . . . 26
9 FEM influence on the progressive failure predictions . . . 26
10 FPF check . . . 28
11 Time step size dependence . . . 29
12 Residual Stiffness Fraction dependence . . . 31
13 Force Control vs. Displacement Control . . . 32
14 Subcases vs. computational cost . . . 35
15 Subcases vs. result's quality . . . 35
16 Finite elements . . . 43
17 VT static test reaction forces . . . 45
18 Fin and rudder loading points (csys A/C) . . . 46
19 Fin and rudder test loads (Test LC UL) . . . 47
20 Single Point Constraint . . . 50
21 Transducers application points . . . 51
22 Current model: trasducers displacements . . . 56
23 Aluminium alloy 7050 T7451 (1.5-2.0 inch) . . . 61
24 Aluminium alloy 7050 T7451 (5.0-6.0 inch) . . . 62
25 Hexcel 8552/IM7 Unidirectional Tape . . . 63
26 HRH-10 Aramid Fiber/Phenolic Resin Honeycomb . . . 67
27 Element geometry check . . . 74
28 Epsilon . . . 75
29 OLOAD card . . . 75
30 SPCFORCE card . . . 75
31 Current model: bolt applied load . . . 76
32 First 10 eigenvalues and relevant cycles . . . 77
33 FPF: differences between SOL 106 and SOL 400 . . . 90
34 Spar model FPF vs. current model specifications . . . 94
35 Spar model FPF: nodes displacement . . . 95
36 Spar model FPF vs. spar model PFA: weight . . . 97
37 Spar model PFA vs. current model specifications . . . 103
38 Spar model PFA: nodes displacement . . . 104
39 Honeycomb: elastic modulus and allowable values . . . 109
40 Honeycomb: knock down allowable values . . . 109
41 Sandwich model FPF: stresses acting on the honeycomb . . . 110
42 Sandwich model FPF: margin of safety . . . 110
43 Sandwich model FPF vs. current model specifications . . . 112
44 Sandwich model FPF: nodes displacement . . . 113
45 Sandwich model FPF vs. sandwich model PFA: weight . . . 115
46 Sandwich model PFA: stresses acting on the honeycomb . . . 120
47 Sandwich model PFA: margin of safety . . . 120
48 Sandwich model PFA vs. current model specifications . . . 122
49 Sandwich model PFA: nodes displacement . . . 123
50 Comparison between all models specifications . . . 125
51 MATF - format . . . 131
52 MATF - example . . . 131
53 NLSTEP - format . . . 132
54 NLSTEP - default . . . 132

1 Introduction

Composite materials have been increasingly used in aerospace and automotive applications over the last three decades and have seen a dramatic increase in usage in non-aerospace products in the few years.

The use of composite materials is very attractive because of their outstanding strength, stiffness, and light-weight properties. An additional advantage of using composites is the ability to tailor the stiffness and strength to specific design loads. However, a reliable methodology for fully predicting the performance of composite structures beyond initial localized failure has yet to be developed.

Since most composite materials exhibit brittle failure, with little or no margin of safety through ductility, as offered by many metals, most of aircraft companies, including Alenia Aermacchi, knock down the allowable values and do not allow the components to buckling. Furthermore, the various parts are designed with the First Ply Failure analysis. This means that, regardless of how many plies is composed a component, as soon as one of these breaks, it has to be considered broken and replaced, even though the material is able to withstand much higher loads. This dimensioning criteria implies that for any structure does not occur the FPF before reaching the ultimate load.

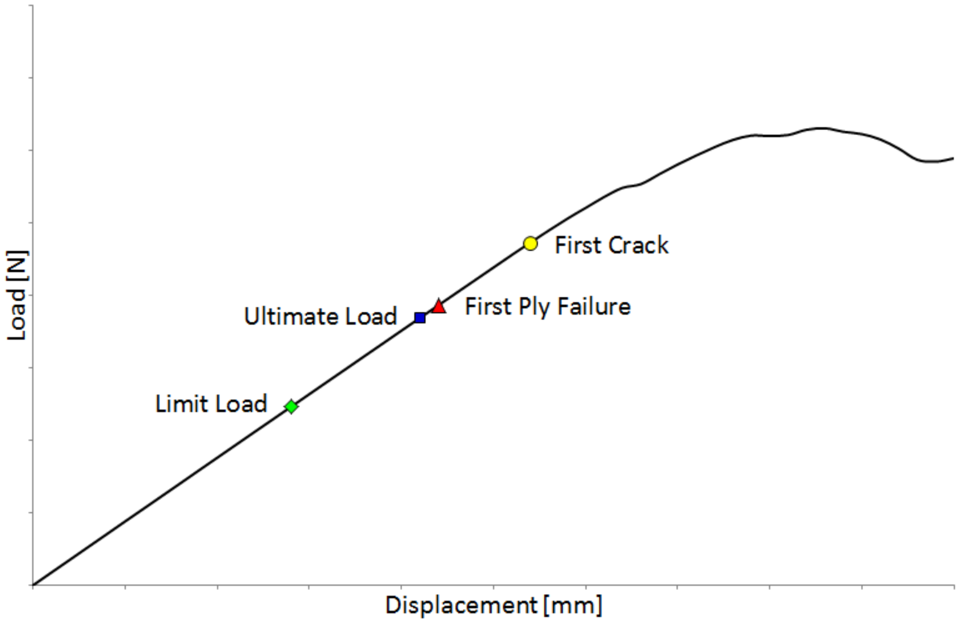

Figure 1: First Ply Failure design

Laminated composite structures can develop local failures or exhibit local damage such as matrix cracks, fiber breakage, fiber-matrix debonds, and delaminations under normal operating conditions which may contribute to their failure.

The ability to predict the initiation and growth of such damage is essential for predicting the performance of composite structures. With the Progressive Failure Analysis it will be possible for example to find the area of the structure where is more probable the birth of the First Crack. If this condition were accepted immediately after the threshold of the Ultimate Load it would be possible to lower the FPF above the Limit Loads (which are the maximum loads that the aircraft should never exceed), thus allowing considerable savings in weight without sacrificing safety.

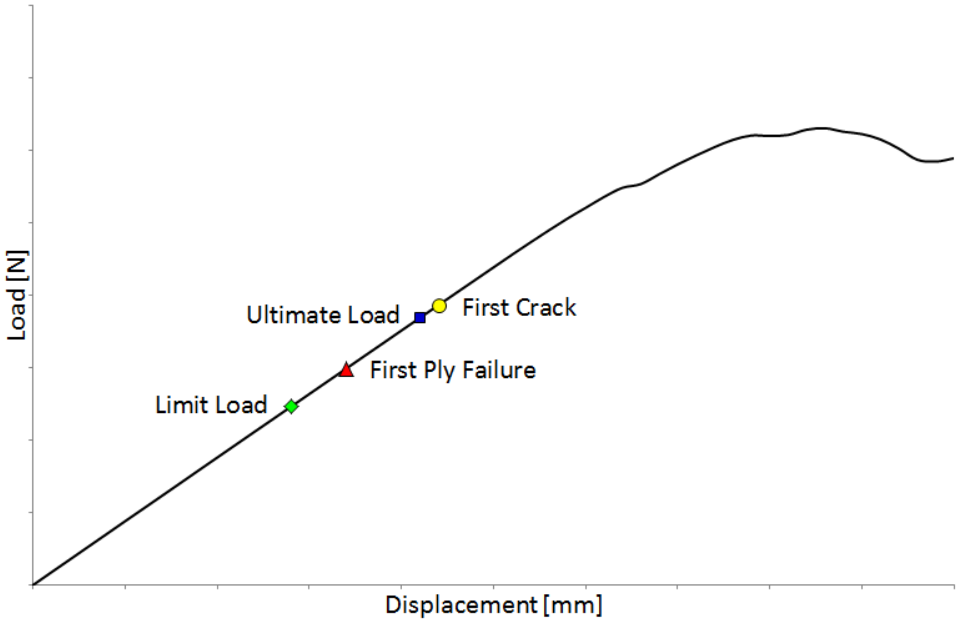

Figure 2: Progressive Failure Analysis design

Hence, the need for a reliable methodology for predicting failure initiation and propagation in composite laminated structures is of great importance to the development of reliable, safe designs which will exploit the advantages offered by composite materials.

1.1 AleniaAermacchi M-346

Figure 3: AleniaAermacchi M-346 Aircraft

The twin-turbofan M-346 is the most advanced Lead-In Fighter Trainer flying today, designed to provide the best possible balance between high training effectiveness and operational capabilities but with low life-cycle cost. It is designed to the latest “design-to-cost” and “design-to-maintain” concepts, with avionics modeled upon those of fifth-generation combat aircraft.
It is capable of transonic flight without using an afterburner, which is designed to reduce acquisition and operating costs. Two engines and triple-quadruple redundant systems enhance reliability. The aerodynamic design of the M-346 uses wing LERXs (Leading Edge Root eXtensions) to generate vortex lift providing maneuverability and controllability at very high angle of attack (up to 40° degrees) using a fly-by-wire control system. The Flight Control System, quadruple redundant, self-reconfigurable in case of failure, gives the aircraft both manual and automatic capability and in conjunction with peculiar aerodynamics, provides M-346 with flight characteristics similar to latest fighter.

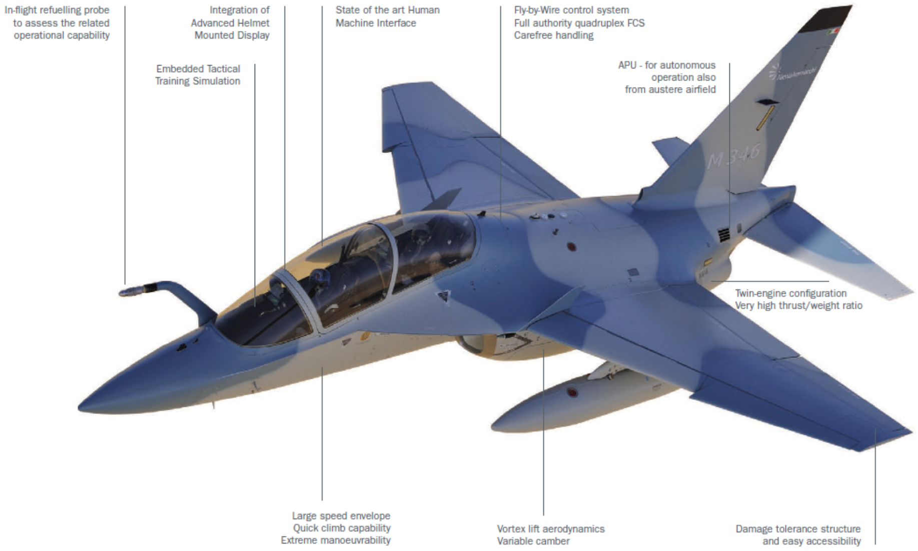
In-flight refuelling probe to assess the related operational capability
Integration of Advanced Helmet Mounted Display
Embedded Tactical Training Simulation
State of the art Human Machine Interface
Fly-by-Wire control system Full authority quadruplex FCS Carefree handling
APU - for autonomous operation also from austere airfield
M-346
Twin-engine configuration Very high thrust/weight ratio
Large speed envelope Quick climb capability Extreme manoeuvrability
Vortex lift aerodynamics Variable camber
Damage tolerance structure and easy accessibility

Figure 4: M-346 features

The M-346 exploits non-conventional features and advanced technologies to provide superior performance, flying qualities and safety of operations. These characteristics, together with a man-machine interface and advanced mission management suite within its ETTS (Embedded Tactical Training Simulation), make the M-346 truly representative of the next generation combat aircraft. Furthermore the performance level, flight characteristics and on-board system, offer significant capabilities in the M-346 also as an operational aircraft.

Dimensions	
Wing Span	9.72 m^2
Length	11.49 m^2
Height	4.76 m^2
Wing area	23.52 m^2
Weights	
Take-off (clean)	7400 kg
Take-off (ext. tanks)	9500 kg
Full internal fuel	2000 kg
Power plant	
Engines, turbofan	2 Honeywell F-124-GA-200
Thrust, max, sl, ISA	2 x 2850 kg

Performance (clean, ISA)	
Max level speed	1092 km/h
Stall speed (reference)	175 km/h
Rate of climb	111 m/s
Service ceiling	13700 m
Limit Load Factors	+8 / − 3 g
Take-off run	450 m
Landing roll	655 m
Range (clean)	1980 km
Range (ext. tanks)	2720 km
Endurance (clean)	2h 45min
Endurance (ext. tanks)	4h

Table 1: M-346 technical data

Actually the airframe design is based on damage tolerance concept. Main structural elements are made of aluminium alloys, titanium alloys and steel used in specific areas. Most fuselage skin, access doors and panels, air intakes and ducts are made of composites (carbon fiber, Kevlar). The aircraft is equipped with a S-HUMS (Structural Health & Usage Monitoring System) segment to evaluate expired/residual airframe fatigue life of individual aircraft usage which is up to 10,000 flight hours.

1.2 Project's specification

The new design, in composite material, of M-346 aircraft's VT must respect the project's specification which are the reduction of the weight and the increase of flexural stiffness of at least 30%, compared to the current design. This last can be determined through the maximum deflection at ultimate load.

Considering in a first approximation, the VT as a cantilever beam loaded in the extremity, it is possible to calculate the maximum deflection with the following equation:

$$f = \frac{Pl^3}{3EJ}$$

where P is the applied load, l is the length and EJ is the flexural stiffness. Denoting by 0 and 1 the current VT and the new configuration, can be done the following comparison:

$$\frac{f_0}{f_1} = \frac{\frac{Pl^3}{3(EJ)_0}}{\frac{Pl^3}{3(EJ)_1}}$$

Geometry and loads of both model are the same therefore equation simplifies:

$$\frac{f_0}{f_1} = \frac{(EJ)_1}{(EJ)_0}$$

Is thus demonstrated that, to obtain a comparison between the stiffnesses, it is possible to perform a simple comparison between the maximum deflection.

In virtue of business secret is not allowed to post any value of variables through which it is possible to determine the stiffness of the current fin. For this reason, all the displacement values will be reported as a percentage of maximum displacement of the current model. Even all the weights will be reported as a percentage of FEM weight of the current model

$$d\% = \frac{d}{d_{ref}} \cdot 100 \qquad\qquad w\% = \frac{w}{w_{ref}} \cdot 100$$

1.3 List of abbreviations

For sake of simplicity during the writing of this document will be used the abbreviations summarized below:

Abbreviations and meanings

A/C	Aircraft
AAEM	AleniaAermacchi
CFC	Carbon Fiber Composite
DOF	Degree of Freedom
FC	First Crack
FEM	Finite Element Model
FI	Failure Index
FPF	First Ply Failure
KDF	Knock Down Factor
LC	Load Case
LL	Limit Load
LVDT	Linear Variable Differential Transformer
MS	Margin of Safety
PFA	Progressive Failure Analysis
RSF	Residual Stiffness Fraction
RT	Room Temperature
TD	Total Damage
TRF	Temperature Reduction Factor
UL	Ultimate Load
VT	Vertical Tail

Table 2: Abbreviations

2 Overview of Progressive Failure Analysis

A typical methodology for a progressive failure analysis is illustrated in Figure 5.
At each load step, a nonlinear analysis is performed until a converged solution is obtained assuming no changes in the material model. Then using this equilibrium state, the stresses within each lamina are determined from the nonlinear analysis solution. These stresses are compared with material allowable values and used to determine failure according to certain failure criteria. If lamina failure is detected, as indicated by a failure criterion, the lamina properties are changed according to a particular degradation model.
Since the initial nonlinear solution no longer corresponds to an equilibrium state, equilibrium of the structure needs to be re-established utilizing the modified lamina properties for the failed lamina, while maintaining the current load level. This iterative process, about obtaining nonlinear equilibrium solutions each time a local material model changes, is continued until no additional lamina failures are detected.
The load step is then incremented until catastrophic failure of the structure is detected as defined by the progressive failure methodology.

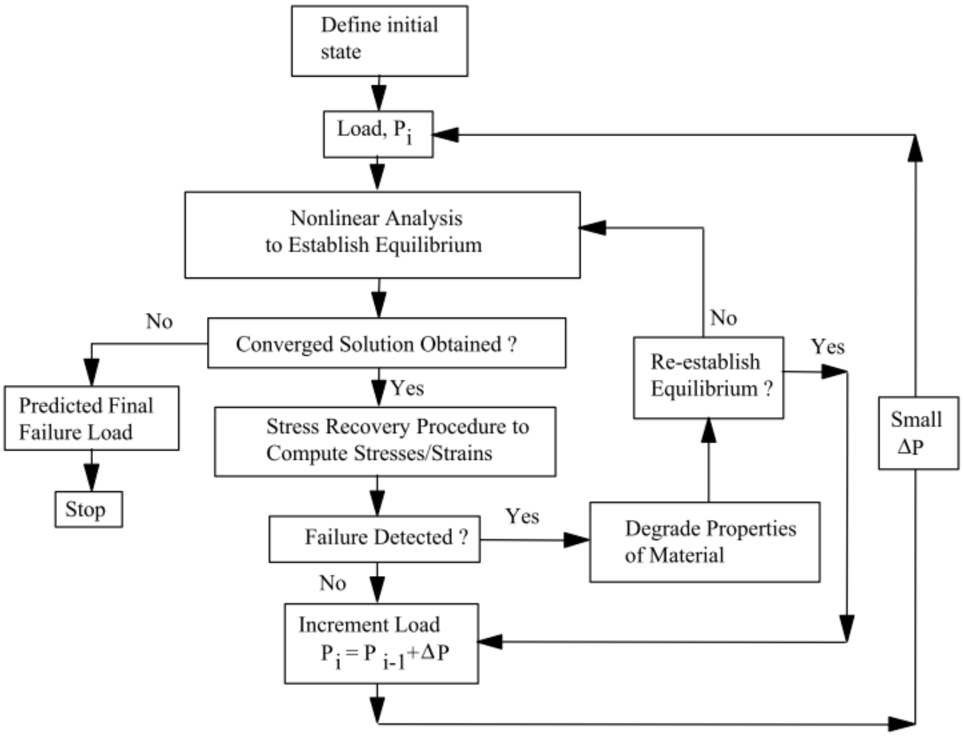
Define initial state
Load, P_i
Nonlinear Analysis to Establish Equilibrium
No
Converged Solution Obtained ?
Yes
Predicted Final Failure Load
Stop
Stress Recovery Procedure to Compute Stresses/Strains
Failure Detected ?
Yes
No
Degrade Properties of Material
Re-establish Equilibrium ?
No
Yes
Small ΔP
Increment Load
P_i = P_i-1+ΔP

Figure 5: Typical progressive failure analysis methodology

Therefore, typical progressive failure analysis methods involve five key features:

- ✈ First: a nonlinear analysis, used to establish equilibrium.
- ✈ Second: an accurate stress recovery procedure, necessary to define the local lamina stress state.
- ✈ Third: failure criteria, required to detect local lamina failure and determine the mode of failure.
- ✈ Fourth: material degradation or damage models, needed to propagate the failure and establish new estimates for the local material properties.
- ✈ Fifth: a procedure to re-establish equilibrium after modifying local lamina properties.

2.1 Nonlinear Analysis

A nonlinear analysis is performed to account for the geometrically nonlinear behavior in the Progressive Failure Analysis. The assembled finite element equations are given by

$$[K_T]\{D\} = \{P\}$$

in which $\{D\}$ is the displacement vector, $\{P\}$ is the applied load vector, and $[K_T]$ is the assembled tangent stiffness matrix.
Composite laminates typically behave in a linear elastic manner until local structural failures develop. After local failures within the laminate, the global structural stiffness changes. Hence, the tangent stiffness matrix $[K_T]$ depends on the material properties as well as the unknown displacement solution $\{D\}$.
In this PFA, a nonlinear analysis is performed until a converged solution is obtained for a constant set of material properties. The nonlinear analysis involves the solving of linearized finite element equations for the k^{th} iteration

$$[K_T]^k\{\Delta D\} = \{R\}^k$$

$$\{D\}^{k+1} = \{D\}^k + \{\Delta D\}$$

where the tangent stiffness matrix $[K_T]^k$ and force imbalance vector $\{R\}^k$ are functions of the displacements $\{D\}^k$.
Solving the equilibrium equations is an iterative process where the k^{th} step requires computing the displacement increment $\{\Delta D\}$ for the $k+1$ load step using the k^{th} tangent stiffness matrix. Then the k^{th} displacement vector $\{D\}$ is updated using $\{\Delta D\}$.
Having a new displacement solution, the force imbalance vector $\{R\}$ and possibly the tangent stiffness matrix $[K_T]$ are updated, and the process is continued for the next iteration. The solution process is continued until convergence is achieved by reducing the force imbalance $\{R\}$, and consequently $\{\Delta D\}$, within some tolerance.

Using this nonlinear solution, corresponding to a given load step, the lamina stresses are determined and used with a failure criterion to determine whether any failures have occurred during this load increment. If no failures are detected, then the applied load is increased, and the analysis continues. When a failure in the lamina occurs, a change in the stiffness matrix due to a localized failure is calculated, based on the material degradation model. This adjustment accounts for the material non-linearity associated with a progressive failure analysis, embedded within a nonlinear finite element analysis.
If the load step size is too large, static equilibrium needs to be re-established by repeating the nonlinear analysis at the current load step using the new material properties in the tangent stiffness matrix. This process is repeated until no additional failures are detected. Alternatively, small load step sizes can be used thereby minimizing the effect of not re-establishing equilibrium at the same load level. This incremental iterative process is performed until a lack of convergence in the nonlinear solution occurs.

The most popular iterative schemes for the solution of nonlinear finite element equations are forms of the Newton-Raphson procedure which is widely used because it generally converges quite rapidly. However, one of the drawbacks of the Newton-Raphson procedure is the large amount of computational resources needed to evaluate, assemble, and decompose the tangent stiffness matrix at each iteration.
To reduce the computational effort, a modified Newton-Raphson procedure is commonly used. The modified Newton-Raphson procedure differs from the Newton-Raphson method because the tangent stiffness matrix is not updated on each iteration but periodically during the analysis, at the beginning of each new load step.
Another disadvantage of the Newton-Raphson method is that the increment within a load step can only grow. For for this reason will be taken into account also the Arc-Length methods in which the increments are allowed to increase or decrease.

2.2 Strain/Stress Recovery

Once the nodal values of generalized displacements have been obtained, by performing the nonlinear analysis at a particular load step, the element strains are evaluated by differentiating the displacements. Since the displacements calculated from the finite element analysis are in global coordinates, and the failure criteria used in the laminate analysis require the material coordinates, strains and stresses must be transformed from global coordinates to material coordinates for each layer of the laminate. Once the strains are transformed to the material coordinates, the lamina constitutive equations are used to compute the in-plane stresses.

2.3 Failure Analysis

The catastrophic failure of a composite structure rarely occurs at the load corresponding to the First Ply Failure. Instead, the structure ultimately fails due to the propagation or accumulation of local failures (or damage) as the load is increased. Laminated composites may fail by fiber breakage, matrix cracking, or by delamination of layers, however, the PFA only includes predictions for the first two.

Failure criteria are intended to predict macroscopic failures in the composite laminate and are based on the tensile, compressive, and shear strengths of the individual lamina. The criteria, that can be implemented in a PFA, are the same that can be used in linear static solutions:

- Maximum Stress
- Maximum Deformation
- Hill
- Hoffman
- Tsai-Wu
- Hashin
- Puck
- Hashin-Tape
- Hashin-Fabric

If an allowable stress limit or failure criterion within a layer is not exceeded, the material properties are not changed and the other layers within the laminate are checked. When a material allowable value or failure criterion is exceeded, in a given layer, the engineering material constants, corresponding to that particular mode of failure, are reduced depending on the material degradation model. As consequence the load is redistributed.

2.4 Material Degradation

If failure is detected, in a particular lamina of the composite material, the properties of that lamina must be adjusted according to a material property degradation model. Most of these material degradation models belong to one of three general categories: instantaneous unloading, gradual unloading, or constant stress at ply failure.

Figure 6 illustrates these three categories. For the instantaneous loading case, the material property, associated with that mode of failure, is degraded instantly to zero. For the gradual unloading case, the material property is degraded gradually (perhaps exponentially) until it reaches zero. For the constant stress case, the material properties are degraded such that the material cannot sustain additional load.

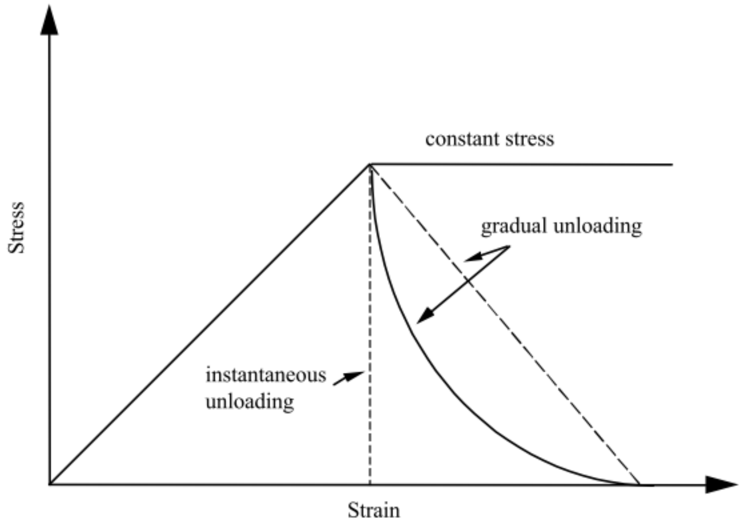

Figure 6: Post-failure degradation behavior in composite laminates

Is immediate to understand how the instantaneous unloading case is a design choice much more conservative than the models constant stress and gradual unloading. That is because, once properties are degraded, the elements are no longer able to support the load and can no longer contribute to the total stiffness.

One of the most common methods used for degradation of material properties is the ply-discount theory which belongs to the instantaneous unloading category. In this method, one or more of the elastic material properties of a lamina are set to equal zero or a small fraction of the original value once failure is detected. It is assumed that the material degradation is restricted to the ply that fails.

The behavior of the lamina as it fails, as well as which elastic constants are degraded, depends on the failure mode of the composite laminate, as shown in Table 3:

Primary Failure	**Degraded Properties**
Fiber Failure	E_{xx}, ν_{xy}
Matrix Failure	E_{yy}, ν_{xy}
Shear Failure	G_{xy}

Table 3: Material degradation for maximum strain criteria

3 Bibliographic Research

Few studies have been performed on predicting the failure of composite material based on nonlinear analysis and compared with experimental data.
The following example, from the *American Institute of Aeronautics and Astronautics* consider a tension loaded laminate with a hole. In this case the Progressive Failure Analysis has been performed by mean of ABAQUS/Standard but the obtained result can be used as reference for an equivalent analysis performed with NASTRAN.

3.1 Problem Statement

In order to assess the accuracy of the progressive failure methodology, a 16-ply tensile specimen containing a centrally located circular hole is considered. The calculated results are compared with available test data.
The composite laminate is 9-inches long and 1-inch wide with a hole diameter of 0.25 inches. The thickness of each ply is 0.00645 inches for a 0.1032-inches total laminate thickness. Two stacking sequences are analyzed: a $[(0/90)_4]_s$ cross-ply laminate and a $[(0/45/90/-45)_2]_s$ quasi-isotropic laminate. The specimen is fabricated from T800H/3900-2 graphite/epoxy. The lamina properties and the allowable values are reported in the following tables:

Material Properties		**Values**	
Longitudinal Young's Modulus	E_{xx}	23.2	[Msi]
Transverse Young's Modulus	E_{yy}	1.3	[Msi]
In-Plane Shear Modulus	G_{xy}	0.90	[Msi]
Out-of-Plane Shear Modulus	G_{yz}	0.50	[Msi]
Out-of-Plane Shear Modulus	G_{xz}	0.90	[Msi]
Interlaminar Strength	S_B	0.86	[lb/in^2]
Poisson's Ratio	ν_{xy}	0.28	

Table 4: T800/3900-2 graphite-epoxy properties

Material Allowable		**Value**
Longitudinal Tensile Strain	X_ε^T	0.0178
Transverse Tensile Strain	Y_ε^T	0.0067
Out-of-Plane Tensile Strain	Z_ε^T	0.0067
Longitudinal Compression Strain	X_ε^C	0.0097
Transverse Compression Strain	Y_ε^C	0.0187
Out-of-Plane Compression Strain	Z_ε^C	0.0187
In-Plane Shear Strain	S_ε^{xy}	0.0153
Out-of-Plane Shear Strain	S_ε^{yz}	0.0153
Out-of-Plane Shear Strain	S_ε^{xz}	0.0153

Table 5: T800/3900-2 graphite-epoxy allowable values

The tensile and compressive elastic moduli are the same, and the response is assumed to be linear elastic up to the ultimate strength values of the material.
Figure 7 shows the Finite Element Model of the open hole tension specimen. The boundary conditions were imposed on opposite ends of the finite element model to simulate the clamped edge and the edge with an imposed uniform longitudinal end displacement δ. In the analysis, the bottom edge is fully restrained, while the top edge is restrained except for the applied displacement. This mean that the nonlinear solution process of ABAQUS/Standard is under displacement control.

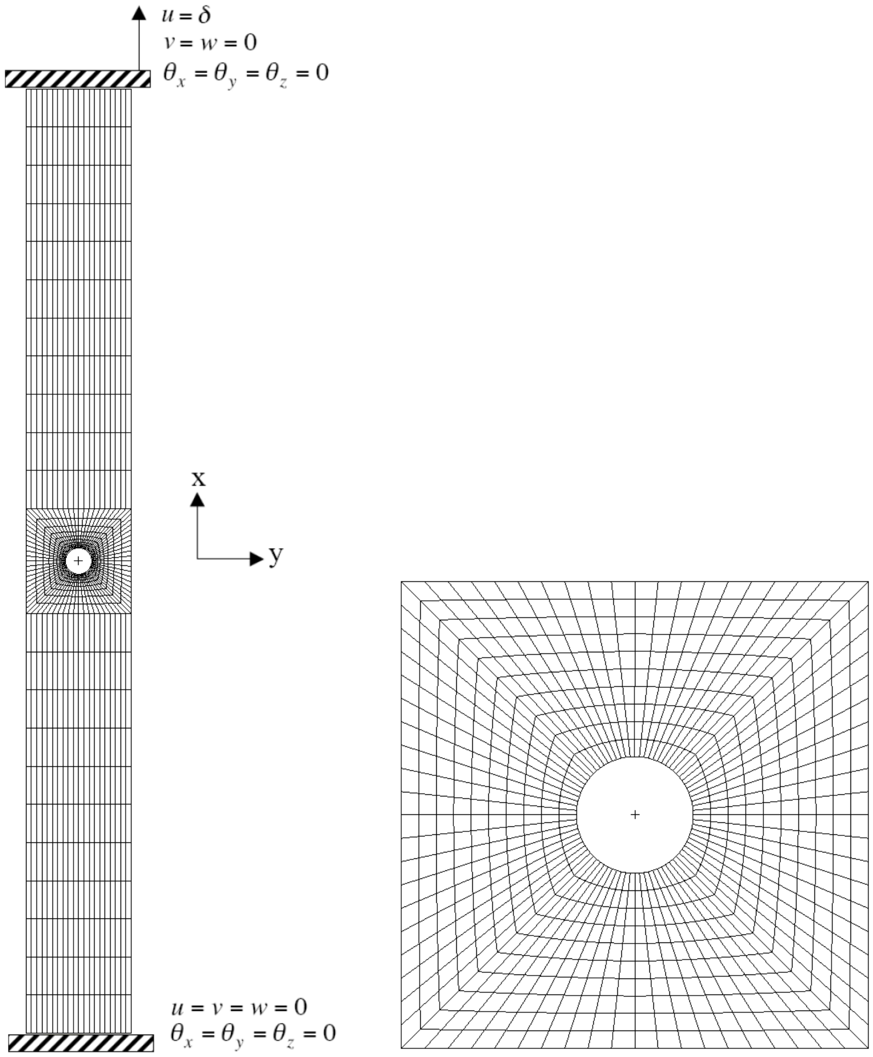
$u = \delta$
$v = w = 0$
$\theta_x = \theta_y = \theta_z = 0$
x
y
$u = v = w = 0$
$\theta_x = \theta_y = \theta_z = 0$

(a) Complete model (b) Close-up view of region near the hole

Figure 7: Finite element model of the open hole tension specimen

Nonlinear analysis are performed using a full Newton-Raphson procedure without extrapolation for the next solution increment. The initial factor for the solution increment size is set at 0.005 with a minimum value specified as 0.0001. The maximum solution increment size factor is used as parameter. Automatic solution increment size control is permitted. Progressive failure simulations are performed using different failure criteria such as Max Stress, Max Strain, Hashin, Tsai-Wu.

3.2 Numerical Results and Discussion

First of all the cross-ply stacking sequence will be analyzed. The applied tension loads, as a function of end displacement, are summarized in the following figures for two values of the maximum solution increment size and for different failure criteria. The short-dash line indicates the average failure load from three tests reported in Table 6. The long-dash line represents the linear elastic response from the finite element analysis.
Progressive failure analysis results were generated using the nominal lamina material data, a single integration point through the thickness of each lamina within the 16-ply laminate, and recursive degradation with a degradation factor β of 0.5. In Figure 8 and Figure 9 is shown the comparison between different PFA models which prediction are obtained respectively using the values 0.02 and 0.01 for the maximum solution increment size factor.

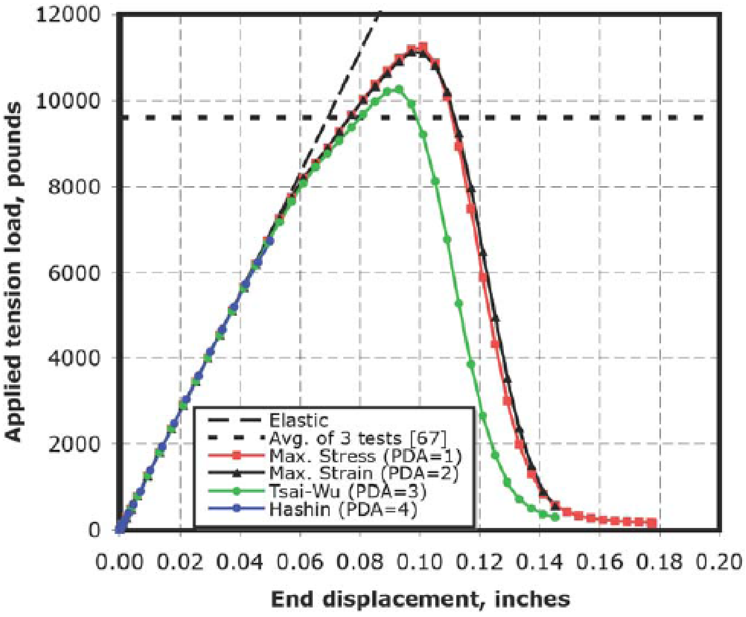

Figure 8: Comparison of different PFA models for the cross-ply laminate (0.02)

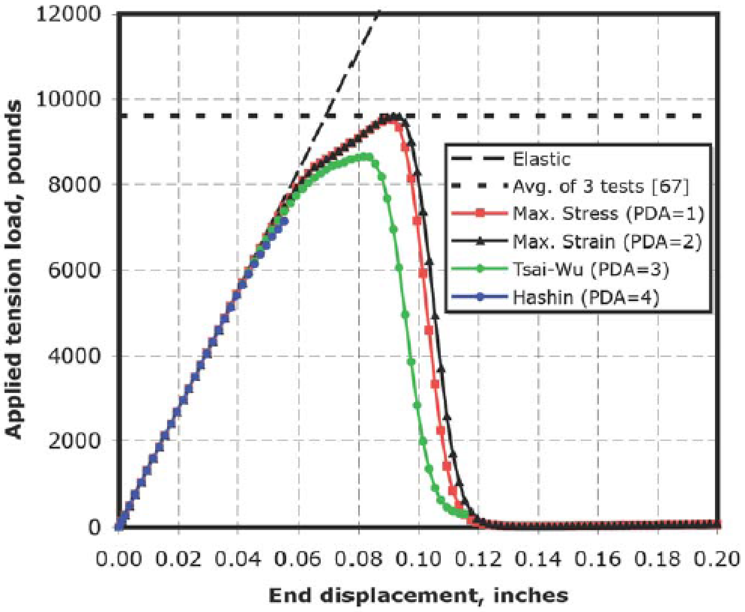

Figure 9: Comparison of different PFA models for the cross-ply laminate (0.01)

The maximum stress criteria and the maximum strain criteria predict nearly the same failure load of approximately 11200 pounds using the 0.02 value for the maximum solution increment size factor and approximately 9500 pounds using the 0.01 value. The Tsai-Wu criteria predicts a lower failure load (10300 pounds using the 0.02 value and 8700 using the 0.01 value). The Hashin criteria under predict the failure load by nearly 30%.

As the maximum solution increment size factor is reduced, the peak load predictions obtained from the other failure criteria are reduced. By reducing the maximum solution increment size, a smooth response is still predicted, and numerical drift in the simulation due to smaller solution increments is minimal.

The influence of the maximum solution increment size on the progressive failure predictions is shown in Figure 10 for the maximum strain criteria.

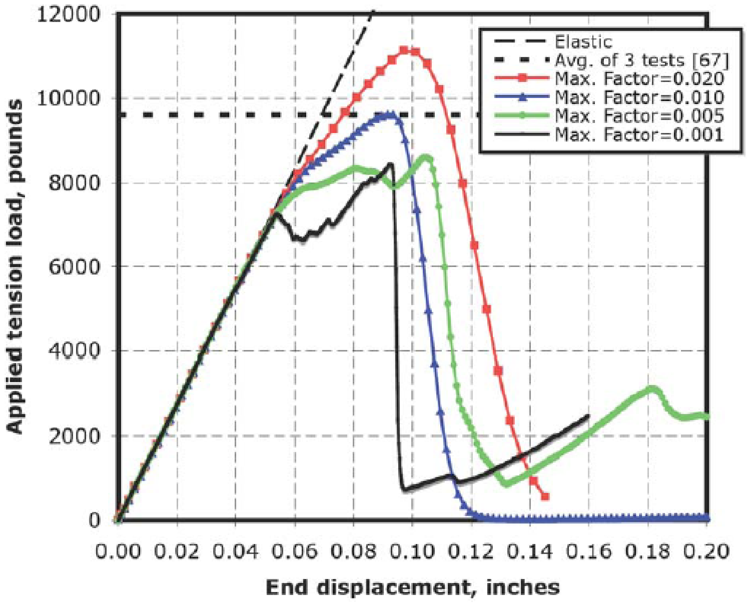

Figure 10: Maximum solution increment size influence on the progressive failure predictions

As the factor is reduced in size, the peak load prediction is also reduced. However, the load value corresponding to local fiber failure near the hole is the same for all values, approximately 7000 pounds.

The maximum solution increment size factor, which is used in the nonlinear solution strategy, apparently influences the post-ultimate behavior of the simulation.

Progressive failure simulations performed on the quasi-isotropic open-hole-tension specimen using different failure criteria are summarized in Figure 11.

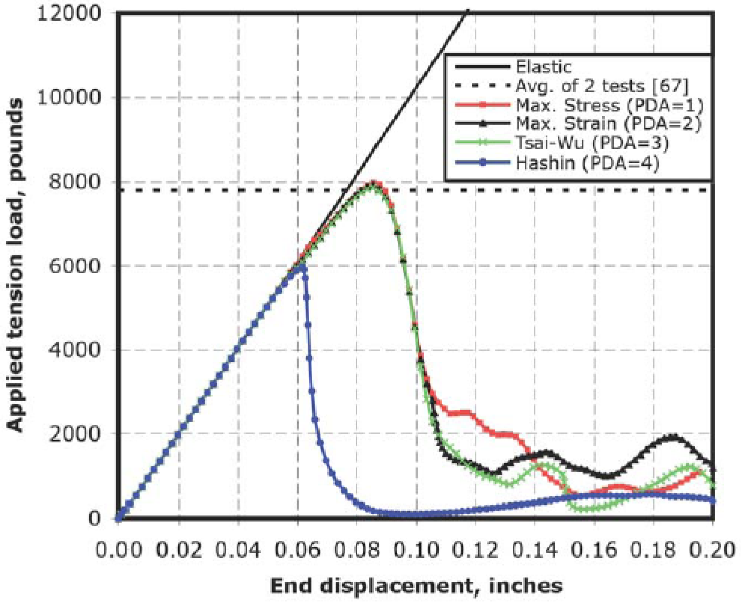

Figure 11: Comparison of different PFA models for the quasi-isotropic laminate

These progressive failure analysis results are generated using the nominal lamina material data, a single integration point through the thickness of each lamina, recursive degradation with a degradation factor β of 0.5, and a maximum solution increment size factor of 0.01.

The maximum stress and maximum strain criteria again give essentially the same result because the material is a linear elastic brittle material. The Tsai-Wu failure polynomial predicts a similar behavior and failure load since the laminate is quasi-isotropic.

The Hashin criteria under predict the peak load.
The predicted peak failure loads are summarized in Table 6. The different failure criteria have the maximum solution increment size of 0.01, and a recursive degradation with a degradation factor β of 0.5.

PFA Failure Criteria	**Peak Failure Load** [lbs] **Cross-ply**	 **Quasi-isotropic**
Max Stress	9531	7975
Max Strain	9620	7941
Tsai-Wu	8655	7869
Hashin	7129	5985
Test Average	9605	7810

Table 6: Comparison between test peak failure loads and different PFA models

For the cross-ply laminate case, the peak failure loads predicted by the maximum stress, maximum strain, and Tsai-Wu criteria are within 10% of the average failure load from test. The Hashin criteria gave very conservative predictions (lower by more than 25%).
For the quasi-isotropic laminate case, the peak failure loads predicted by the maximum stress, maximum strain, and Tsai-Wu criteria are within 2% of the average failure load from test. The Hashin criteria again gave conservative predictions (lower by 23%).

3.3 Concluding Remarks

From the achieved results it can be deduced that it is possible to obtain a good approximation regardless of the failure criteria adopted, being careful to choose a sufficiently tight step. This factor acts mainly on the peak load and on the post-failure behavior without affecting the birth of the crack near the hole. According to what seen so far will be considered as failure criteria the criterion of maximum deformation, being the one closest to reality. It must be said that the possibility to define a reliable model for the prediction of damage beyond the first crack can not prescind from the knowledge of behavior of the specific material.

4 Open Hole Tension Laminate

To understand how to properly set a Progressive Failure Analysis in NASTRAN will be taken as reference the uniaxial tensile test presented in section 3 reproducing accurately the model used, both in terms of properties that in terms of geometry. It will be analyzed only the quasi-isotropic lamination, much more similar to the one that will be used for the VT. Since the characteristics of T800H/3900-2 are very similar to those of 8552/IM7 (material that will be used for the VT), the results obtained here will also apply to the design of the structure.

Material Properties			**T800H/3900-2**	**8552/IM7**
Longitudinal Young's Modulus	E_{xx}	[MPa]	159958	155000
Transverse Young's Modulus	E_{yy}	[MPa]	8963	8400
In-Plane Shear Modulus	G_{xy}	[MPa]	6205	3200
Out-of-Plane Shear Modulus	G_{yz}	[MPa]	3447	3200
Out-of-Plane Shear Modulus	G_{xz}	[MPa]	6205	3200
Interlaminar Strength	S_B	[MPa]	125	56
Poisson's Ratio	ν_{xy}		0.28	0.28

Table 7: Comparison between T800H/3900-2 and 8552/IM7

As failure criteria will be considered the one currently used by AAEM, of which are available all the necessary allowable values, ie the maximum strain criteria. As regards the model of degradation, will be used the instantaneous unloading as more conservative.
After summarizing the results of interest, will be carried out checks regarding the dependence of these latter on the mesh size and how the parameters of the analysis affect the "goodness" of the solution.

4.1 Results of Interest

In order to explain the interesting data provided by a PFA it has been considered an analysis with Time Step of 2% (see sub 4.3), that is divided into 50 steps, performed on a mesh of medium density.

4.1.1 First Ply Failure

The first result to be searched is the load at which it occurs the FPF. This value is easily identifiable by the Failure Index (FI) defined as follows:

$$FI = \frac{Applied\,Load}{Allowable\,Load}$$

The FI is a quantity "layered" therefore it can be displayed ply per ply in order to understand which of these comes first to breakage. To know the value of the FPF is necessary to display the maximum value of FI in all the plies.
It is also important to exclude any kind of interpolation in order not to over/underestimate the result through the shape functions of finite elements. In this way are displayed the maximum values of FI, namely those used by the solver to perform the calculations.
When the FI exceeds unity means that the specimen is subjected to a load greater than the FPF. Figure 12 shows a visualization of the FI in the region near the hole at Time Step 20%. As can be noted, in 8 elements (shown in red, 4 per side) there is a FI very close to the unit equal to 0.992. This means that, in the transition between the 20% and 22% of the load, there is the breaking of at least one lamina.

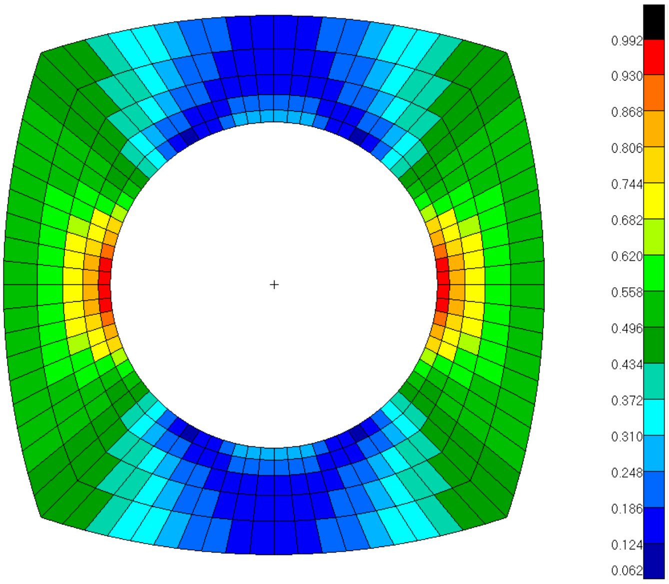

Figure 12: Open-hole-tension specimen FPF: Time Step 20%

Assuming to have used an integration step sufficiently tight to be able to consider a linear behavior between two consecutive step, it can be searched the exact FPF load and the displacement associated, using the definition of the FI.

$$F_{FPF} = \frac{F_{app}}{FI} \quad d_{FPF} = \frac{d_{app}}{FI}$$

4.1.2 Total Damage

The degradation model of the material is activated in elements subject to the FPF, whereby the progressive failure will originate from them.

The integrity of the individual lamina is expressed by the Total Damage whose value is the complement of the Residual Stiffness Fraction (see sub 4.4).

In the case of instantaneous unloading the TD may assume two values:

$$TD = \begin{cases} 0 \\ 1 - RSF \end{cases}$$

A null value indicates that the lamina has not been broken, while the value $1-RSF$ indicates that it is broken while maintaining a fraction of the original stiffness, as defined by the RSF. As well as the FI, also the TD is a quantity “layered” so, considering all the plies and displaying the maximum value of the TD, it is possible to draw a map of the damage propagation within the laminate.

Looking at Figure 13 is seen as, at the Time Step 20%, the TD is still null because the FI does not exceed unity. At Time Step 22% the maximum strain criteria indicates the presence of the FPF hence the material property is degraded in the elements with FI higher than unit. Subsequently the damage propagates with a path which is a function of geometry and type of lamination.

If, considering all the laminae, is displayed the minimum value of TD, is possible to draw a map of the crack propagation within the laminate. A non-zero value means that all the laminae of that element are broken therefore is born a crack.

Looking at Figure 14 can be seen as the crack propagates perpendicular to the load direction. The prediction of rupture is very similar to those found experimentally on specimens with quasi-isotropic lamination.

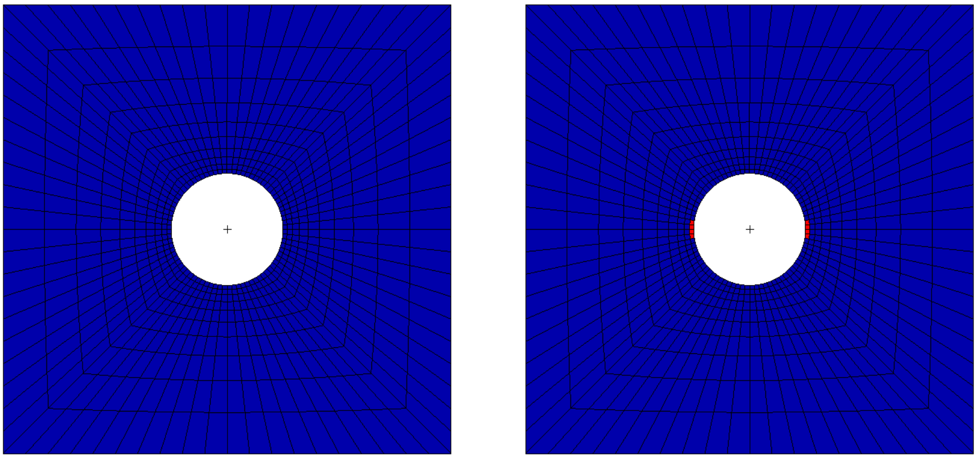

TD_{max} - Time Step 20% TD_{max} - Time Step 22%

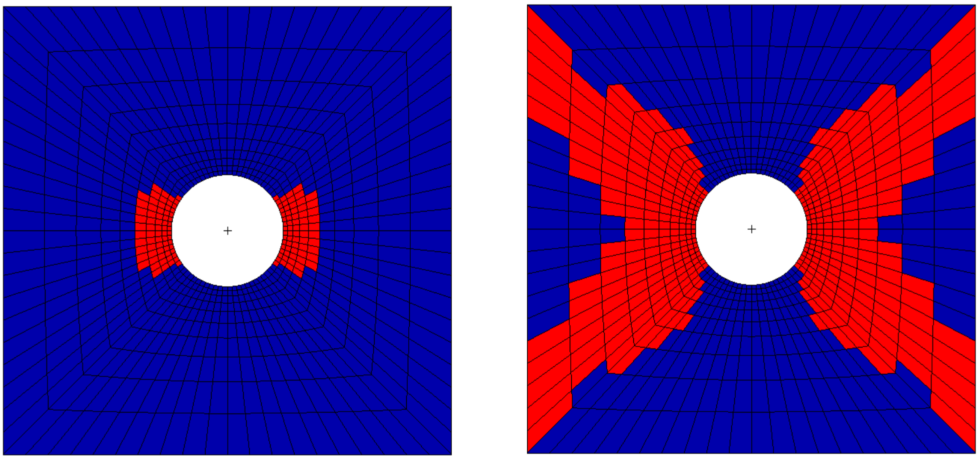

TD_{max} - Time Step 42% TD_{max} - Time Step 54%

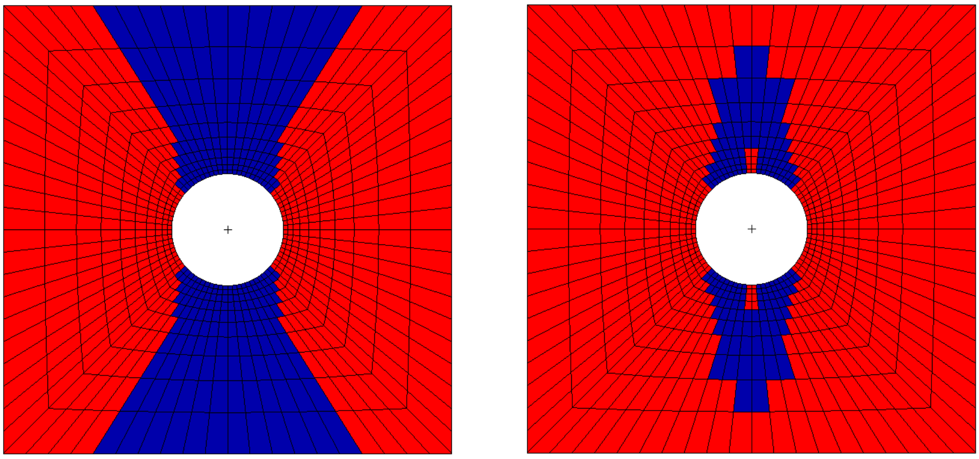

TD_{max} - Time Step 60% TD_{max} - Time Step 100%

Figure 13: Open-hole-tension specimen TD: maximum (all layer)

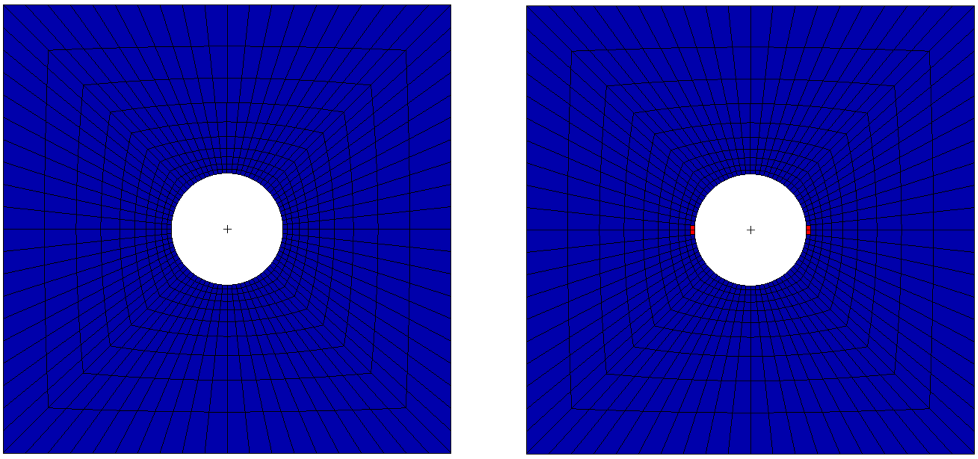

TD_{min} - Time Step 50% TD_{min} - Time Step 52%

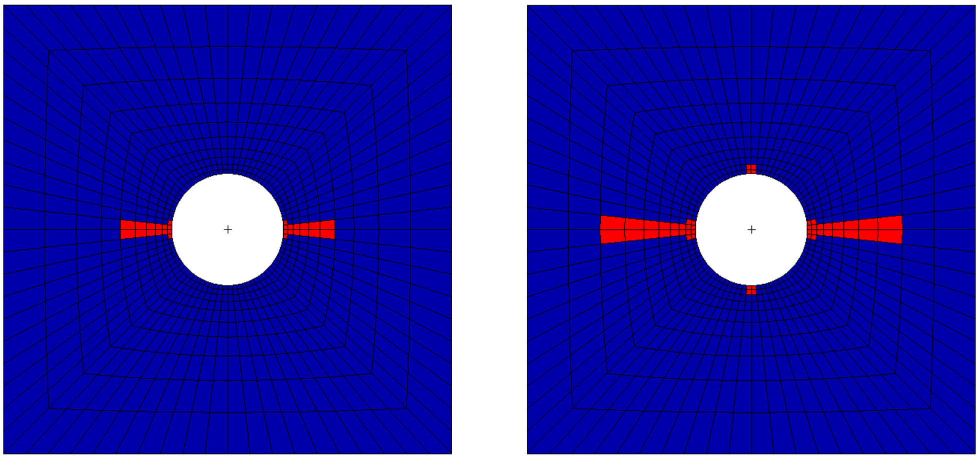

TD_{min} - Time Step 72% TD_{min} - Time Step 82%

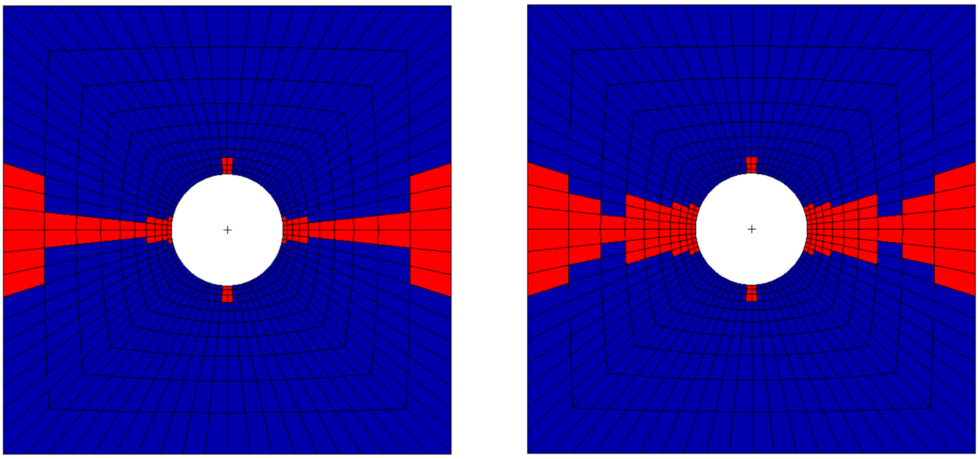

TD_{min} - Time Step 90% TD_{min} - Time Step 100%

Figure 14: Open-hole-tension specimen TD: minimum (all layer)

The birth of the first crack will be the new condition for the design of the structure. The more the FPF will be far from the onset of the crack, the greater will be the margins to optimize the model. In addition, the PFA allows to have a greater awareness about the propagation of the damage and consequently take countermeasures to limit it, for example through thickenings or by the introduction of crack stoppers.

4.1.3 Final Failure

The catastrophic failure is not identifiable in a unique way but depends from case to case. In a simple example, such as that of the specimen, the break can be identified by the crossing of the entire section by the crack (TD_{min} - Time Step 90%).

For more complex cases, which may be the internal structure of VT, the identification is not so simple. In theory it would be possible to associate to the peak of the force-displacement curve the maximum sustainable load of the structure, but this would inevitably lead to an overestimation due to the contribution of the residual stiffness.

Another more effective method would be the observation of large entities displacements on the load curve, symptom of complete rupture of some stiffening element, and consequently attribute to the failure load the one associated to the previous step.

4.2 Mesh Size Influence

To investigate the mesh size influence on the quality of the results will be compared four different finite element models of the specimen made with 620, 1240 (model from literature), 2480 and 4960 elements. All analysis will be performed without varying any parameters and maintaining a step sufficiently tight to ensure the goodness of the solution.

It has been maintained a modellation similar to that used in the example given in the subsection 3.1 in which the mesh is uniform approaching the edge of the hole, as shown in Figure 15.

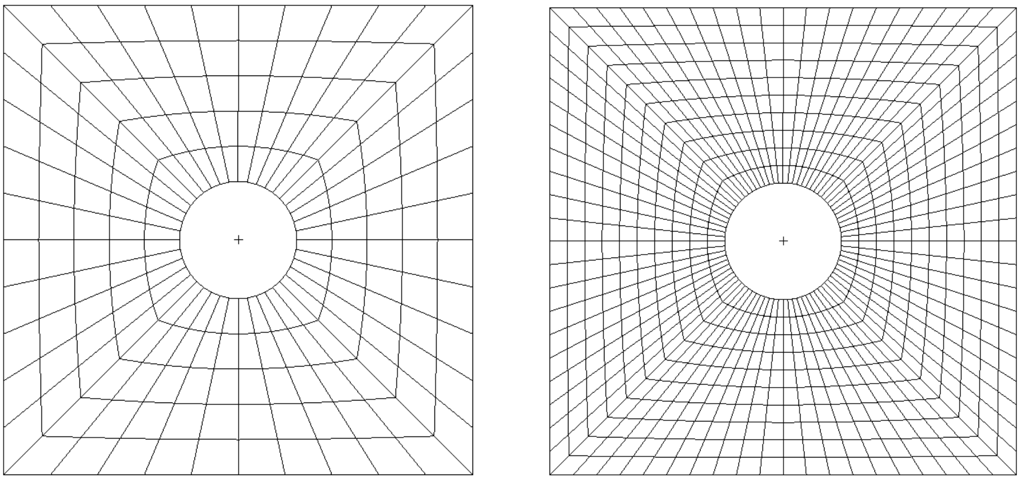

(a) 420 elements (b) 1240 elements

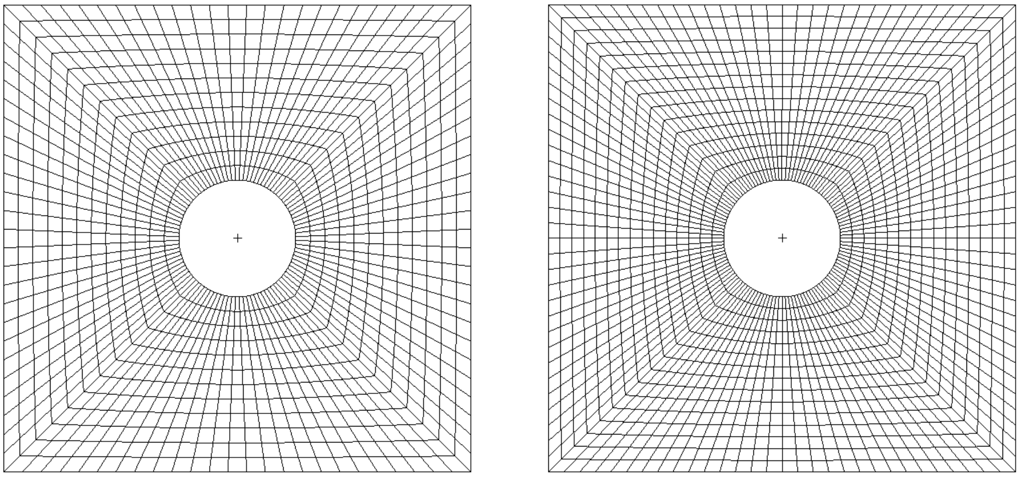

(a) 1240 elements (b) 2460 elements

Figure 15: Different mesh size

In Table 8 are reported the results of interest obtained from the different mesh used.

N° Elem	Force [N]	Δ%	Disp. [mm]	Δ%
	First Ply Failure			
2460	9378	-	0.527	-
1750	9594	2%	0.539	2%
1240	9847	5%	0.559	6%
420	11288	20%	0.645	22%
	First Crack			
2460	23678	-	1.350	-
1750	24107	2%	1.380	2%
1240	24537	4%	1.400	4%
420	28216	19%	1.650	22%
	Failure			
2460	32636	-	2.030	-
1750	32901	1%	2.050	1%
1240	31263	4%	1.950	4%
420	31372	4%	1.980	2%

Table 8: Mesh size influence on the progressive failure predictions

As the number of elements, which is composed the mesh, increase, the results tend to converge. This means that the mesh with 2460 elements provides more reliable data, which will therefore be used as a reference.
Comparing them with the mesh of 420 elements we will immediately notice that they deviate too far from those considered good, therefore must be discarded.
As regards the mesh with 1240 and 1750 elements their results can be considered acceptable. In addition, taking into account the computational cost, these mesh are more attractive than tighter ones.
Unlike the failure load, which has a minimum variation, FPF and FC are strongly influenced by the size of the mesh.
To better understand the dependence of the results from the mesh it has been considered a different modellation. In Table 9 are reported the results of interest obtained for different mesh used.

N° Elem	Force [N]	Δ%	Disp. [mm]	Δ%
	First Ply Failure			
2460	8734	-	0.496	-
1750	8780	1%	0.498	1%
1240	8878	2%	0.504	2%
420	9372	7%	0.532	7%
	First Crack			
2460	22376	-	1.275	-
1750	22811	2%	1.300	2%
1240	22811	2%	1.300	2%
420	24109	8%	1.375	8%
	Failure			
2460	31714	-	1.950	-
1750	31870	0%	1.950	0%
1240	30520	4%	1.875	4%
420	30918	3%	1.900	3%

Table 9: FEM influence on the progressive failure predictions

Unlike the previous case it can be seen in Figure 16 how the mesh has been thickened in the area around the hole, in which it is expected the birth of the first crack.

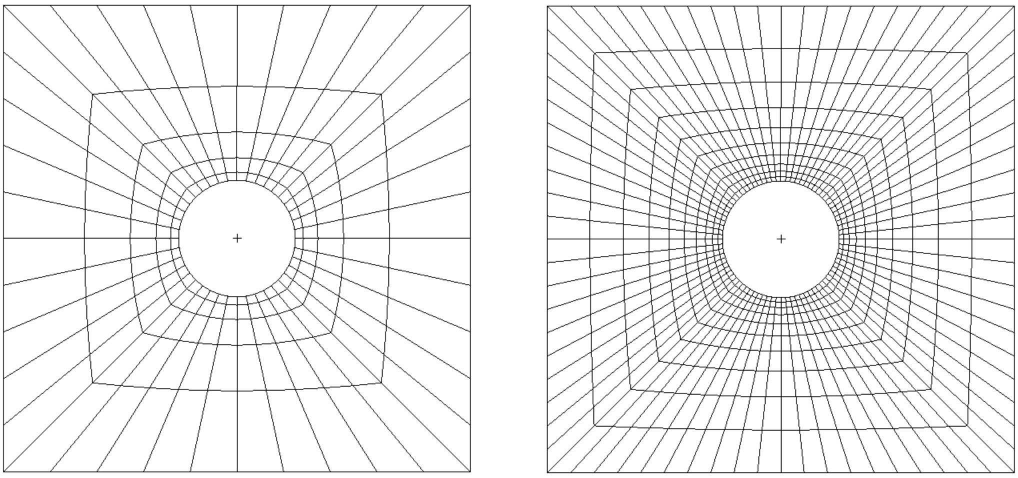

(a) 420 elements (b) 1240 elements

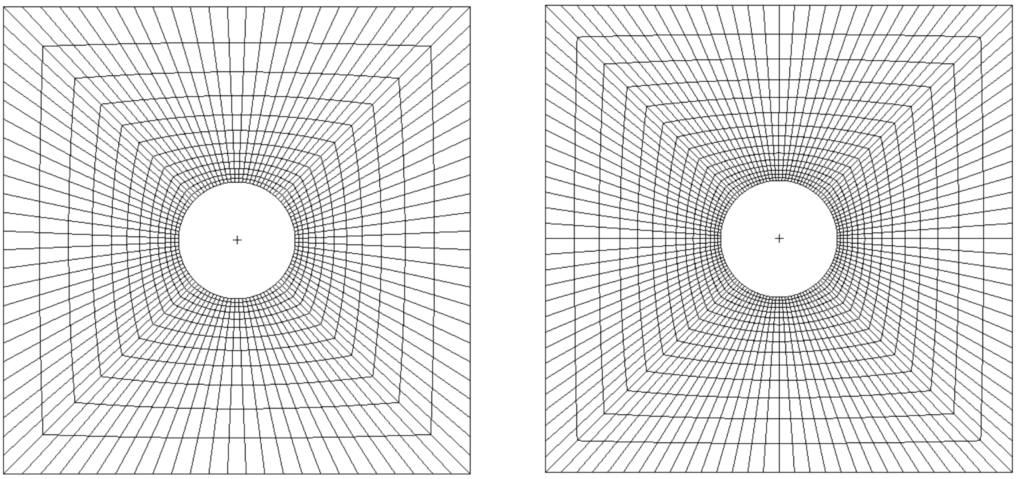

(a) 1240 elements (b) 2460 elements

Figure 16: Different Finite Element Models

As expected, the denser mesh provides the best results, but unlike before, the variations of the other results, has decreased substantially.
The mesh with 1240 elements proves to be a good compromise between quality of results and computational cost, therefore, will be used for the following checks.
The graph of Figure 17 shows the load-displacement curves in function of the mesh size. In addition is reported the trend curve of the static solution and the mean value of the test breaking load (taken from literature).

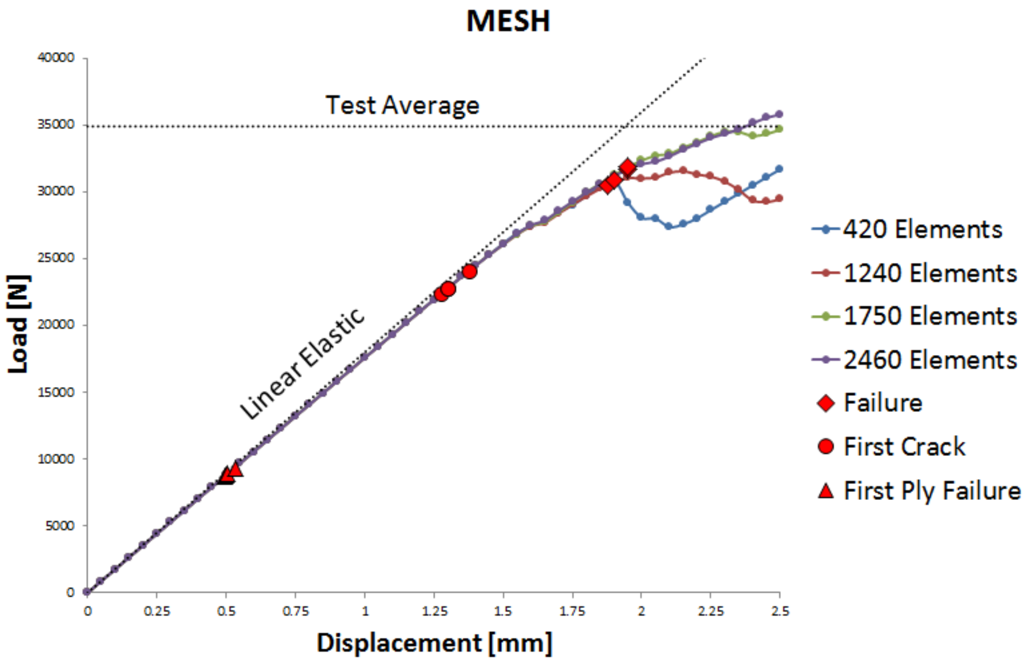

Figure 17: FEM influence on the progressive failure predictions

Before the FPF all the curves overlap each other with the same inclination of the static solution. This means that prior to the FPF, when the material degradation model is not yet activated, the solutions are very similar. This is very important since it allows to dimension a component with a static analysis, very fast, and subsequently to check with the PFA that cracks do not occur before the ultimate load.

N° Elem	Force [N]			Displacement [mm]		
	Static	PFA	Δ%	Static	PFA	Δ%
2460	9018	8734	3%	0.511	0.496	3%
1750	9149	8780	5%	0.519	0.498	5%
1240	9324	8878	7%	0.529	0.504	7%
420	10259	9372	17%	0.581	0.532	17%

Table 10: FPF check

4.3 Time Step Size Influence

A key parameter for the success of the analysis is the integration step, implemented in NASTRAN through the card NLSTEP (see Appendix).
This parameter indicates in how many increments is divided the load to which is subjected the structure under examination. The smaller are these increments (or the greater is the number of integration steps), the easier will be finding an equilibrium solution.
Four different adaptive analysis were performed with respectively 25, 50, 75 and 100 steps of integration. The term “adaptive analysis” is to indicate that, in presence of strong non-linearity, the program is able to decrease the integration step to facilitate convergence.
Table 11 shows the results of interest obtained from the various analysis.

N° Step	Force [N]	Δ%	Disp. [mm]	Δ%
	First Ply Failure			
100	8878	-	0.504	-
75	8885	0%	0.505	0%
50	8879	0%	0.504	0%
25	8881	0%	0.504	0%
	First Crack			
100	22811	-	1.300	-
75	22808	0%	1.300	0%
50	22818	0%	1.300	0%
25	22829	0%	1.300	0%
	Failure			
100	30520	-	1.875	-
75	31452	3%	1.933	3%
50	35379	16%	2.250	20%
25	39104	28%	2.400	28%

Table 11: Time step size dependence

Is evident how the number of steps affects only the failure load, decreasing it as the analysis thickens. For clarity, in Figure 18 is shown only the final part of the load-displacement curve.

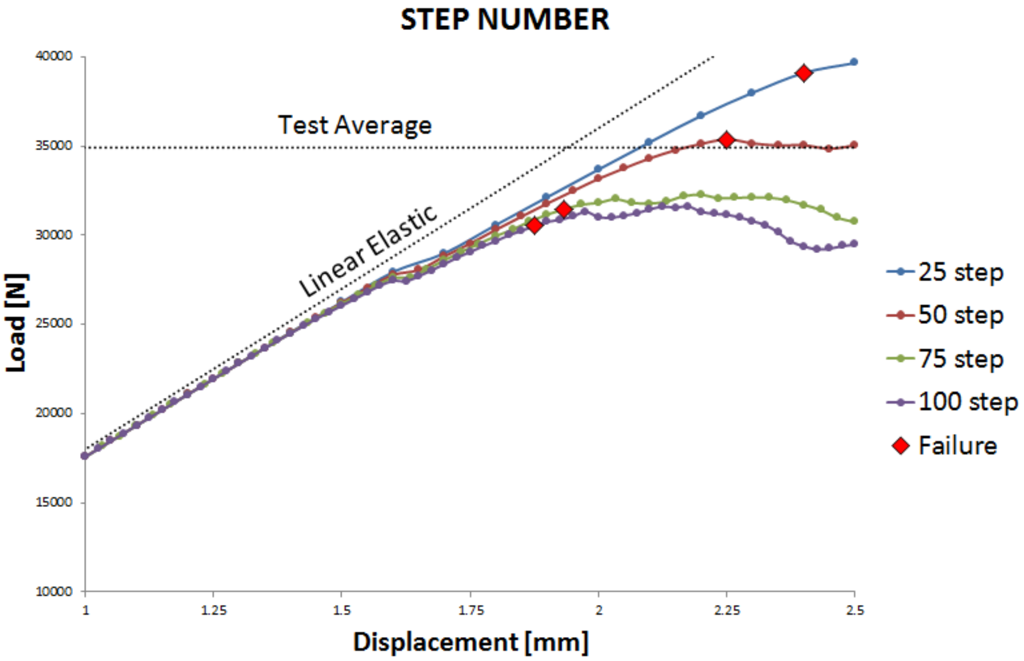

Figure 18: Time step influence on the progressive failure predictions

The reason of this behavior is the following: whenever the FI exceeds unity the material properties are degraded and the overall stiffness of the component is decreased. In a dense analysis the load condition is updated more frequently as well as the properties. While for a wide step many element are degraded at once, for a fine step are broken continuously. This means that, for the same displacement, dense analysis presents more broken elements compared to sparse analysis and therefore loses its stiffness faster. Figure 19 shows the number of broken items as a function of displacement.

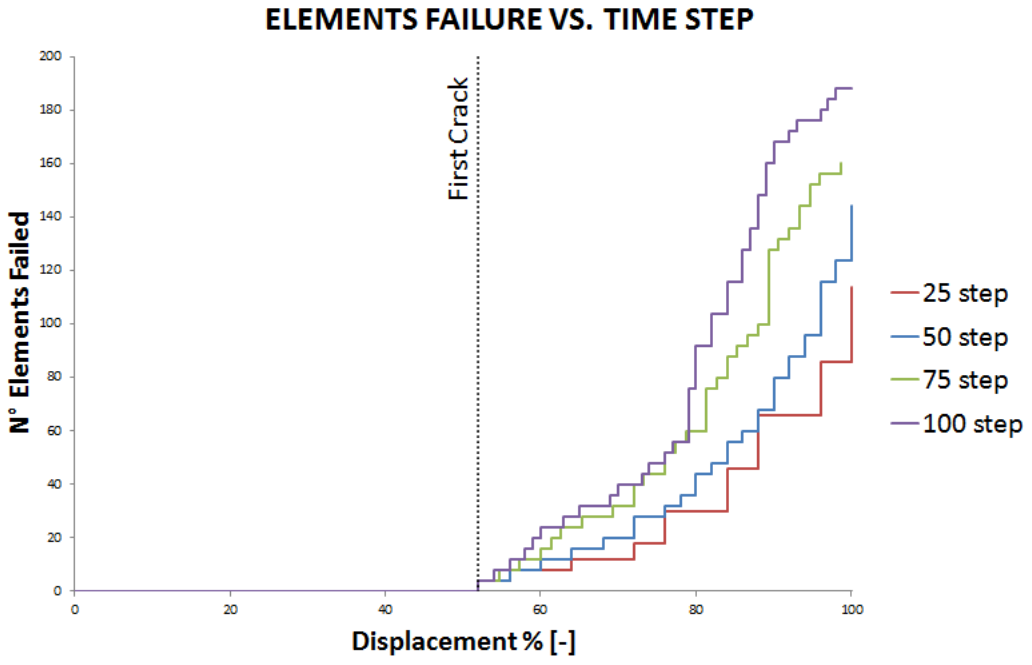

Figure 19: Time step influence on the failure

In order to have the curve as accurate as possible the best solution would be to have the steps tight enough to break one element at a time; obviously this is not possible without admitting high computational costs.
Since getting the real value of the failure load is of secondary importance, compared to the identification of the FC, for follow-up checks will be considered the intermediate analysis with 50 steps.

4.4 Residual Stiffness Fraction

For the previous analysis has been used the instantaneous unloading as material degradation model. This choice lies in the intrinsic properties of carbon. In fact, because of its brittle behavior, the drastic reduction of the lamina's properties after the rupture is more close to reality, in addition to being a more conservative choice. Everything is implemented in NASTRAN through the card MATF (see Appendix) using the Residual Stiffness Fraction (RSF), which is defined in the following way:

$$RSF = \frac{K_f}{K_i}$$

where K_i and K_f are respectively the stiffness of the integral element and the broken one.
To understand the effects of this parameter on the results, four analysis were performed on the same model simply varying the RSF. As can be seen from Figure 20 and the Table 12 there is a substantial variation of the results only in the final part of the curve, close to the failure.

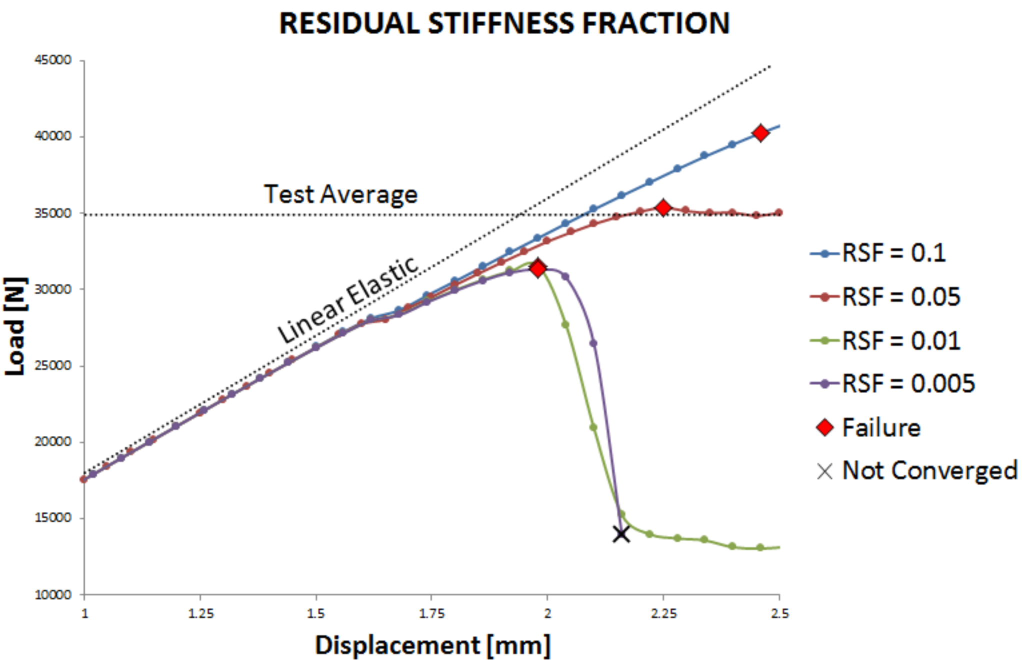

Figure 20: Residual Stiffness Fraction influence on the progressive failure predictions

RSF	Force [N]	Δ%	Disp. [mm]	Δ%
	First Ply Failure			
0.1	8878	0%	0.504	0%
0.05	8878	-	0.504	-
0.01	8878	0%	0.504	0%
0.005	8878	0%	0.504	0%
	First Crack			
0.1	22811	0%	1.300	0%
0.05	22811	-	1.300	-
0.01	22811	0%	1.300	0%
0.005	22811	0%	1.300	0%
	Failure			
0.1	40273	14%	2.460	9%
0.05	35379	-	2.250	-
0.01	31555	11%	1.980	12%
0.005	31317	11%	1.980	12%

Table 12: Residual Stiffness Fraction dependence

What happens after the FC is useful to study the propagation of the rupture. In this case, where is of interest the identification of the first crack, the RSF plays a role only for reasons of computational cost.

4.5 Force Control vs. Displacement Control

In this section, will be studied the effect on the results of different type of loading. In particular, will be analyzed: a force controlled loading (Force 50) and displacement controlled loading (DISP 50) with the Newton-Raphson method, and a force controlled loading with the Arc-Length method (ARCL 50), all with 50 step analysis.

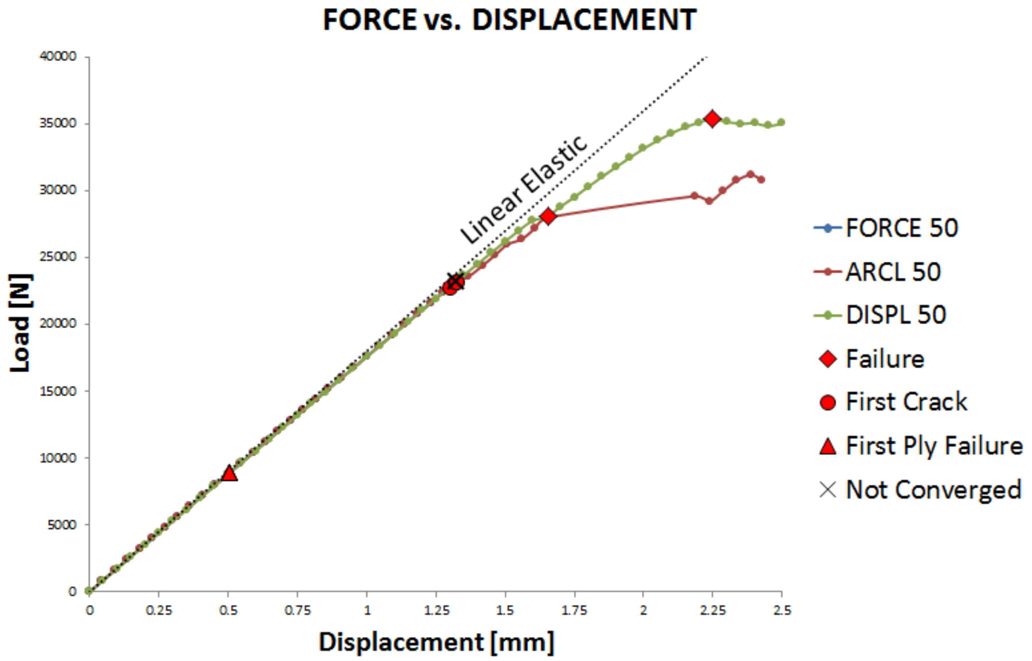

Figure 21: Force Control vs. Displacement Control

Method	Force [N]	Δ%	Disp. [mm]	Δ%
	First Ply Failure			
DISP 50	8879	-	0.504	-
ARCL 50	8908	0%	0.506	0%
FORCE 50	8880	0%	0.505	0%
	First Crack			
DISP 50	22818	-	1.300	-
ARCL 50	23253	2%	1.320	2%
FORCE 50	23200	2%	1.322	2%
	Failure			
DISP 50	35379	-	2.250	-
ARCL 50	28080	21%	1.654	26%
FORCE 50	Not Converged			

Table 13: Force Control vs. Displacement Control

After the first crack the ARCL50 method has more difficulties to follow the load curve with respect to the DISP50 method while the FORCE50 method fails to converge.
As regards FPF and FC the three methods can be considered equivalent therefore the choice to apply one respect to another will be taken afterward.

4.6 Computational Cost

This section summarizes the costs, both in terms of time and memory, that the various analysis, performed so far, have required. The analysis time was obtained from the output file .sts while for the memory occupied has been considered the size of the output file .op2, used to import the results in PATRAN.
Time and memory are directly proportional to the number of elements in the model and the number of steps used. The necessity of fast analysis and acceptable memory costs leads to analysis with few steps and to reduced models. However the need of high quality results contrast with this choice so a compromise have to be found.

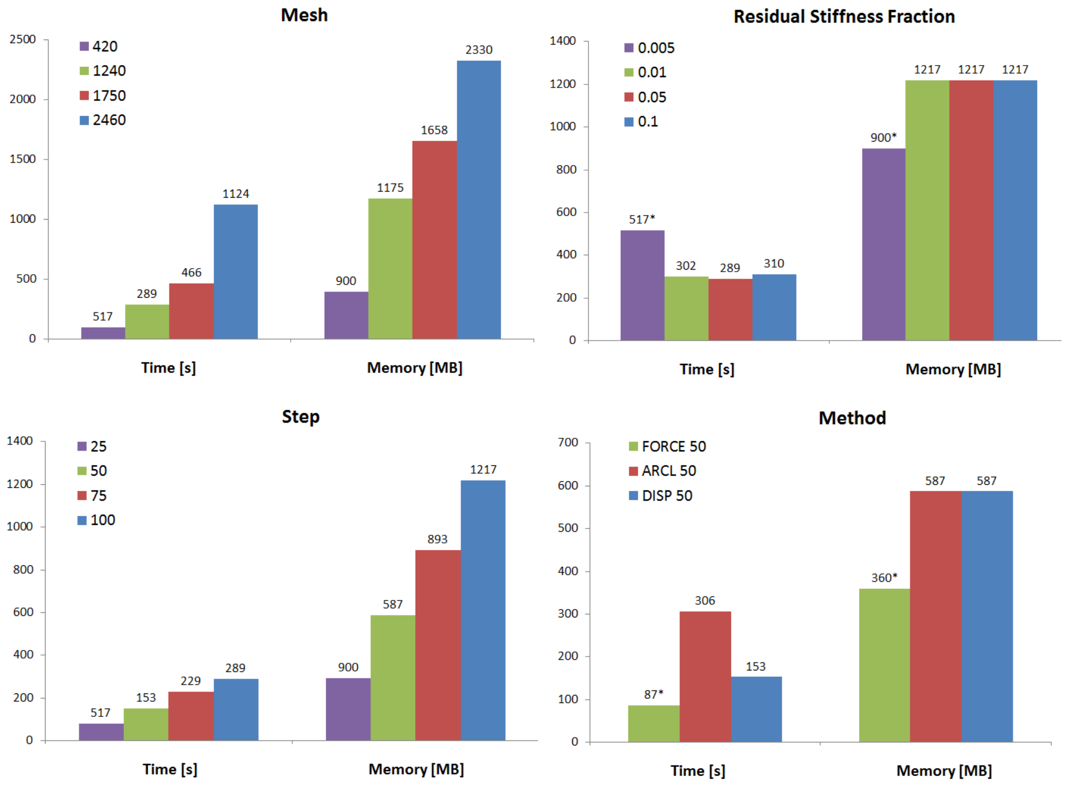

Figure 22: Computational cost

The RSF has no effect on the computational cost but an excessive reduction of its value can lead to ill-conditioned problems. This happens because the analysis has difficulties in reversing the stiffness matrix since the damaged elements introduce stiffness almost nil. Not having available reference values, for future analysis will be chosen as RSF an arbitrary value corresponding to the stiffness of the resin

$$\frac{\text{matrix stiffness}}{\text{fibre stiffness}} = \frac{8963}{159958} \cong 0.05$$

The type of loading control has an influence only on the time of the analysis. The faster is the Newton-Raphson method with displacement controlled loading.

As regards the force controlled loading, the Newton-Raphson method is definitely faster than the Arc-Length method but, exceeded the first crack, presents considerable difficulties to converge due to the impossibility of using negative load increments. A solution to this problem may be to set an analysis with Newton-Raphson up to FC followed by an analysis with Arc-Length. This can be done using the subcases.

4.6.1 Subcases

In order to save time and memory it is possible to split the analysis into several subcases in order to densify the step only in critical areas.

In particular is convenient to consider a wide step before the FPF, where there are only geometric non-linearity, and subsequently densify when appear the non-linearity of the material. In this way, with a lower number of steps, it is possible to reduce the computational time and the memory required, obtaining a solution with the same quality.

Taking into account, from a 50 step analysis, the conditions of FPF and FC, two similar analysis but with lower number of steps are performed. The subcases 5-22-5 consider:

- a number of steps equal to 5 before the FPF
- a number of steps equal to 22 just before the FPF and immediately after the birth of the FC

- ✈ a number of steps equal to 5 after the birth of the FC.

The subcase 1-22-5 is different from the previous one simply because before the FPF performs a single step.

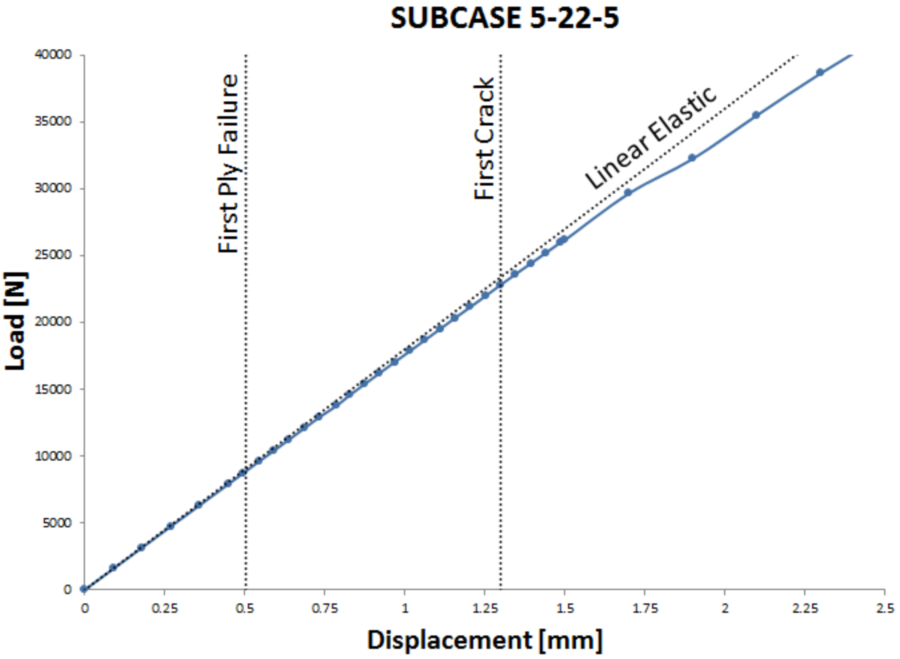

Figure 23: Subcase 5-22-5: computational cost

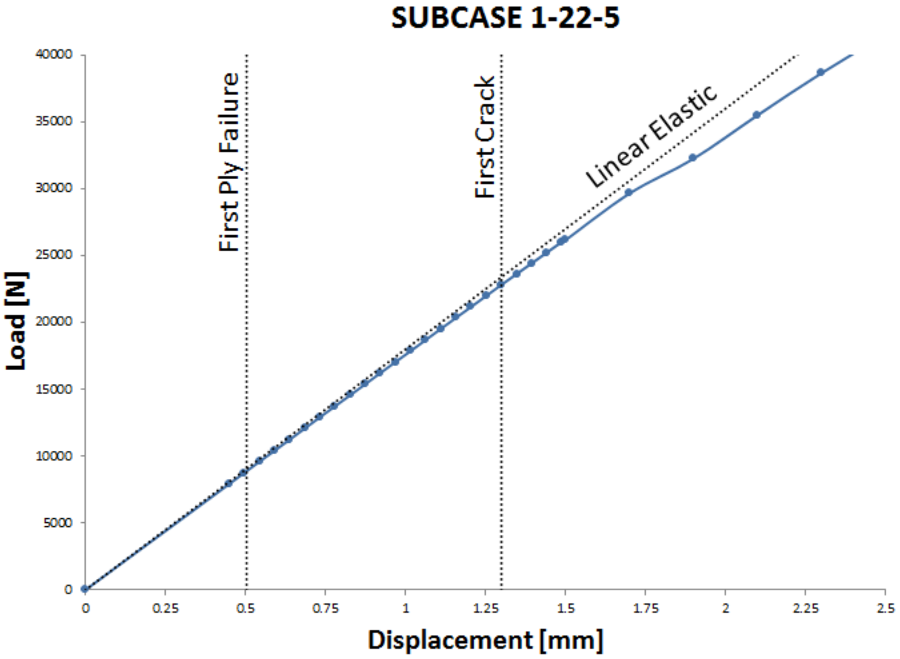

Figure 24: Subcase 1-22-5: computational cost

Subcase	Time [s]	Δ%	Memory [MB]	Δ%
50 Step	153	-	587	-
5-22-5	105	31%	387	34%
1-22-5	92	40%	340	42%

Table 14: Subcases vs. computational cost

Subcase	Force [N]	Δ%	Disp. [mm]	Δ%
	First Ply Failure			
50 Step	8879	-	0.504	-
5-22-5	8887	0%	0.504	0%
1-22-5	8887	0%	0.504	0%
	First Crack			
50 Step	22818	-	1.300	-
5-22-5	22826	0%	1.301	0%
1-22-5	22828	0%	1.301	0%

Table 15: Subcases vs. result's quality

As can be seen from Table 14 the computational costs, both in terms of time and memory, are reduced significantly. In Table 15 is immediately evident how the results of interest have not been affected by the changes of analysis.

Obviously this argument can be made only by knowing in advance the position of the FPF, easily identifiable through a static analysis, and the location of the FC, obtained through an analysis of PFA reasonably dense. However, the advantage remains and it is represented by the possibility to reduce the computational cost in successive stages of model optimization.

4.7 Other Results

To better understand what has been done so far, here is shown in detail the behavior of some elements adjacent to the specimen hole. It has been considered a standard analysis with mesh composed by 1240 elements, a time step of 2% and a RSF of 0.05.

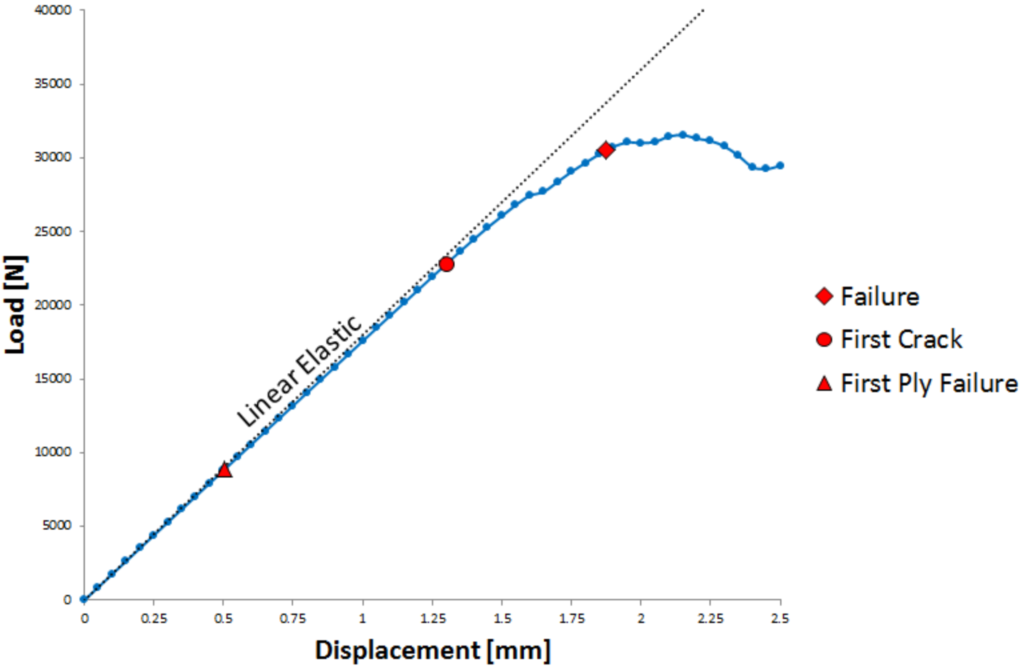

Figure 25: Standard analysis: load displacement curve

Are taken into consideration only 3 elements in order to make the following graphs easy to read. The choice of these is not accidental: the element 1851 is among the first elements subjected to the FPF as well as one of the elements from which is originated the crack; the elements 1871 and 1891, are on the path of the crack propagation, so their failure takes place in sequence as the load increases.

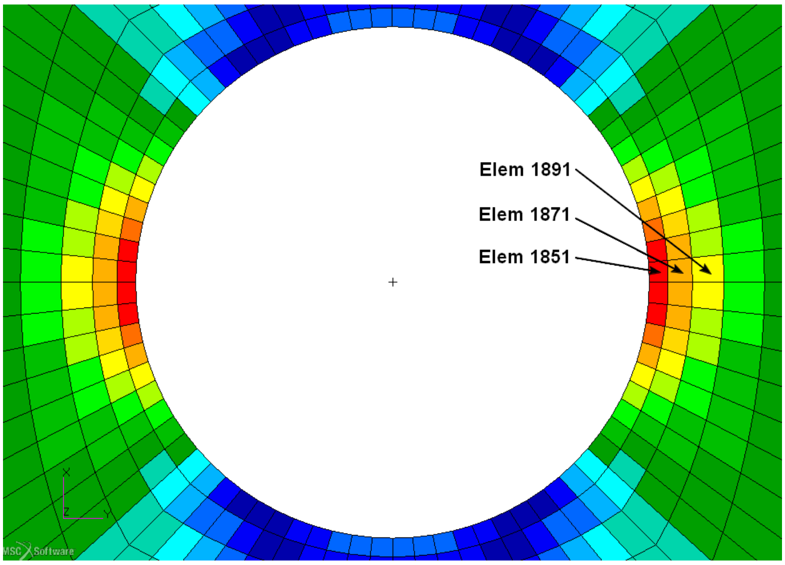

Figure 26: Elements considered

To be able to compare the results, the graphs are expressed as function of a parameter independent from the element taken into consideration, namely the time step of the analysis (expressed in terms of maximum displacement %). Furthermore, only the laminae oriented at 0° and 90°, with respect to the direction of load, are considered as they provide results most interesting.

As anticipated, observing the TD in Figure 27 and Figure 28, it can be seen how the fiber breakage occurs in sequence starting from the edge of the hole and moving towards the outside. The first break occurs at the FPF load for the laminae oriented at 90°. This is due to the fact, that for these laminae, the load acts on the matrix, whose tensile strain allowable is much lower than the tensile strain allowable of fiber for the laminae oriented at 0°.

$$X_\varepsilon^T = 0.0178$$

$$Y_\varepsilon^T = 0.0067$$

As the load rises, the deformation increases, up to overcome even the allowable of the laminae oriented at 0°. This leads to the complete rupture of the laminate and then to the birth of the first crack and its propagation towards the outside.

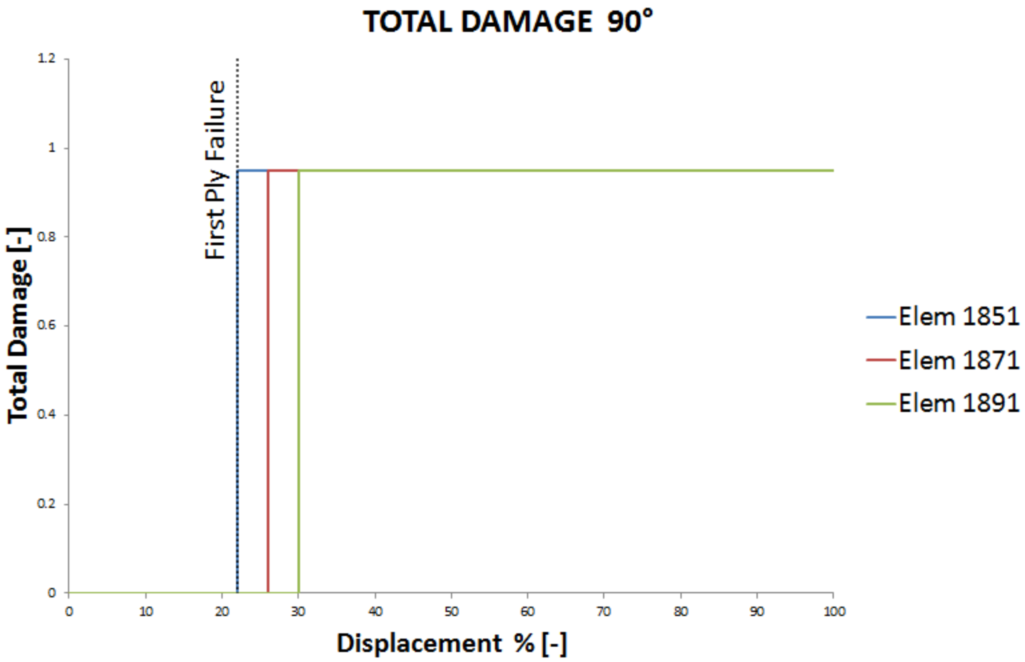

Figure 27: Total Damage: 90°

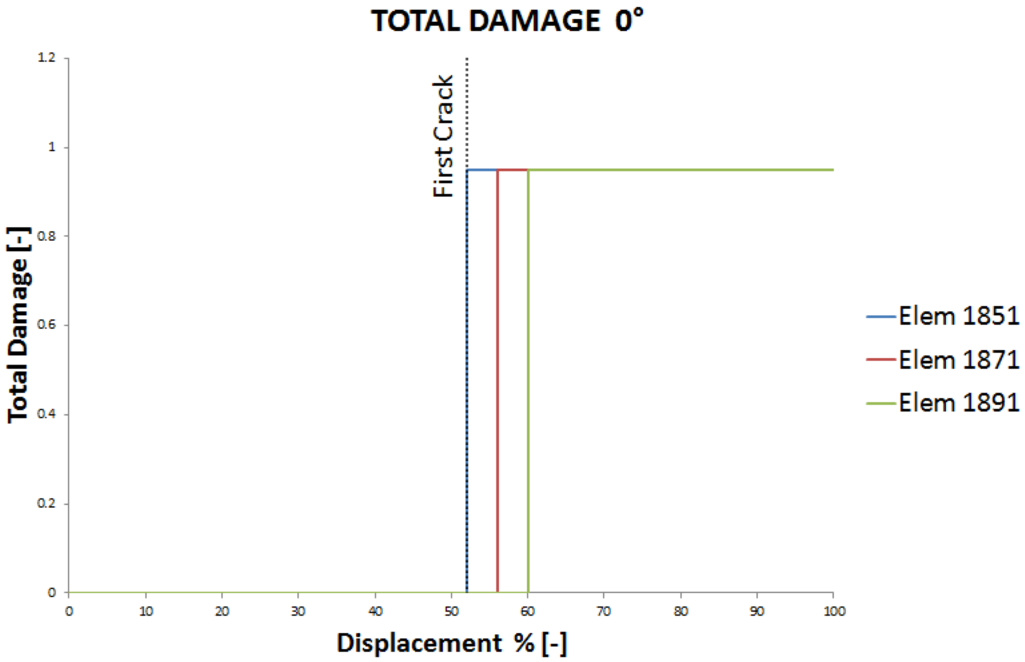

Figure 28: Total Damage: 0°

In the first portion of the strain-displacement curve, deformation has a nearly linear trend. The gradient does not change even after the advent of the FPF as the plies at 90° give a small contribution to the stiffness of the element. In fact, almost all of the stiffness is given by the laminae at 0° which have an elastic modulus 2 orders of magnitude higher.

$E_{xx} = 159958$

$E_{yy} = 8963$

The curves in Figure 29 show a sudden increase of the gradient after the breakage of the first lamina at 0°. The broken element, having only residual stiffness, can not more sustain the load and begins to deform considerably.

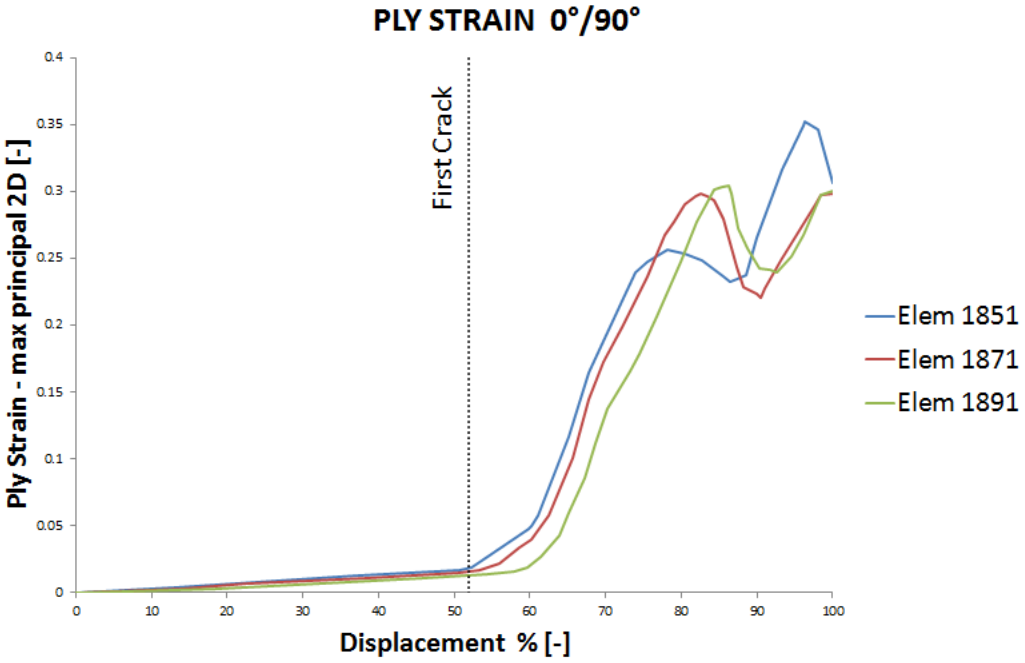

Figure 29: Ply strain

Figure 30 and Figure 31 show respectively the evolution of stresses in the laminae at 90° and 0°. It can be seen how the element 1851 loads faster than the others and therefore is the first to reach the breakage. As for the laminae at 90° this does not cause appreciable variations in the behavior of the other elements because, as already specified, the lost stiffness is negligible. Instead, when the rupture of the laminae at 0° occurs, it is noted in the elements 1871, and 1891 a fairly marked increase of the supported load.

After the FC has taken place, the stress begins to increase in all broken laminae because of the residual stiffness. This behavior is not realistic therefore dimensioning a structure before the FC is the best choice as these phenomena are still negligible.

The level of stress at which rupture occurs within the laminae at 90° and 0° can be easily checked using the following formulas:

$$\sigma_y = E_{yy} Y_\varepsilon^T = 8963 \cdot 0.0067 = 60\,\text{MPa}$$

$$\sigma_x = E_{xx} X_\varepsilon^T = 159958 \cdot 0.0178 = 2847.2\,\text{MPa}$$

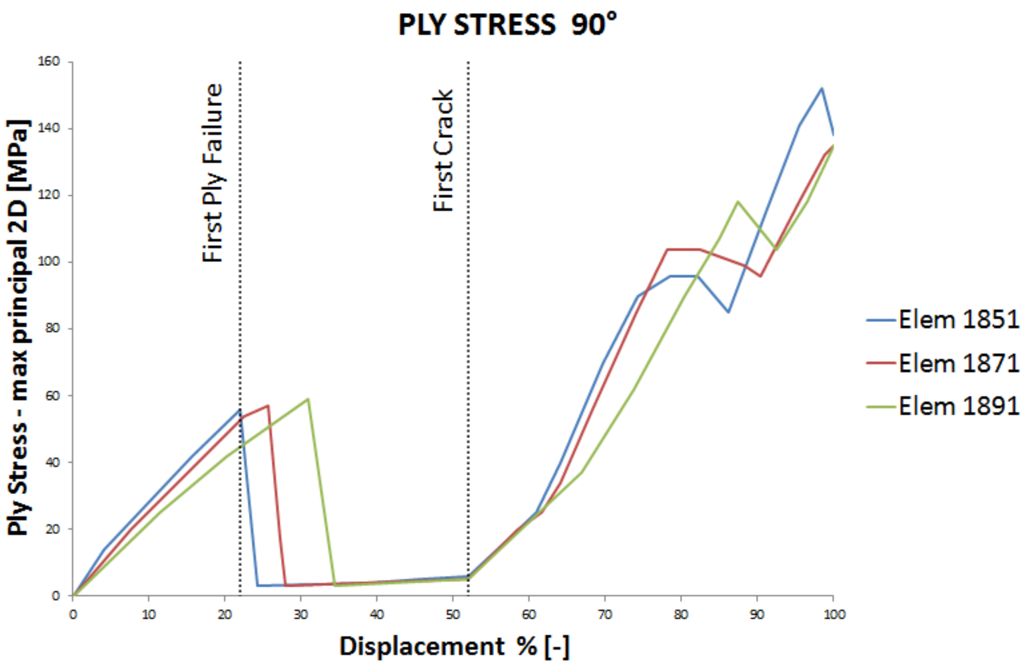

Figure 30: Ply stress: 90°

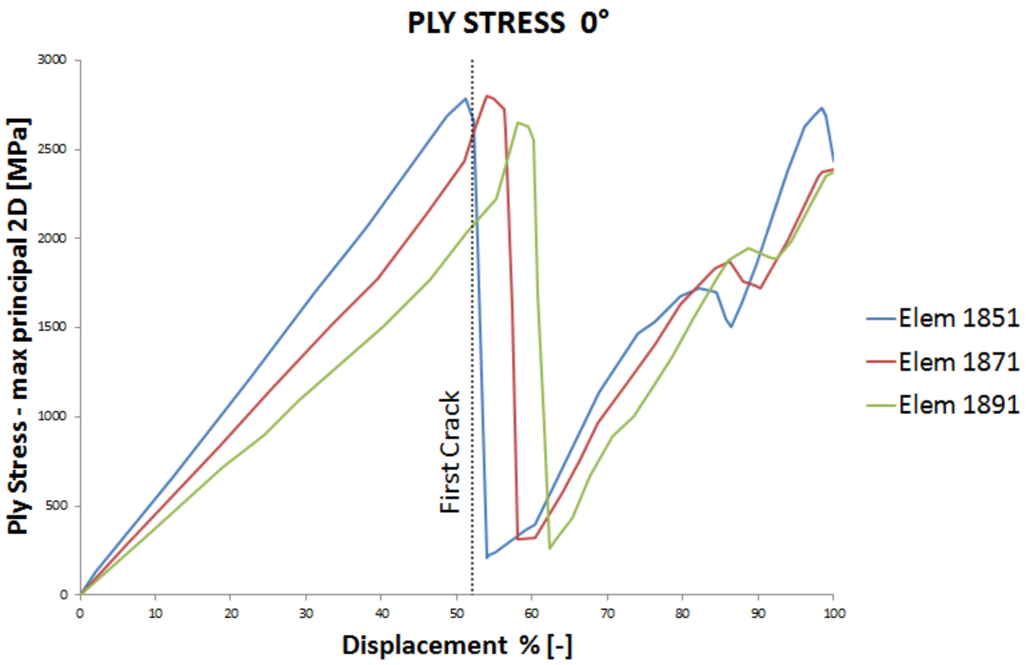

Figure 31: Ply stress: 0°

5 Planning

Understood how to properly set a Progressive Failure Analysis it is possible to start working on the real goal of this thesis, namely the dimensioning of the VT in composite material. At the beginning a simple static analysis will be performed, on the FEM structure currently in use, to obtain reference values.
Subsequently will be performed a bibliographic research to identify the most common construction methods used on the major aircraft in order to choose the internal configurations. Then we will proceed to the finite element modeling for two configurations of the VT, being careful to check all the procedures for the validation of the model.
After choosing the materials, which will be used to realize the structures, will be performed a preliminary analysis using the method of FPF. For sake of simplicity will be described in detail the analysis on the first structure while for the other will be reported only the results. At this point, having the two configurations statically dimensioned, we will proceed with their verification, by applying the PFA, and their optimization.
Finally, the obtained results will be compared to the current configuration. The foregoing is shown schematically in Figure 32.

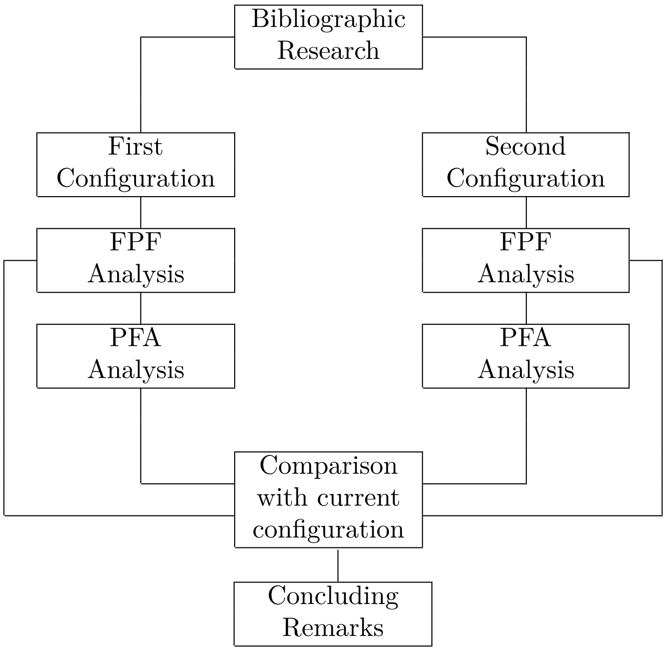
Bibliographic Research
First Configuration
Second Configuration
FPF Analysis
FPF Analysis
PFA Analysis
PFA Analysis
Comparison with current configuration
Concluding Remarks

Figure 32: Planning

During the modellation some components will be maintained equal to the current. In particular, these elements are:

- root machined parts (connection fin/fuselage)
- hinges (connection fin/rudder)

6 Vertical Tail FEM

Finite Element Models (FEMs) are the basis for a variety of engineering computations such as stress and stability analysis, vibration and dynamic load analysis. When the model is being used in the preliminary stages of a project, FEM developers must use their best engineering judgment to model the structure accurately and to ensure that the model is mathematically correct and does not contain any inadvertent errors.

6.1 FEM Idealization

6.1.1 Element Selection

MSC/NASTRAN contains a large library of structural elements. The criteria for the selection of an element may include its capabilities (for example, whether it supports anisotropic material properties), its cost (in general, the more DOF an element has, the more expensive it is), and/or its accuracy.

It is critical to have a fairly good idea of how the structure will behave prior to generating the FEM. The best source of such insight is usually experience with similar structures. In other words, understanding the load path is crucial in the selection of the appropriate element. A fairly good idea of how the structure will behave permits to avoid incorrect results due to errors or incorrect assumptions in input data preparation. The common element to be used are listed in the table below:

Category	**Spring Elements**	**Line Elements**	**Surface Elements**	**Solid Elements**	**Rigid Elements**
Physical Behavior	Simple Spring	Rod, Bar, Beam	Membrane, Thin Plate	Thick Plate, Brick	Rigid Bar
NASTRAN Element Name	CELAS CBUSH	CROD CBAR CBEAM	CQUAD4 CTRIA3	CHEXA CPENTA CTETRA	RBE2 RBE3
			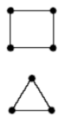	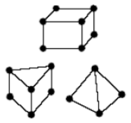	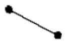

Table 16: Finite elements

It is recommended that when a CELAS element is used, the locations of the two end points be coincident in order to avoid induced significant moment not existing in physical structure. If the two end points are not coincident, CROD or CBUSH elements shall be used instead. If only an axial and/or torsion load is to be transmitted in an element, then the CROD is the easiest element to use. A CBAR is easier to use than a CBEAM element. Use the CBEAM element instead of the CBAR element if any of the following features is important:

- ✈ The cross-sectional properties are tapered.
- ✈ The shear center does not lie on the neutral axis.
- ✈ The effect of cross-sectional warping on torsional stiffness is critical.
- ✈ The difference in the mass center of gravity and the shear center is significant.

In general, quadrilateral elements are preferred over the triangular elements. The CTRIA3 element is excessively stiff, and generally less accurate than the CQUAD4 element, particularly for membrane strain. Whenever feasible, the CQUAD4 element should be used instead of CTRIA3 element which should only be used when necessary for geometric or topological reasons (for example, mesh transition between regions of quadrilateral elements with different mesh densities).

6.1.2 Mesh Density

The mesh density, in a finite element model, is an important topic because of its relationship to accuracy and cost. The number of elements is set by FEM analysis considerations. Global models, like M-346 aircraft structure, are necessary to analyze the structural behavior in terms of internal loads, loads path and stiffness. In general a coarse mesh density guarantees a good results accuracy and time saving. Vice versa, detailed models, necessary to analyze parts of structure in terms of stress/strain or buckling, require a suitable fine mesh.
In this specific study will be used a single global model for both static and instability analysis, whereby the mesh density must be a good compromise between the two cases mentioned. The progressive failure analysis will be applied on the same model but, for future insights, it will be necessary to create detailed models of the most critical areas such as the junctions.

6.2 FEM Loading

In finite element analysis only nodal forces can be applied (pressure and force fields are converted anyway, by the program, into nodal forces with the same resultant). Inevitably this leads to a direct dependence between forces and mesh.
The preliminary design stage of the model involves a continuous updating of the mesh so it would be expensive to change the loading on each iteration. To overcome the problem, saddles and pad-ups can be used, in a similar way to those used in the experimental field. These, modeled through interpolation elements RBE3, easily editable, approximate at the best the trends of the internal actions of distributed load, by means of a limited number of concentrated loads. Figure 33 shows an example of static loading on the VT M-346.

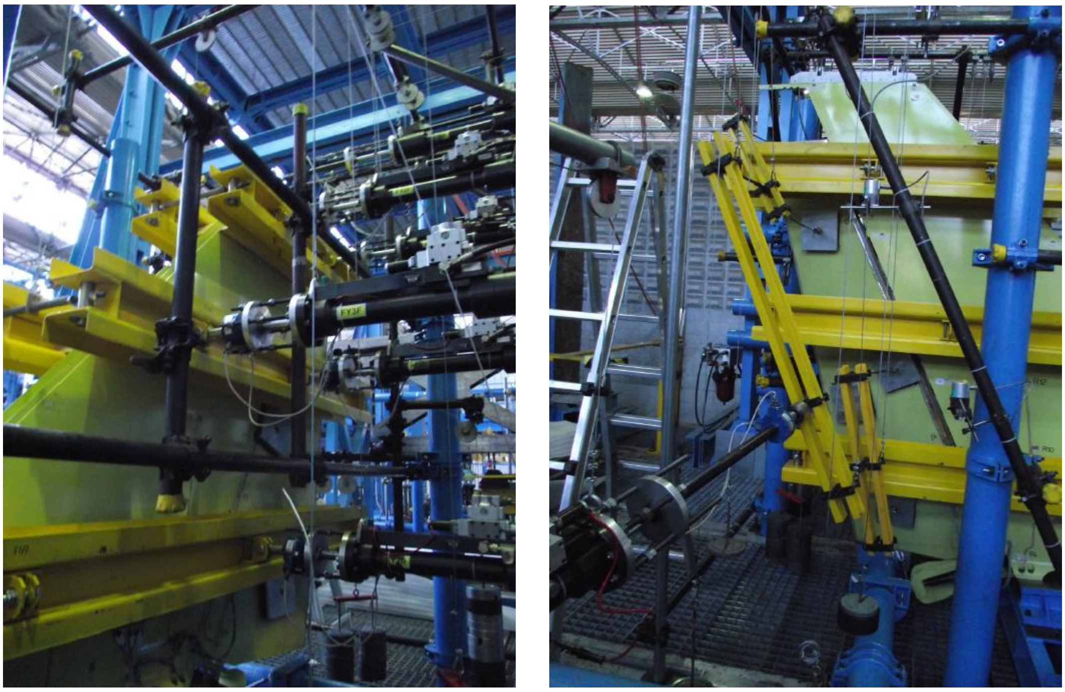

Figure 33: VT loading by mean of saddle and pad-ups

For structures such as the VT the bending moment is the most critical internal action so it must be reproduced as accurately as possible. By varying the load application points also the torque can be approximated accurately while for the shear we have to settle for an average fair value.
For the dimensioning have been provided all available loads, both those distributed and those applied by saddles and pad-ups. In virtue of the foregoing we will proceed with the first dimensioning by means of saddles, and subsequently will be calculated a load distribution suitable for the final finite element model. This will be necessary because an analysis of progressive failure does not permit the use of RBE3.

6.2.1 Test Load Case

The load conditions considered is representative of the VT static test and is the most critical condition in terms of bending moment. Table 17 shows the reaction forces transferred to the fuselage:

Test LC	$F_y\,[N]$	$M_x\,[Nmm]$	$M_z\,[Nmm]$
LL	33205	-36151526	20145515
UL	48807	-54227289	30218272

Table 17: VT static test reaction forces

The term LL indicates the Limit Loads while UL specifies the Ultimate Loads obtained by multiplying the limit loads by a factor of safety of 1.5.
This load condition uses an arrangement of forces with points of application referred to the reference system Coord 360008, which has the x axis laying in the floor plane of the root rib, and the y axis coincident with basic y axis:

origin

$$\begin{bmatrix} 8383. & 0. & 827.469 \end{bmatrix}$$

rotation matrix referred to A/C coordinate system

$$\begin{bmatrix} 0.997 & 0. & -0.074 \\ 0. & 1. & 0. \\ 0.074 & 0. & 0.997 \end{bmatrix}$$

6.2.2 Loading Scheme

In order to reproduce the vertical tail internal forces (shear, bending moment, torque), the aerodynamic and inertial loads will be simulated by means of four saddles on the fin and four pad-ups on the rudder. The loading points are shown in Figure 34 and reported in Table 18. Coordinates have been referred to A/C coordinate system (Coord 0) with rudder at zero deflection.

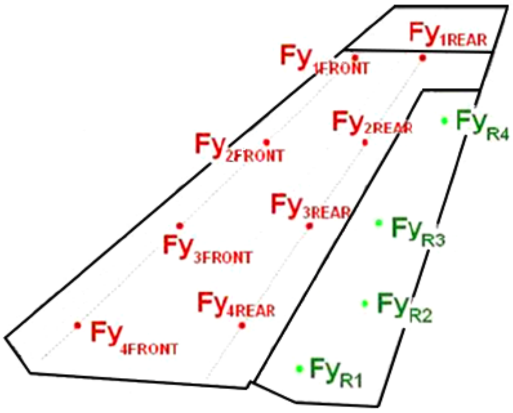

Figure 34: Fin and rudder loading points (csys A/C)

FIN Locations	x [mm]	z [mm]
$F_{y_1\,front}$	10357	3209
$F_{y_1\,rear}$	10730	3209
$F_{y_2\,front}$	9856	2649
$F_{y_2\,rear}$	10403	2649
$F_{y_3\,front}$	9217	1935
$F_{y_3\,rear}$	9986	1935
$F_{y_4\,front}$	8603	1249
$F_{y_4\,rear}$	9585	1249

RUDDER Locations	x [mm]	z [mm]
$F_{y_{R4}}$	10843	2808
$F_{y_{R3}}$	10670	2397
$F_{y_{R2}}$	10453	1516
$F_{y_{R1}}$	10177	966

Table 18: Fin and rudder loading points (csys A/C)

As mentioned earlier these nodes are connected to the aerodynamic surfaces by means of RBE3. In order to transfer only forces but not moments will be constrained only the degrees of freedom U_x, U_y e U_z.

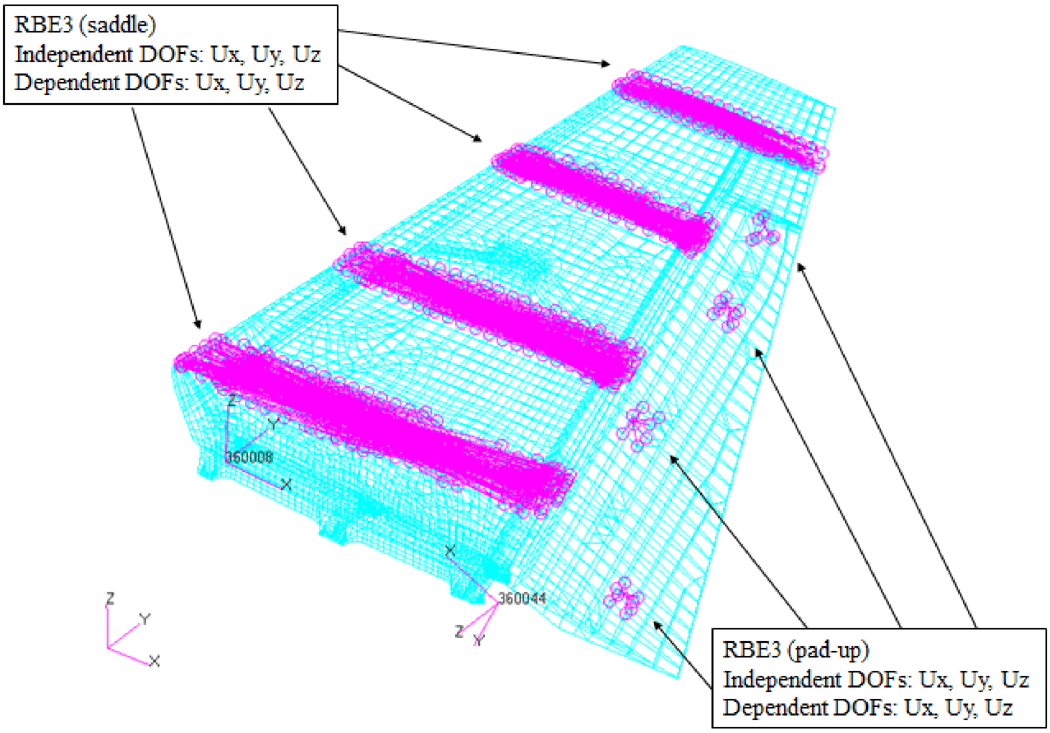
RBE3 (saddle)
Independent DOFs: Ux, Uy, Uz
Dependent DOFs: Ux, Uy, Uz
Z
Y
360008
X
Z
Y
X
X
360044
Z
Y
RBE3 (pad-up)
Independent DOFs: Ux, Uy, Uz
Dependent DOFs: Ux, Uy, Uz

Figure 35: VT saddles and pad-ups

Unlike the RBE2, which simulates an infinitely rigid element which couple a set of nodes/DOFs by enforcing the same amount of motion for each of them, the RBE3 is an interpolation element which defines a linear relationship between nodal DOFs. It distribute the loads upon the corresponding nodes and constrain the displacement of one node (master) by the weighted average of the displacement of the other nodes (slaves). This means that it will not introduce added stiffness to the structure as it happens with the RBE2.

The fin and rudder test force are summarized in Table 19. Force on rudder have non-null components in all of the three aircraft reference direction because of the rotation of the rudder of about 11°.

FIN Test Loads	F_y [N]
$F_{y_1\,front}$	2910
$F_{y_1\,rear}$	3390
$F_{y_2\,front}$	7455
$F_{y_2\,rear}$	4845
$F_{y_3\,front}$	11700
$F_{y_3\,rear}$	0
$F_{y_4\,front}$	12345
$F_{y_4\,rear}$	2355

RUDDER Test Loads	F_x [N]	F_y [N]	F_z [N]
$F_{y_{R4}}$	0	0	0
$F_{y_{R3}}$	255	1473	-128
$F_{y_{R2}}$	333	1914	-163
$F_{y_{R1}}$	461	2651	-230

Table 19: Fin and rudder test loads (Test LC UL)

Thanks to the linearity of the static solution only one analysis will be performed. In particular the analysis will be carried out by applying the UL so the result for the LL will be obtained simply dividing by the safety factor.

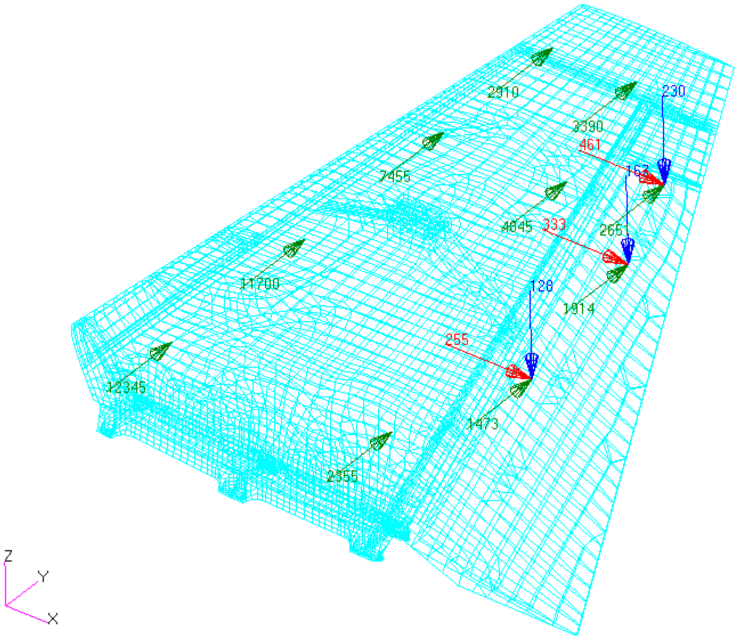
2910
230
3390
461
163
7455
4845
333
265
11700
128
1914
255
12345
1473
2355
Z
Y
X

Figure 36: Fin and rudder test loads (Test LC UL)

6.2.3 Internal Forces Comparison

The comparison between theoretical loads (static analysis) and test loads of the fin (in term of shear F_y , bending M_x and torque M_z) have been carried out in the A/C reference frame (Coord 0) using the current finite element models. The results are shown in the following figure:

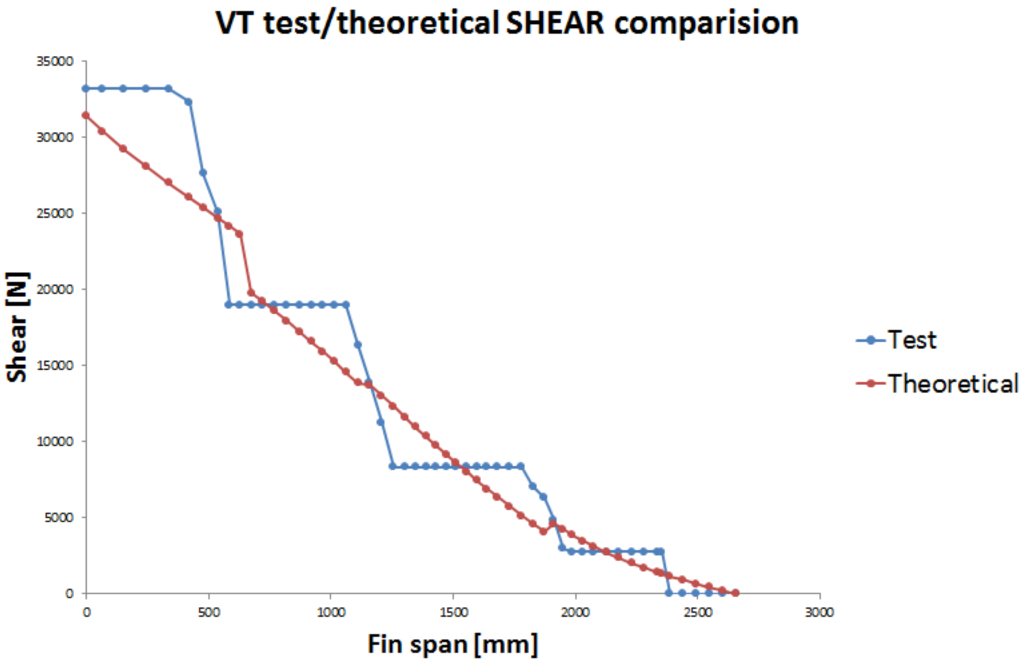

Figure 37: VT test/theoretical SHEAR comparison

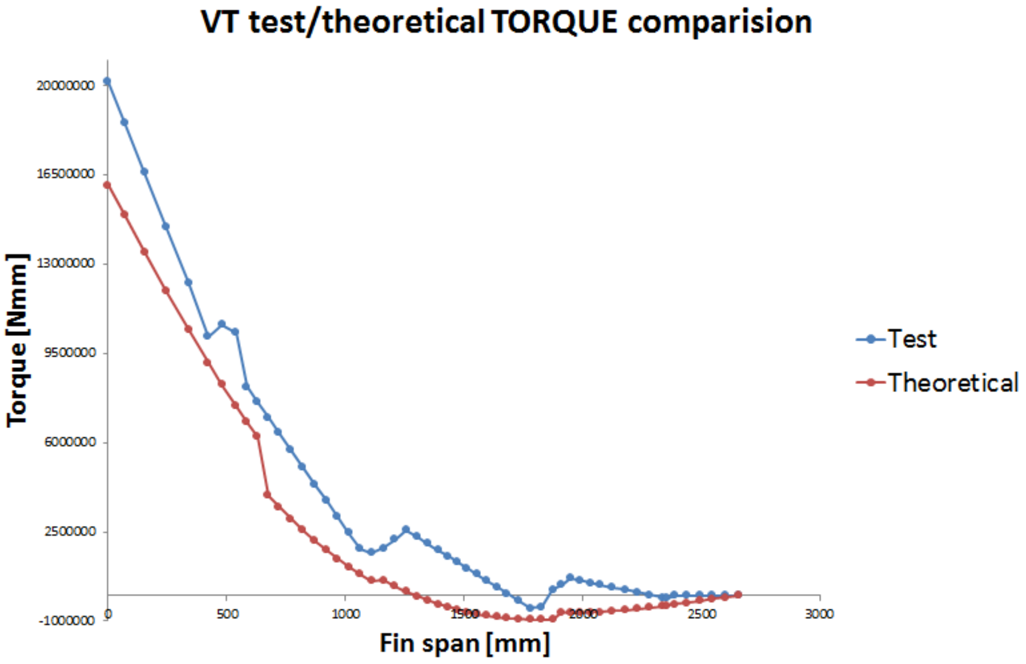

Figure 38: VT test/theoretical TORQUE comparison

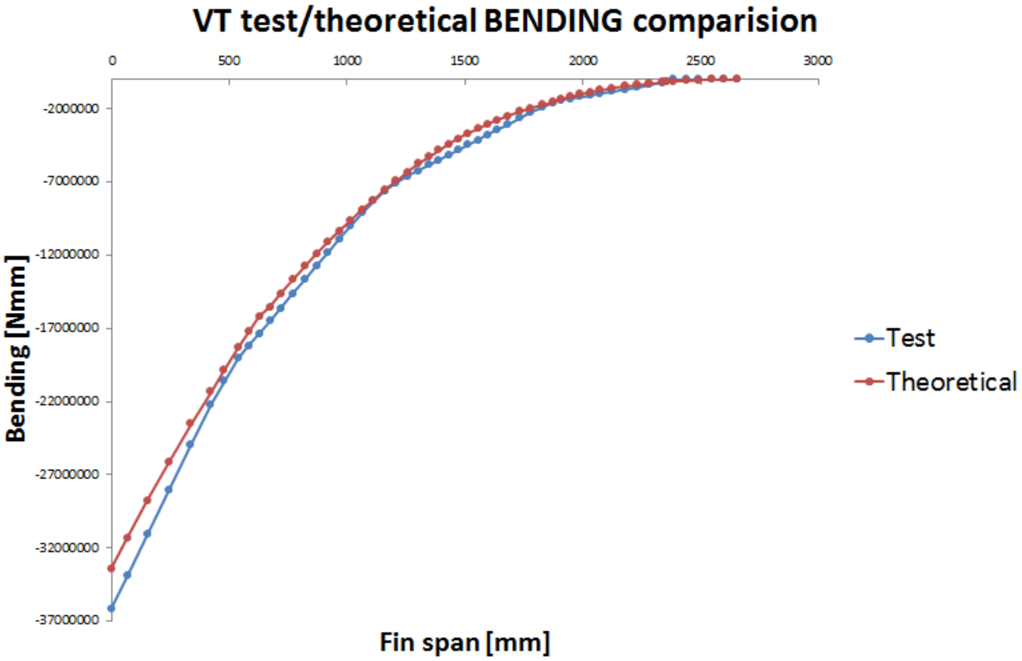

Figure 39: VT test/theoretical BENDING comparison

It may be noted as said before, namely that the bending moment is more burdensome internal action and that it has been accurately reproduced.

6.3 FEM Constraints

The connection fin/fuselage will be modeled by means of RBE2 whose constrained DOFs will be defined in the local coordinate system (Coord 360008).

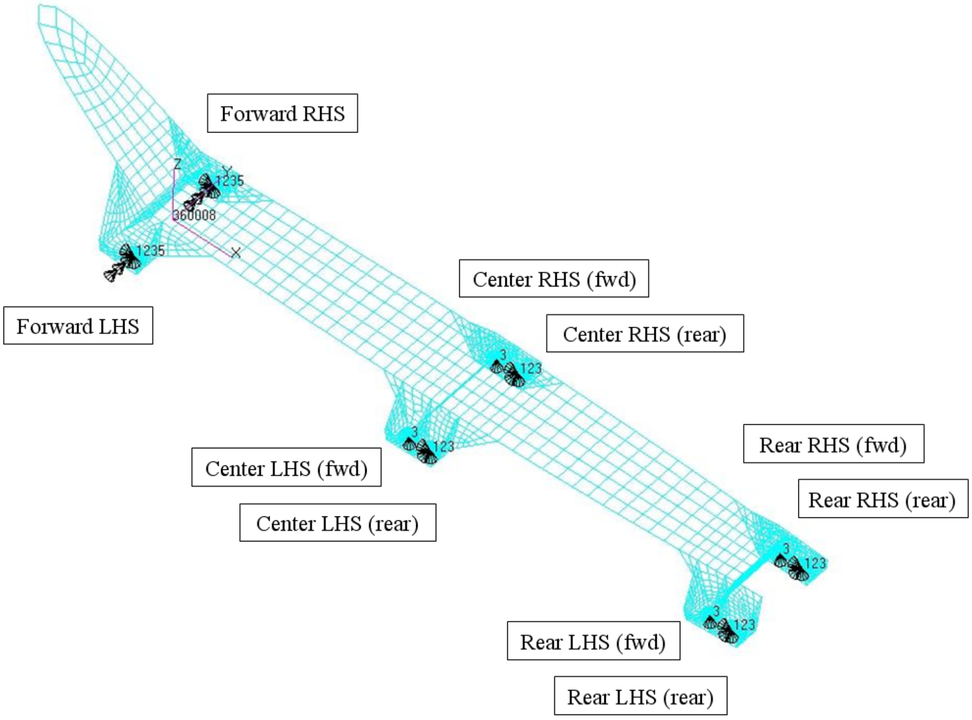
Forward RHS
Forward LHS
1235
1235
360008
Z
Y
X
Center RHS (fwd)
Center RHS (rear)
3
123
Center LHS (fwd)
Center LHS (rear)
3
123
Rear RHS (fwd)
Rear RHS (rear)
3
123
Rear LHS (fwd)
Rear LHS (rear)
3
123

Figure 40: Connection to fuselage

The following table shows the NASTRAN card of SPC.

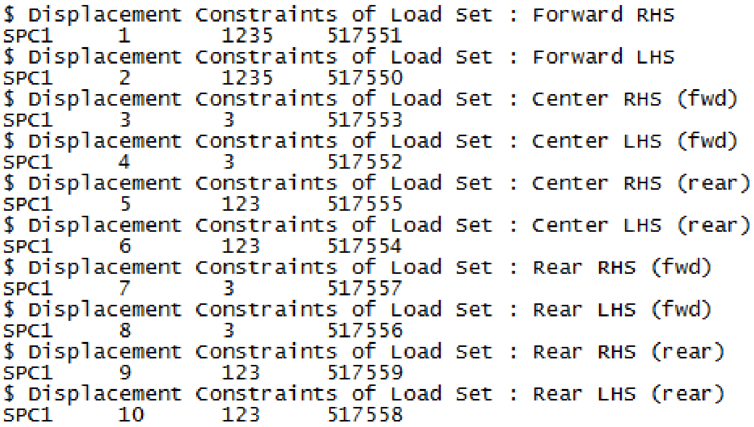

```
$ Displacement Constraints of Load Set : Forward RHS
SPC1     1       1235    517551
$ Displacement Constraints of Load Set : Forward LHS
SPC1     2       1235    517550
$ Displacement Constraints of Load Set : Center RHS (fwd)
SPC1     3       3       517553
$ Displacement Constraints of Load Set : Center LHS (fwd)
SPC1     4       3       517552
$ Displacement Constraints of Load Set : Center RHS (rear)
SPC1     5       123     517555
$ Displacement Constraints of Load Set : Center LHS (rear)
SPC1     6       123     517554
$ Displacement Constraints of Load Set : Rear RHS (fwd)
SPC1     7       3       517557
$ Displacement Constraints of Load Set : Rear LHS (fwd)
SPC1     8       3       517556
$ Displacement Constraints of Load Set : Rear RHS (rear)
SPC1     9       123     517559
$ Displacement Constraints of Load Set : Rear LHS (rear)
SPC1     10      123     517558
```

Table 20: Single Point Constraint

It can be seen how the constraints (fwd) block only the DOF 3 while the constraints (rear) block also the DOFs 1,2. This is because, in order to avoid hyperstaticity, the tolerances of the rear holes are deliberately tighter than the front ones.

The interface fin/rudder is realized through three hinges, each consisting of a RBE3 and a RBE2 connected to each other by means of an element CELAS, as shown in Figure 41. The constrained DOFs are defined in a local coordinate system (Coord 360044), where the y axis coincides with the hinge axis of the rudder and the axes x, y lie in the plane of symmetry.

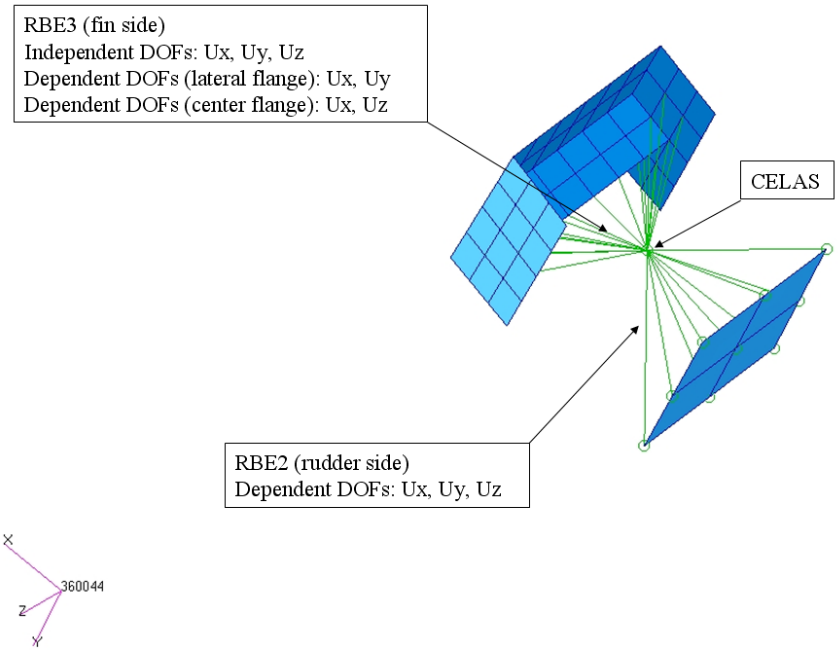
RBE3 (fin side)
Independent DOFs: Ux, Uy, Uz
Dependent DOFs (lateral flange): Ux, Uy
Dependent DOFs (center flange): Ux, Uz
CELAS
RBE2 (rudder side)
Dependent DOFs: Ux, Uy, Uz
X
360044
Z
Y

Figure 41: Hinges

6.4 Nodal Displacements

A further verification of the model can be done by comparing its displacements with those obtained in the test. Since there are no nodes in the corresponding positions the displacements are recovered by introducing RBE3 positioned in correspondence of the transducers. During the test a total of 12 transducer were fitted to the vertical tail left skin. Their position is reported in the following table and refers to the A/C coordinate system.

Transducers Location		x [mm]	y [mm]	z [mm]
Leading Edge	1	8389	-66.29	908
	3	8762	-57.32	1346
	5	9134	-48.34	1784
	7	9507	-39.35	2221
	9	9880	-30.37	2660
	11	10253	-21.39	3094
Trailing Edge	2	9555	-57.68	821
	4	9829	-49.39	1346
	6	10057	-42.39	1784
	8	10287	-35.43	2221
	10	10515	-28.47	2660
	12	10742	-21.57	3094

Table 21: Transducers application points

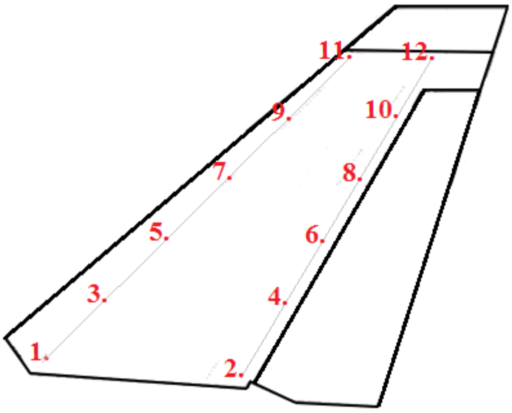

Figure 42: Transducers application points

Displacements are obtained as difference between the position of the 12 nodes in the undeformed and deformed configurations. Obviously, the displacement is given in its three components x, y, z therefore, to derive the axial action measured by the trasducers, it would be necessary to calculate the resulting displacement. However, displacements in the direction x and y are negligible compared to those in the z direction, for which it will be used only the latter without committing significant errors.

6.5 Verification Procedure

After defining the model, it is necessary to check if it will produce reliable results. In subsection 10.3 will be listed some of the methods used to verify the quality of the model.

7 Vertical Tail Current Design

The fin is mainly a metallic honeycomb panel, close in the upper side by the top rib, in the lower part by the two halves of the root rib (connected together by doublers, splice and spar webs), in the rear part by the rear spar and in the front part by the front spar. The skin is connected to the root rib flanges by fastener groups and it is also joined to the spars and to the top rib by joints in line all along its boundary.

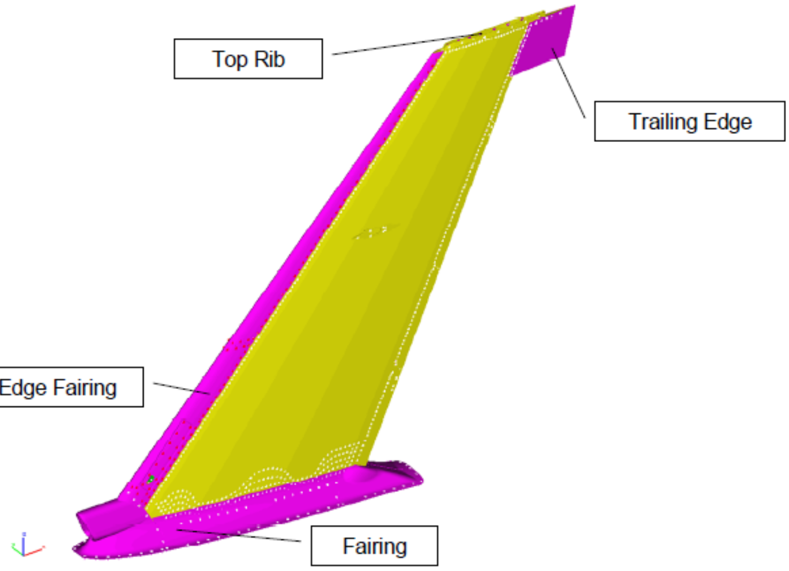
Top Rib
Trailing Edge
Leading Edge Fairing
Fairing

Figure 43: Fin box assembly

The root rib provides the connection with three frame of the rear fuselage by means of 10 bolts, and with the rudder mount by means of 4 bolts, as shown in the following figure.

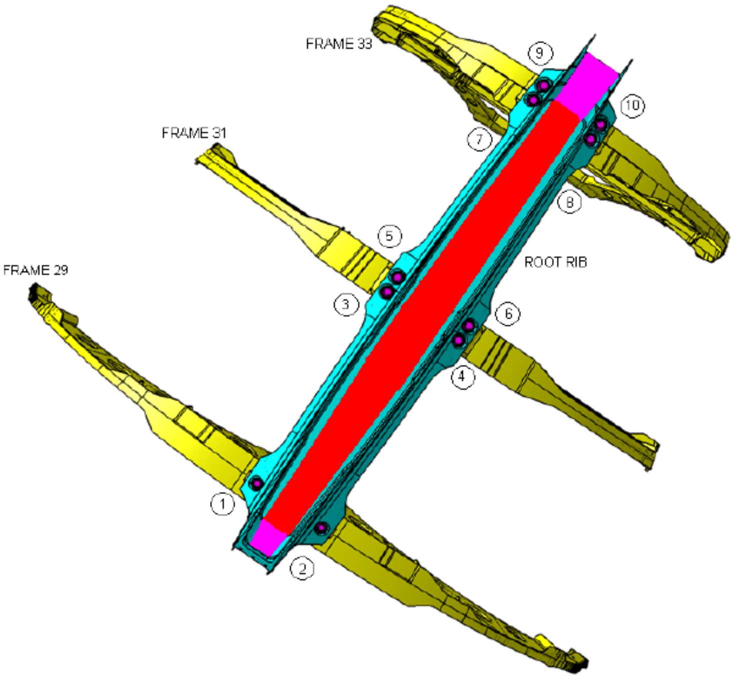
FRAME 33
FRAME 31
FRAME 29
ROOT RIB
⑨
⑩
⑦
⑧
⑤
③
⑥
④
①
②

Figure 44: Root rib to rear fuselage connection

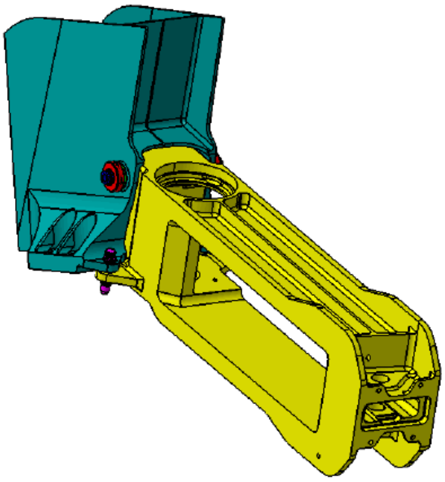

Figure 45: Root rib to VT rudder mount connection

The rear spar provides the connection with the rudder by means of three hinges.

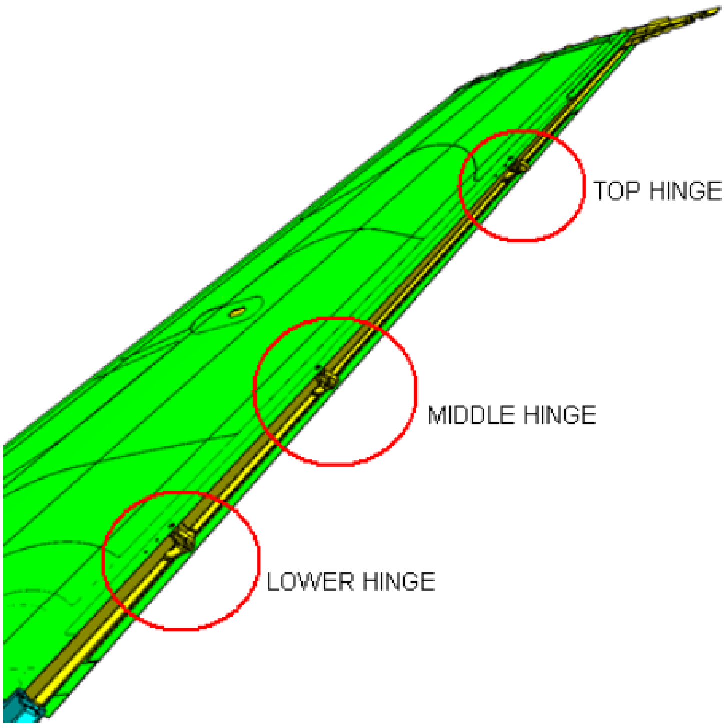

Figure 46: Rudder connection

The skin is made of Alluminium Alloy 7475 T761 with variable thickness obtained by chemical milling. The inner area is filled with the metal honeycomb composed by four different component of different density, starting from a more dense near the root, up to a less dense towards the end (the hole in the center is necessary for the attachment of the ILS antenna). In the following pictures is possible to see the thickness distribution of the skin and the density in the honeycomb respectively.

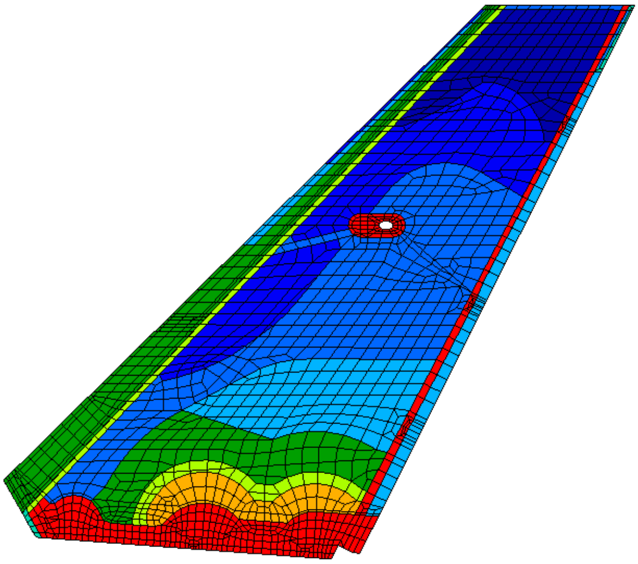

Figure 47: Skin thickness distribution

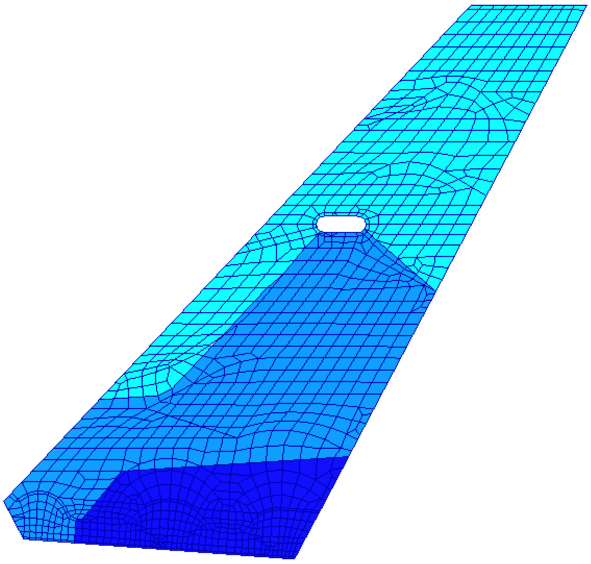

Figure 48: Fin honeycomb core components

The leading edge is a solid laminate made of layers of aramid fiber and epoxy resin and it is connected to the fin main structure through the front spar.

7.1 Parameters of Interest

In this section, have been gathered all the necessary data for comparison with the models in CFC that will be created later. The first reference value is the FEM[1] weight of the VT. The second value is the maximum deflection, calculated at ends of the fin for the ultimate load, whose deformation is shown in Figure 49. As already specified the exact values of weight and displacement can not be reported due to business secret, therefore they will be indicated as a percentage value of 100%.

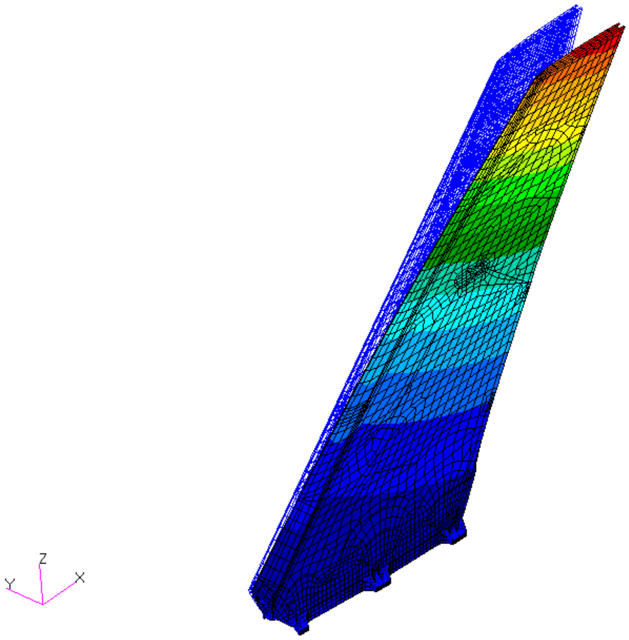

Figure 49: Current model deformed: maximum deflection 100%

Lastly, will be taken as reference the readings provided by the trasducers (see sub 6.4). All the displacement are reported in function of the maximum deflection.

Trasducers		Δy
Leading Edge	1	1.6%
	3	7.6%
	5	17.8%
	7	35.3%
	9	59.0%
	11	86.8%
Trailing Edge	2	3.2%
	4	14.0%
	6	27.4%
	8	46.6%
	10	69.8%
	12	95.8%

Table 22: Current model: trasducers displacements

---

[1] The FEM weight is different from the real weight as in the model are not considered the elements such as bolts or rivets, the fittings between the surfaces, etc.. Usually the FEM weight is lower than the real one.

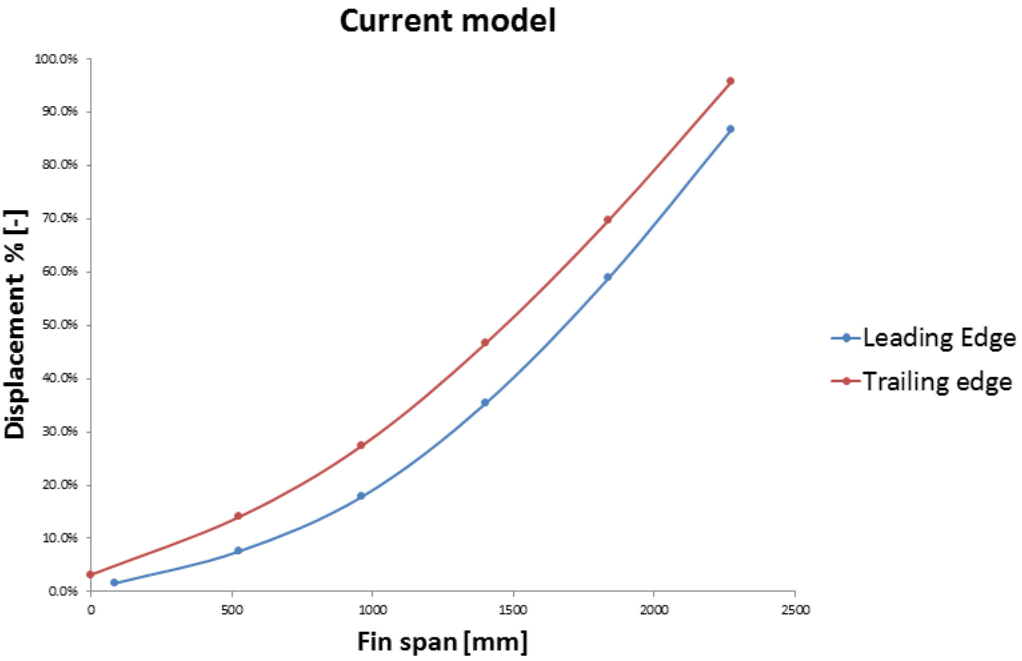

Figure 50: Current model: trasducers displacements

8 New Possible Design

The choice of the new internal configuration of the vertical tail had as a prerequisite the possibility of realization of the structure with established technologies. To define some plausible designs has been made a research in which have been compared different configurations of several aircraft. The most common configurations are two: a single full-sandwich structure such as that adopted in the current configuration and a structure mainly composed of ribs and spars.

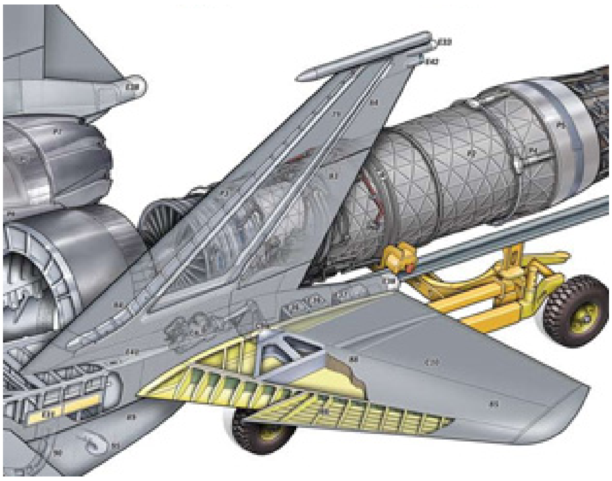

Figure 51: Boeing F15 Silent Eagle

The main problem of the first type of structure is the possibility of an extended unstuck which can lead to the complete detachment of one of the two skins. On the other hand this type of structures are hardly subject to the phenomena of instability.

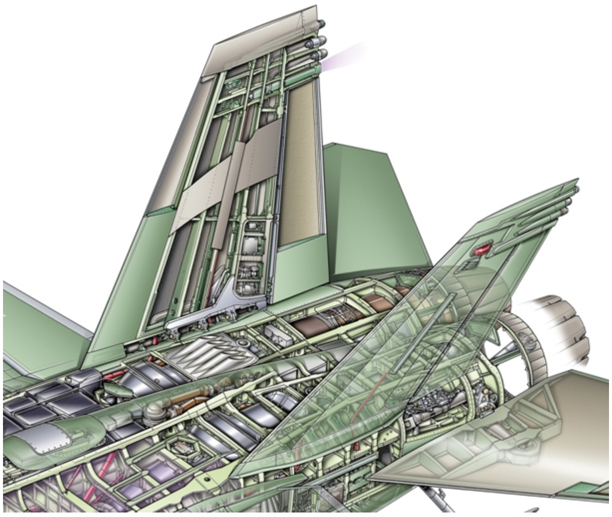

Figure 52: Boeing EA-18G Growler

The structure of the second type are very light with excellent performance but easily subjected to buckling.
There are also other configurations in which there is a large number of stringers such as the VT of the Eurofighter.

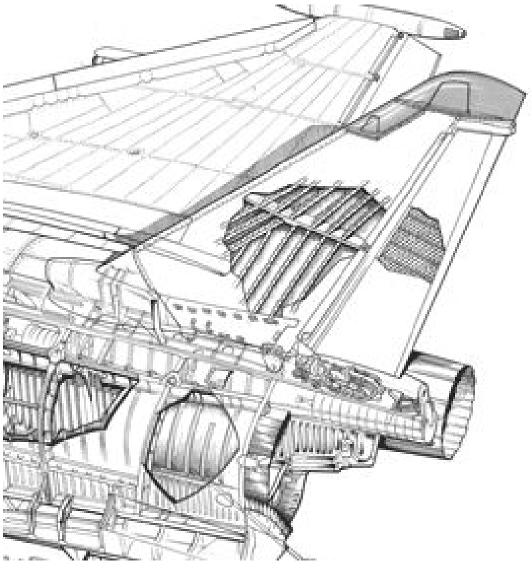

Figure 53: Eurofighter Typhoon

According to what was seen will be studied two configurations similar to those mentioned above but with some changes:

- a full-sandwich structure with in addition a certain number of ribs, both to transfer the load from the rudder both to limit the phenomenon of ungluing
- a structure with many longitudinal members but without ribs. In their place, to limit the buckling of the panels, will be used the stringers which at the same time increase the global stiffness of the structure

9 Materials

The structure of the M-346 is composed by different materials, metallic and non-metallic, modeled in NASTRAN by cards MAT1 and MAT8.

In the following paragraphs will be shown the properties of composites and metals that will be used in the design of the Vertical Tail. These properties are enclosed in an AAEM program which collects data of all the materials described in the Military Handbook (MIL-HDBK-H5) and calculate the allowable values at different temperatures using the variation laws of of the parameters.

9.1 Metallic Materials

The metallic material allowable values are strongly influenced by the size of the raw, from which is extracted the machined part by mechanical milling. This is because the residual stresses, generated during the thermal treatments, knock down the mechanical properties of the material, as the thickness increases.

The root's constraints are composed by two symmetrical parts, jointed together during the assembly phase. This allows to obtain the machined part from less thick raw material with better properties.

9.1.1 Aluminium Alloy 7050 T7451

The 7050 is a lightweight aluminum alloy composed by Al-Zn-Mg-Cu-Zr and density equal to 2823 kg/m^3. It has been developed to have a good combination of high allowable stress, high corrosion resistance and good toughness. The words T7451 refers to a type of tempering that provides the largest high corrosion resistance for this alloy.

The mechanical properties of the raw, from which are derived the rudder's hinges are shown in Table 23:

Al 7050 T7451 Raw Thickness 1.5-2.0 inch Specification AMS 4050		**Temperature** **RT** **[MPa]**	**TRF** **/**	**90 °C** **[MPa]**
Tensile Elastic Modulus	E_T	71016	0.952	67607
Compressive Elastic Modulus	E_C	73084	0.952	69576
Shear Modulus	G	26890	0.952	25599
Ultimate Tensile Strength	σ_T^U	510	0.849	433
Yield Tensile Strength	σ_T^Y	441	0.932	411
Yield Compressive Strength	σ_C^Y	427	0.941	402
Ultimate Shear Strength	σ_S^U	296	0.982	291
Yield Shear Strength	σ_S^Y	255	0.982	251
Ultimate Bearing Strength	σ_B^U	883	0.877	774
Yield Bearing Strength	σ_B^Y	648	0.963	624

Table 23: Aluminium alloy 7050 T7451 (1.5-2.0 inch)

In the table above is possible to note a column labeled RT (Room Temperature) which indicates the value of the allowable values at an ambient temperature of 20 °C. These are then multiplied to the TRF (Temperature Reduction Factor) to take into account a maximum operating temperature of the VT at 90 °C.

The mechanical properties of the raw, from which are derived the connections with the fuselage are shown in Table 24:

Al 7050 T7451		**Temperature**		
Raw Thickness 5.0-6.0 inch		**RT**	**TRF**	**90 °C**
Specification AMS 4050		[MPa]	/	[MPa]
Tensile Elastic Modulus	E_T	71016	0.952	67607
Compressive Elastic Modulus	E_C	73084	0.952	69576
Shear Modulus	G	26890	0.952	25599
Ultimate Tensile Strength	σ_T^U	483	0.849	410
Yield Tensile Strength	σ_T^Y	414	0.932	386
Yield Compressive Strength	σ_C^Y	393	0.941	370
Ultimate Shear Strength	σ_S^U	296	0.982	291
Yield Shear Strength	σ_S^Y	234	0.982	230
Ultimate Bearing Strength	σ_B^U	945	0.877	828
Yield Bearing Strength	σ_B^Y	724	0.963	697

Table 24: Aluminium alloy 7050 T7451 (5.0-6.0 inch)

9.1.2 Calculation Methods for Metals

To define the calculation methods for metal are considered the following norms:

> JAR 23.301 - Loads
>
> (a) Strength requirements are specified in term of limit loads (the maximum load to be expected in service) and ultimate loads (limit load multiplied by prescribed factor of safety).
>
> JAR 23.305 - Strength and Deformation
>
> (a) The structure must be able to support limit load without detrimental, permanent deformation. At any load up to limit loads, the deformation may not interfere with safe operation.
>
> (b) The structure must be able to support ultimate load without failure for at least three seconds, except for local failures or structural instabilities between limit and ultimate load are acceptable only if the structure can sustain the require ultimate load for at least three seconds.

The metallic material shall be considered failed if the maximum Von Mises stress exceed the yield strength, in limit load conditions, or exceed the ultimate strength, in ultimate load conditions. In general is defined the margin of safety as follow:

$$MS = \left(\frac{Allowable\,Load}{Applied\,Load} \right) - 1 \geq 0$$

In this particular case the margins of safety are:

$$\begin{aligned} MS_{LL} &= \frac{\sigma^Y}{\sigma_{VM}^{max}} - 1 \\ MS_{UL} &= \frac{\sigma^U}{\sigma_{VM}^{max}} - 1 \end{aligned}$$

9.2 Composite Materials

For the design of the Vertical Tail it has been decided to use only unidirectional tape. This choice is due to their better performance compared to the fabrics and the possibility of automating the production process.

Although unidirectional tapes have low drapability, the slight curvature of the skins of the VT allows to use the Automated Tape Layup (ATL), which is the robotic placement of prepreg composite strips. ATL machines have developed a refined process capable of repeated automated production with low waste and a high level of quality control therefore, when possible, are to be preferred to manual labor.

The allowable values will be considered in a condition of 100 °C/wet, as provided in the bibliography and conservative compared to the operating conditions (90 °C).

9.2.1 Hexcel 8552/IM7 Unidirectional Tape

Hexcel 8552/IM7 is an amine cured, toughened epoxy resin system supplied with carbon fibers and density equal to 1583 kg/m^3. It is recommended for structural applications requiring high strength, stiffness, and damage tolerance.
The mechanical properties of the prepreg unidirectional tape are shown in Table :

Material Properties	**Values** [**MPa**]	
Longitudinal Young's Modulus	E_{xx}	155000
Transverse Young's Modulus	E_{yy}	8400
In-Plane Shear Modulus	G_{xy}	3200
Out-of-Plane Shear Modulus	G_{yz}	3200
Out-of-Plane Shear Modulus	G_{xz}	3200
Interlaminar Strength	S_B	56
Longitudinal Tensile Strength	X_σ^T	2200
Longitudinal Compression Strength	X_σ^C	1100
Transverse Tensile Strength	Y_σ^C	25
Transverse Compression Strength	Y_σ^C	140
In-Plane Shear Strength	S_τ	76

Table 25: Hexcel 8552/IM7 Unidirectional Tape

It is possible to notice how the unidirectional composite works very well along the direction of the fibers, while has very low characteristics in the transverse direction, even two orders of magnitude less. This is because the only task of the matrix is to transfer the loads to the fibers and not to bear them.
The strain allowable values are obtained by dividing the strength allowable values by the elastic modulus for that component:

$$X_\varepsilon^T = \frac{X_\sigma^T}{E_{xx}} = 0.014$$

$$X_\varepsilon^C = \frac{X_\sigma^C}{E_{xx}} = 0.007$$

$$Y_\varepsilon^T = \frac{Y_\sigma^T}{E_{yy}} = 0.003$$

$$Y_\varepsilon^C = \frac{Y_\sigma^C}{E_{yy}} = 0.017$$

$$S_\varepsilon = \frac{S_\tau}{G_{xy}} = 0.0238$$

The following hypotheses have been made:

- the tensile and compressive elastic moduli are the same
- the shear modulus are the same, $G_{xy} = G_{xz} = G_{yz}$

Due to damage tolerance consideration the fiber strain allowable values are usually limited below typical values here reported:

- pure tension strain is limited to $5500\,\mu\varepsilon$
- pure bending strains are limited to $\pm 5500\,\mu\varepsilon$
- in-plane shear strains are limited to $10000\,\mu\varepsilon$
- for thin skin on honeycomb, core compression strains are limited to $2600\,\mu\varepsilon$
- pure compression strain are limited, as shown in Figure 54 depending on the laminate thickness and the impact energy. For simplicity, while remaining conservative, will be considered an impact energy of $20\,J$.

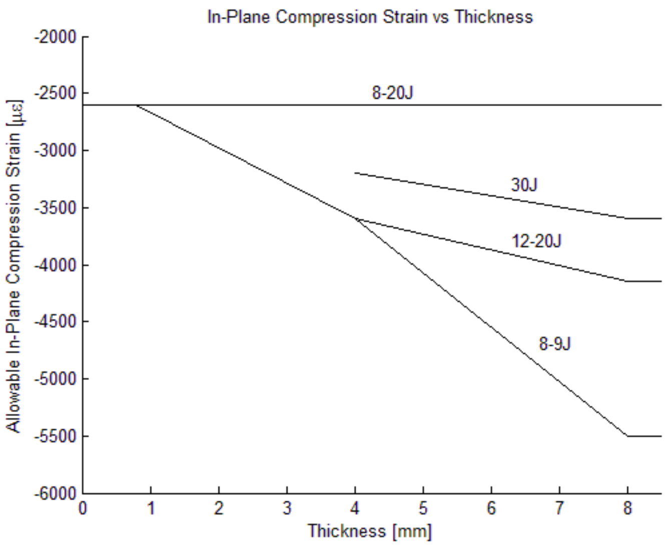

Figure 54: Typical compression strain allowable values as a function of the impact energy

As the case are used higher allowable values in transverse direction where the experimental evidence has shown to be too conservative (for example in laminates fiber-dominated).

9.2.2 Calculation Methods for Laminates

The laminate shall be considered failed, when the First Ply Failure occurs (i.e. matrix failure or fiber failure, whatever is least). The failure modes of a unidirectional composite lamina include:

- ✈ axial failure, dominated by the fiber
- ✈ transverse failure, dominated by the matrix
- ✈ shear failure, dominated by the matrix

Among the various failure criteria will be taken into account the maximum strain criteria. A critical assumption of this criterion is that the laminate behavior is fiber-dominated.

Maximum Strain Criteria It decrees the failure of a lamina, under plane stress, if one of the following relations is satisfied:

$$\varepsilon_x \geq X_\varepsilon^T \text{ o } |\varepsilon_x| \geq X_\varepsilon^C \quad \text{fiber failure}$$

$$\varepsilon_y \geq Y_\varepsilon^T \text{ o } |\varepsilon_y| \geq Y_\varepsilon^C \quad \text{matrix failure}$$

$$|\gamma_{xy}| \geq S_\varepsilon \quad \text{shear failure}$$

$$\tau_{xz} \geq S_B \text{ o } \tau_{yz} \geq S_B \quad \text{interlaminar shear}$$

The absolute value of γ_{12} indicates that the sign of the shear does not influence the criterion.

X_ε^T, X_ε^C	tensile and compression strain allowable values, in the plane of the lamina, in the fiber direction
Y_ε^T, Y_ε^C	tensile and compression strain allowable values, in the plane of the lamina, in transverse direction
S_ε	shear strain allowable in the plane of the lamina

S_B inter-laminar strength allowable[2]

The strain allowable values are defined in NASTRAN through the card MAT8 while the allowable stress is specified in the PCOMPG. Not considering the interaction between the failure modes leads to the simultaneous verification of the four distinct sub-criteria. This is done by means of the Failure Index:

$$Failure\ Index = max\left(\frac{\varepsilon_x}{X_\varepsilon^T}, \frac{\varepsilon_x}{X_\varepsilon^C}, \frac{\varepsilon_y}{Y_\varepsilon^T}, \frac{\varepsilon_y}{Y_\varepsilon^C}, \left|\frac{\gamma_{xy}}{S_\varepsilon}\right|, \frac{\tau_{xz}}{S_B}, \frac{\tau_{yz}}{S_B}\right)$$

The Margin of Safety is calculate as:

$$MS = \left(\frac{Allowable\, Load}{Applied\, Load}\right) - 1 = \frac{1}{FI} - 1$$

In order that there is no failure, the MS must be greater than or equal to zero, or the FI must be less than unity.

9.2.3 Laminate Design

The lamination of composite parts should meet the following criteria:

- The stacking sequence should be symmetrical; this is because a non-symmetrical laminate presents a coupling between the contraction (due to cooling at the end of the production phase) and the flexion, making difficult the production of panels with the desired curvature. Deviation from the symmetry criterion should be restricted to small areas.
- The laminate should be fiber-dominated meaning that there are fibers in sufficient multiple direction such that strain are limited by the presence of the fiber to inhibit matrix cracking.
- The laminate should be “balanced” that is, equal number of layers with opposite orientation (e.g. equal numbers of ±45° layers).
- The angle between two stacked plies has to be small as possible to reduce inter-laminar stresses

  $$0°/+45°/90°/-45°|-45°/90°/+45°/0°$$
  is better than
  $$0°/+45°/-45°/90°|90°/-45°/+45°/0°$$
- When rivets or bolted joints are involved, the laminate should mainly consist of about 50% of ±45° layers to have high bearing strength.
- The number of adjacent layers with the same fiber orientation angles should not exceed three layers of fabric or six layers of tape in order to inhibit matrix macro-cracking. Their combined thickness should not exceed 0.84 mm.
- The number of dropped layers per thickness step should not exceed three layers of fabric or six layers of tape. Furthermore the thickness step should fall below the minimum value between 0.84 mm and the 20% of the lower thickness.
  Note: surface layers should not be dropped in order to minimize the inter-laminar stress concentration at the fiber ends.
- The distance between two thickness steps should not be less than 0.5 inch.
- The minimum laminate thickness should not be lower than 0.8 mm in order to provide sufficient handling strength during manufacturing and assembly.

The face sheet of sandwich parts should additionally meet the following criteria:

- The number of layers per face should not fall below two layers of fabric or four layers of tape.
- Each of the two face sheets should be stacked symmetrically.

---

[2] The need to introduce a term of stress in a strain criterion is due to the intrinsic properties of the shell elements, which are indeformable out of the plane

9.2.4 Lamination Sequences

To simplify the design phase of the model, were created lamination sequences, for different thickness step, both for components subject to shear and torsion as ribs and spars webs, both for the elements subject to bending and axial force as skins, spars caps and stringers. In the following figures are reported the laminates used which meet all the requirements listed in the previous subsection.

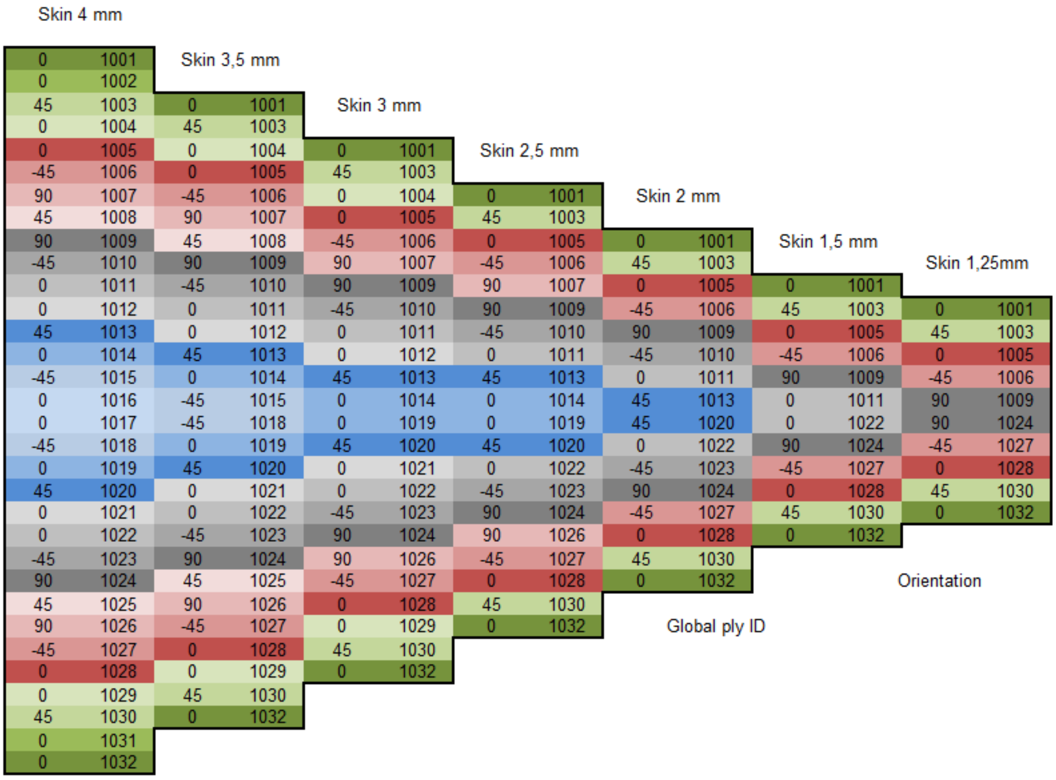

Skin 4 mm	
0	1001
0	1002
45	1003
0	1004
0	1005
-45	1006
90	1007
45	1008
90	1009
-45	1010
0	1011
0	1012
45	1013
0	1014
-45	1015
0	1016
0	1017
-45	1018
0	1019
45	1020
0	1021
0	1022
-45	1023
90	1024
45	1025
90	1026
-45	1027
0	1028
0	1029
45	1030
0	1031
0	1032

Skin 3,5 mm	
0	1001
45	1003
0	1004
0	1005
-45	1006
90	1007
45	1008
90	1009
-45	1010
0	1011
0	1012
45	1013
0	1014
-45	1015
-45	1018
0	1019
45	1020
0	1021
0	1022
-45	1023
90	1024
45	1025
90	1026
-45	1027
0	1028
0	1029
45	1030
0	1032

Skin 3 mm	
0	1001
45	1003
0	1004
0	1005
-45	1006
90	1007
90	1009
-45	1010
0	1011
0	1012
45	1013
0	1014
0	1019
45	1020
0	1021
0	1022
-45	1023
90	1024
90	1026
-45	1027
0	1028
0	1029
45	1030
0	1032

Skin 2,5 mm	
0	1001
45	1003
0	1005
-45	1006
90	1007
90	1009
-45	1010
0	1011
45	1013
0	1014
0	1019
45	1020
0	1022
-45	1023
90	1024
90	1026
-45	1027
0	1028
45	1030
0	1032

Skin 2 mm	
0	1001
45	1003
0	1005
-45	1006
90	1009
-45	1010
0	1011
45	1013
45	1020
0	1022
-45	1023
90	1024
-45	1027
0	1028
45	1030
0	1032

Skin 1,5 mm	
0	1001
45	1003
0	1005
-45	1006
90	1009
0	1011
0	1022
90	1024
-45	1027
0	1028
45	1030
0	1032

Skin 1,25mm	
0	1001
45	1003
0	1005
-45	1006
90	1009
90	1024
-45	1027
0	1028
45	1030
0	1032

Figure 55: Skins, spars caps and stringers lamination sequences

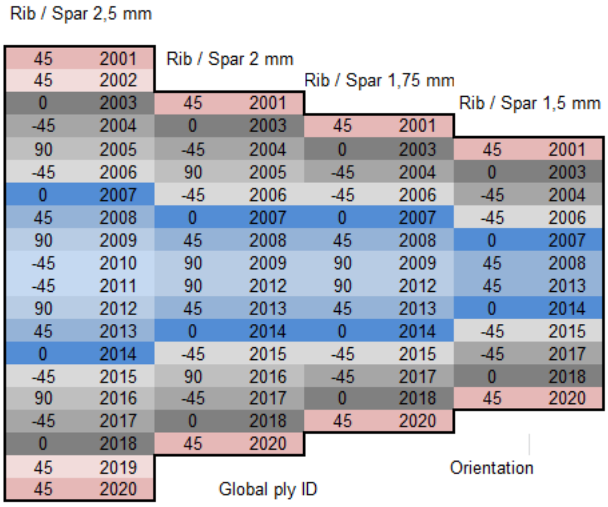

Rib / Spar 2,5 mm	
45	2001
45	2002
0	2003
-45	2004
90	2005
-45	2006
0	2007
45	2008
90	2009
-45	2010
-45	2011
90	2012
45	2013
0	2014
-45	2015
90	2016
-45	2017
0	2018
45	2019
45	2020

Rib / Spar 2 mm	
45	2001
0	2003
-45	2004
90	2005
-45	2006
0	2007
45	2008
90	2009
90	2012
45	2013
0	2014
-45	2015
90	2016
-45	2017
0	2018
45	2020

Rib / Spar 1,75 mm	
45	2001
0	2003
-45	2004
-45	2006
0	2007
45	2008
90	2009
90	2012
45	2013
0	2014
-45	2015
-45	2017
0	2018
45	2020

Rib / Spar 1,5 mm	
45	2001
0	2003
-45	2004
-45	2006
0	2007
45	2008
45	2013
0	2014
-45	2015
-45	2017
0	2018
45	2020

Figure 56: Ribs and spars webs lamination sequences

The first value refers to the orientation of the fibers while the second is the ID of the lamina

9.3 Honeycomb

During the design will also be used as filler an aramid fiber/phenolic resin honeycomb called HRH-10. This type of material provides a significant increase in stiffness for sandwich structures with a minimum increase of weight. Its main function is to keep the skins in composite material at the right distance and stabilize them.

9.3.1 Non Metallic Honeycomb HRH10 - Nomex

The mechanical properties of the aramid fiber filler are shown in the following table, in which have been put in evidence the two types considered for the current project:

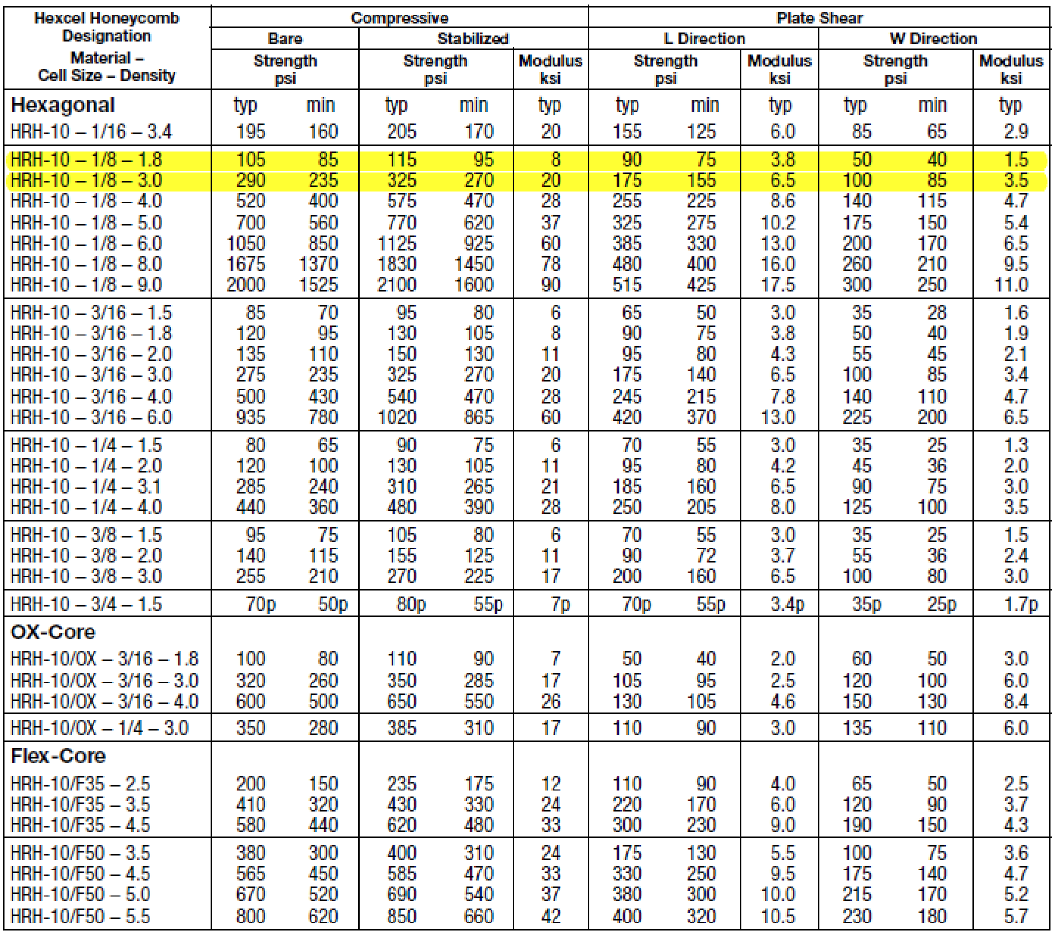

Hexcel Honeycomb Designation Material – Cell Size – Density	Compressive					Plate Shear					
	Bare		Stabilized			L Direction			W Direction		
	Strength psi		Strength psi		Modulus ksi	Strength psi		Modulus ksi	Strength psi		Modulus ksi
Hexagonal	typ	min	typ	min	typ	typ	min	typ	typ	min	typ
HRH-10 – 1/16 – 3.4	195	160	205	170	20	155	125	6.0	85	65	2.9
HRH-10 – 1/8 – 1.8	105	85	115	95	8	90	75	3.8	50	40	1.5
HRH-10 – 1/8 – 3.0	290	235	325	270	20	175	155	6.5	100	85	3.5
HRH-10 – 1/8 – 4.0	520	400	575	470	28	255	225	8.6	140	115	4.7
HRH-10 – 1/8 – 5.0	700	560	770	620	37	325	275	10.2	175	150	5.4
HRH-10 – 1/8 – 6.0	1050	850	1125	925	60	385	330	13.0	200	170	6.5
HRH-10 – 1/8 – 8.0	1675	1370	1830	1450	78	480	400	16.0	260	210	9.5
HRH-10 – 1/8 – 9.0	2000	1525	2100	1600	90	515	425	17.5	300	250	11.0
HRH-10 – 3/16 – 1.5	85	70	95	80	6	65	50	3.0	35	28	1.6
HRH-10 – 3/16 – 1.8	120	95	130	105	8	90	75	3.8	50	40	1.9
HRH-10 – 3/16 – 2.0	135	110	150	130	11	95	80	4.3	55	45	2.1
HRH-10 – 3/16 – 3.0	275	235	325	270	20	175	140	6.5	100	85	3.4
HRH-10 – 3/16 – 4.0	500	430	540	470	28	245	215	7.8	140	110	4.7
HRH-10 – 3/16 – 6.0	935	780	1020	865	60	420	370	13.0	225	200	6.5
HRH-10 – 1/4 – 1.5	80	65	90	75	6	70	55	3.0	35	25	1.3
HRH-10 – 1/4 – 2.0	120	100	130	105	11	95	80	4.2	45	36	2.0
HRH-10 – 1/4 – 3.1	285	240	310	265	21	185	160	6.5	90	75	3.0
HRH-10 – 1/4 – 4.0	440	360	480	390	28	250	205	8.0	125	100	3.5
HRH-10 – 3/8 – 1.5	95	75	105	80	6	70	55	3.0	35	25	1.5
HRH-10 – 3/8 – 2.0	140	115	155	125	11	90	72	3.7	55	36	2.4
HRH-10 – 3/8 – 3.0	255	210	270	225	17	200	160	6.5	100	80	3.0
HRH-10 – 3/4 – 1.5	70p	50p	80p	55p	7p	70p	55p	3.4p	35p	25p	1.7p
OX-Core											
HRH-10/OX – 3/16 – 1.8	100	80	110	90	7	50	40	2.0	60	50	3.0
HRH-10/OX – 3/16 – 3.0	320	260	350	285	17	105	95	2.5	120	100	6.0
HRH-10/OX – 3/16 – 4.0	600	500	650	550	26	130	105	4.6	150	130	8.4
HRH-10/OX – 1/4 – 3.0	350	280	385	310	17	110	90	3.0	135	110	6.0
Flex-Core											
HRH-10/F35 – 2.5	200	150	235	175	12	110	90	4.0	65	50	2.5
HRH-10/F35 – 3.5	410	320	430	330	24	220	170	6.0	120	90	3.7
HRH-10/F35 – 4.5	580	440	620	480	33	300	230	9.0	190	150	4.3
HRH-10/F50 – 3.5	380	300	400	310	24	175	130	5.5	100	75	3.6
HRH-10/F50 – 4.5	565	450	585	470	33	330	250	9.5	175	140	4.7
HRH-10/F50 – 5.0	670	520	690	540	37	380	300	10.0	215	170	5.2
HRH-10/F50 – 5.5	800	620	850	660	42	400	320	10.5	230	180	5.7

Table 26: HRH-10 Aramid Fiber/Phenolic Resin Honeycomb

Among these, have been chosen the cells with hexagonal shape simply because is the most widespread, but nothing prohibits the use of other types of cells. The table lists the different allowable values, but for this case will be used the values “typical” (typ) and “minimal” (min); furthermore, for the compression will be used values “stabilized”.

As can be noted are given two modulus of shear stiffness. The properties in W-direction are attributable to the bonding while the properties in L-direction depend on the characteristics of the core material. This is a direct consequence of the production method (see Figure 57) in fact, the sheets that make up the honeycomb are suitably shaped to desired length L (*ribbon direction*), and subsequently stuck together along the direction W (*transverse to the ribbon*).

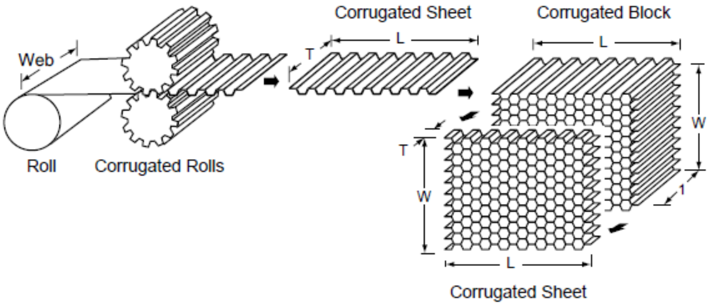

Figure 57: Honeycomb: L and W direction

9.3.2 Calculation Methods for Honeycomb

The failure criteria are simple, identical to those of the metallic materials in which the only difference is in the stresses taken into account. In the honeycomb the compression strain is compared with the allowable (A) in T-direction, and the two shear stresses with the corresponding allowable values. The margins of safety are obtained as:

$$MS_T = \frac{A_T}{\sigma_T} - 1$$

$$MS_L = \frac{A_L}{\tau_{zx}} - 1$$

$$MS_W = \frac{A_W}{\tau_{yz}} - 1$$

9.3.3 Correction Factors for Honeycomb Cores

The characteristics of the honeycomb are highly dependent on the operating temperature and the maximum thickness. There are different Knock Down Factors that reduce the allowable according to the characteristics just mentioned.

Figure 58, generated from actual Hexcel data, shows average shear strength correction factors, for both aluminum and nonmetallic honeycomb, in function of core thickness.

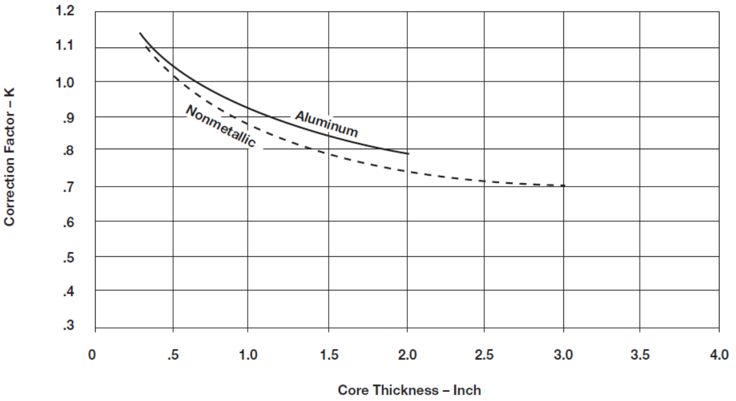

Figure 58: Correction factors for thickness

Thicker cores are not being subjected to pure shear but to a combination of shear and tension. For this reason they have a lower usable shear strength than thinner ones.

Several aircraft company and military specifications, generally test aluminum honeycomb at 0.625” T while nonmetallic honeycomb is tested at 0.500” T.

The curves in Figure 59 compare the typical mechanical properties of several honeycomb types, showing the effect of elevated temperatures on honeycomb strength after 30 minutes of exposure.

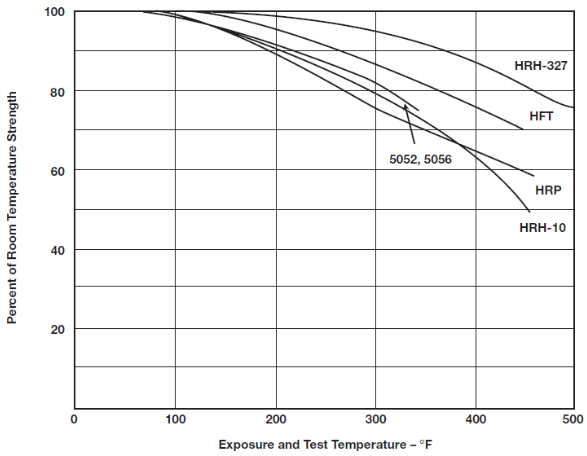

Figure 59: Correction factors for temperature

10 Spar Model FPF

10.1 General Description

The spar model is essentially composed of longitudinal elements, in particular have been used 6 spars and 24 stiffening stringers with trapezoidal shape.
The stringers have the main function to limit the phenomenon of buckling in the panels. They do not continue until the end rib both for reasons of space and because the panels in that area are very elongated and slightly stressed.
In addition to the root and the end ribs, there are also ribs in the front part which are used to maintain the shape of the leading edge and provide additional support in case of bird strike.
The aerodynamic surfaces are defined by the project specifications so it will be possible to operate only on the thickness of the skins that will compose the laminate.
The rear spars webs are very close together so as to create, with the skin, a torsion box for a better transmission of the loads coming from the rudder.

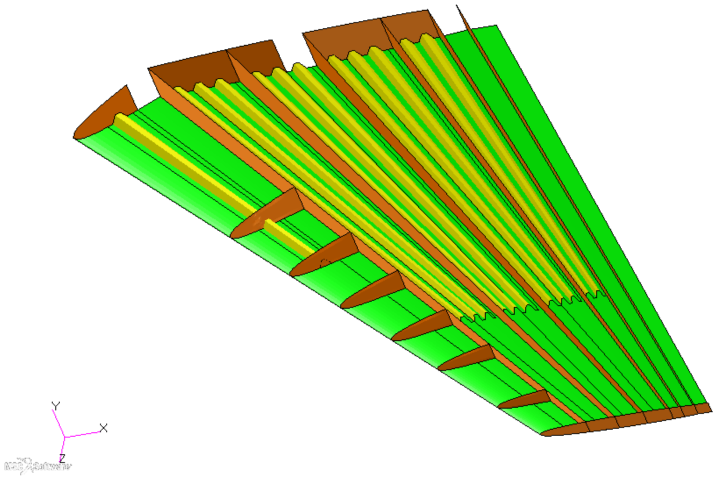

Figure 60: Spar model FPF cutaways

The manufacturing concept of the structure is to realize the spars caps integrated with the skin. One skin will be co-cured together with the J-shaped spars caps and with the stringers. The other skin instead will be co-cured together only with the stringers and subsequentially will be nailed and glued to the other skin.

As can be seen in Figure 61, connection with the fuselage will be done by means of machined parts made of aluminum alloy realized in two symmetrical components which will enclose the composite part of the structure.
As regards the hinges they will be nailed to the rear spar caps and web.
Being a preliminary study, it was decided to model the junction using the MERGE command. Its function is to permanently connect two distinct nodes that are located within a certain tolerance. In this way it is possible to connect two separate surfaces which have in common a number of nodes, such as the spar webs and spar caps integrated in the skin.

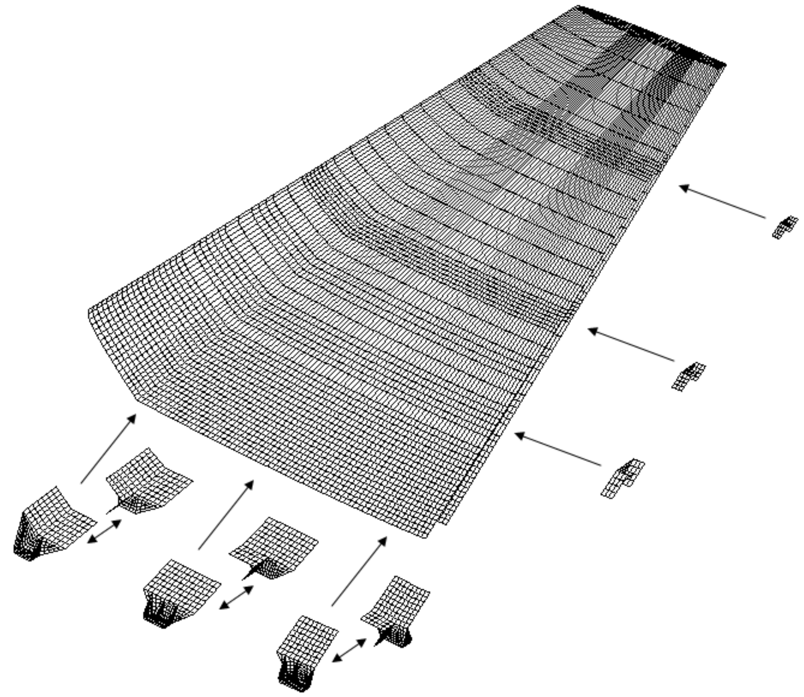

Figure 61: Assembly

10.2 Preliminary Design

10.2.1 Composite Parts

To create a model which was a good starting point for the analysis, have been made some preliminary considerations. Having available the properties of the model of the M346's first prototype, with a structure similar to that choice, but entirely metal, it was decided to determine the equivalent stiffness of the main components, in order to obtain a model already able to sustain the applied loads. Being the first prototype much more rigid than the current VT, the requirement for superior stiffness was already respected.
The load is distributed among the various components in the following way:

- spars caps: transmit bending loads
- spars webs, ribs: transmit shear loads
- skins: transmit axial and torsional loads

Is considered an equivalent bending stiffness EJ for spars and stringers, an equivalent axial stiffness EA for the skins, while for spars web and ribs is considered an equivalent shear stiffness[3] χEA.
In general, the formula used to calculate the moment of inertia has the following form:

$$J = J_{\text{local}} + Ad^2$$

In the case of the fin box, it is possible to demonstrate that the local moments of inertia are negligible compared to the transportation moment. Since the distance d of the skins are unchanged compared to the previous model, the equivalence between the flexural stiffness EJ reduces to:

$$E_{Al}\left(A_{Al}d^2\right) \cong E_{CFC}\left(A_{CFC}d^2\right)$$

$$E_{Al}A_{Al} \cong E_{CFC}A_{CFC}$$

---

[3] For simplicity it has been considered the shape factor χ equal to 1

The first prototype was made for the most part in aluminum alloy whose elastic modulus is around 70 GPa. Instead, the model that we are going to create will be made of composite carbon fiber and epoxy resin.
A symmetrical and balanced laminate, with 40% of fibers in the direction of 0 °, 40% of fibers in the direction of ±45 ° and 20% of fibers in the direction of 90 °, has an elastic modulus $E_{11} = 76,5\,\text{GPa}$. Since the stacking sequences that will be used will have a greater fraction of fibers in the direction of the load, then also the associated elastic modulus will be higher. For the sake of simplicity, while remaining in the conservation field, it is reasonable to assume $E_{Al} \cong E_{CFC}$. Finally, being the geometric proportion between the two models the same, the equivalence reduces to a simple equality between the thicknesses:

$$t_{Al} \cong t_{CFC}$$

10.2.2 Metallic Parts

The new architecture has made it necessary to change the constraint of the root, while maintaining the same interface points with the fuselage. Unlike the current model, the new model has three distinct constraints. As already mentioned each will be made up of two symmetrical parts (see sub 9.1) which will be spliced to each other by means of a joint cover and the web of the spar, which continues up to the base of the constraint. The coupling with the fin box is done by enclosing this one between the two flanges of the constraint, which will remain outside of the box but below the fairing of the aircraft. The real junction will be done using blind rivets. Since the FEM junction has been made using the MERGE command the jump in stiffness between joint and skin would be too sudden leading to Failure Index greater than the real ones. To overcome this problem has been added a dummy strip of variable thickness in order to make gradual the transition between the junction and the skin. The material is the same of the previous model, therefore thicknesses have been adapted to the new geometry.

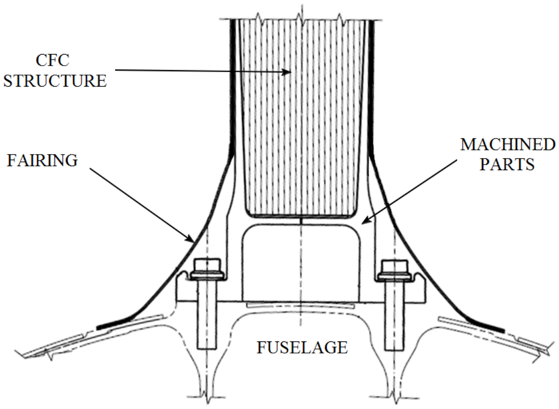

Figure 62: Connection to fuselage

10.3 Vertical Tail FEM Check Validation

The purpose of the analytical checks, described in this paragraph, is to ensure the mathematical soundness of the model and to uncover any gross modeling errors.

10.3.1 Pre-Analysis Check

Several analytical model checks can be performed prior to any static or dynamic analysis because they depend on the mass and/or stiffness matrices and are independent from the specific boundary conditions or applied loads.

Visual Check PATRAN offers a set of graphical tools that allow to check the model geometry and its properties.

- ✈ Shrink plot: this feature is an excellent tool for identifying missing elements.
- ✈ Free edge/face: the existence or not of free edge/face could indicate a modeling problem.
- ✈ Duplicate Grid/Elements: these errors are often due to unintentionally meshing the same line, surface, or volume more than once.
- ✈ Properties/Material Plots: graphic check of assigned incorrect properties.
- ✈ Consistent Plate Normals: elements should always be generated in a consistent manner, because pressure loads can inadvertently be applied in wrong directions.
- ✈ Units: MSC/NASTRAN does not keep track of your units, therefore a consistent set of units shall be used for properties and loads inputs.

Element Geometry Check These geometry tests are typically used to determine whether the element geometry is adequate for finite element matrix generation.
The following table summarizes the acceptable specifications that the model elements should satisfy, as far as possible:

Name	Value Type	Default	Comment
Q4_SKEW	Real≥ 0	30.0	Skew angle in degrees
Q4_TAPER	Real≥ 0	0.50	Taper ratio
Q4_WARP	Real≥ 0	0.05	Surface warping factor
Q4_IAMIN	Real≥ 0	30.0	Minimum interior angle in degrees
Q4_IAMAX	Real≥ 0	150.0	Maximum interior angle in degrees
T3_SKEW	Real≥ 0	10.0	Skew angle in degrees
T3_IAMAX	Real≥ 0	160.0	Maximum interior angle in degrees
TET_AR	Real≥ 0	100.0	Longest edge to shortest edge aspect ratio
TET_EPLR	Real≥ 0	0.50	Edge point length ratio
TET_DETJ	Real	0.0	$\lvert J\rvert$ minimum value
TET_DETG	Real	0.0	$\lvert J\rvert$ minimum value at vertex point
HEX_AR	Real≥ 0	100.0	Longest edge to shortest edge aspect ratio
HEX_EPLR	Real≥ 0	0.50	Edge point length ratio
HEX_DETJ	Real	0.0	$\lvert J\rvert$ minimum value
HEX_WARP	Real≥ 0	0.707	Face warp coefficient
PEN_AR	Real≥ 0	100.0	Longest edge to shortest edge aspect ratio
PEN_EPLR	Real≥ 0	0.50	Edge point length ratio
PEN_DETJ	Real	0.0	$\lvert J\rvert$ minimum value
PEN_WARP	Real≥ 0	0.707	Quadrilateral face warp coefficient
BEAM_OFF	Real≥ 0	0.15	CBEAM element offset length ratio
BAR_OFF	Real≥ 0	0.15	CBAR element offset length ratio

Table 27: Element geometry check

In this specific study all the model's element satisfy the above mentioned conditions.

10.3.2 Static Analysis Check

Simple static analysis can be performed to check a model. If pre-analysis checks have been made, some of the static analysis may be somewhat redundant. However, a static analysis is generally a relatively inexpensive means of checking the soundness of a finite element model.

Epsilon MSC/NASTRAN solves static analysis problems by decomposing the stiffness matrix and then using forward/backward substitution to solve for the displacement vector. A residual load vector is calculated by subtracting the applied load vector from the product of stiffness matrix and calculated displacement vector:

$$\delta P = Ku - P$$

A number called “epsilon” is automatically printed in the .f06 output listing, for each loading condition. Epsilon is based on a strain energy error ratio, and provides an important measure of round off error and numerical ill-conditioning.

$$\varepsilon = \frac{u^T \delta P}{u^T P}$$

A system of linear equations is said to be ill-conditioned if small perturbations in the system lead to large changes in the solution. A high value of epsilon indicates a potential ill-conditioning problem. This does not necessarily result in a FATAL ERROR, but it can result in inaccurate answers. Possible causes of ill-conditioning include a high difference in stiffness between adjacent elements in the model, unconnected degrees of freedom, rigid body motion, or the presence of mechanisms. Epsilon should be one of the first items to examine when reviewing an output file. An epsilon value in the neighborhood of less than 10^{-9} is generally considered acceptable.

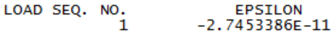

```
LOAD SEQ. NO.             EPSILON
            1       -2.7453386E-11
```

Table 28: Epsilon

Applied Load Check The OLOAD resultant is automatically calculated for each applied load vector. It represents the resultant of all applied loads referenced to a grid point specified. The OLOAD card, shown in the following table, can be found in the .f06 output listing. Although this computation is an applied loads check, and is not really a model check, it is an important consideration when static loads are being used to check out a model.

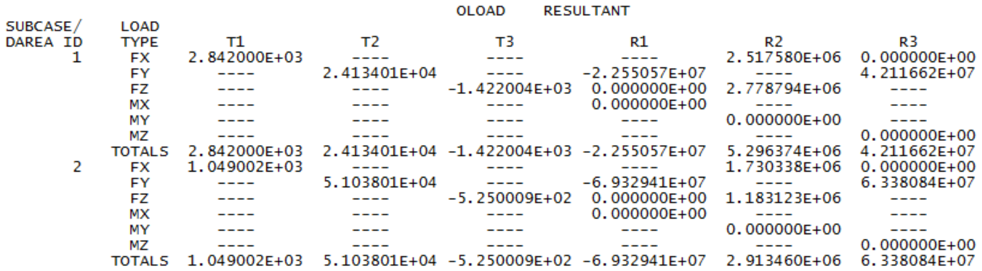

```
                                                     OLOAD     RESULTANT
SUBCASE/      LOAD
DAREA ID      TYPE        T1            T2            T3            R1            R2            R3
       1       FX    2.842000E+03      ----          ----          ----      2.517580E+06  0.000000E+00
               FY        ----      2.413401E+04      ----     -2.255057E+07      ----      4.211662E+07
               FZ        ----          ----     -1.422004E+03  0.000000E+00  2.778794E+06      ----
               MX        ----          ----          ----      0.000000E+00      ----          ----
               MY        ----          ----          ----          ----      0.000000E+00      ----
               MZ        ----          ----          ----          ----          ----      0.000000E+00
             TOTALS  2.842000E+03  2.413401E+04 -1.422004E+03 -2.255057E+07  5.296374E+06  4.211662E+07
       2       FX    1.049002E+03      ----          ----          ----      1.730338E+06  0.000000E+00
               FY        ----      5.103801E+04      ----     -6.932941E+07      ----      6.338084E+07
               FZ        ----          ----     -5.250009E+02  0.000000E+00  1.183123E+06      ----
               MX        ----          ----          ----      0.000000E+00      ----          ----
               MY        ----          ----          ----          ----      0.000000E+00      ----
               MZ        ----          ----          ----          ----          ----      0.000000E+00
             TOTALS  1.049002E+03  5.103801E+04 -5.250009E+02 -6.932941E+07  2.913460E+06  6.338084E+07
```

Table 29: OLOAD card

Reaction Load Check The SPCFORCE Resultant is the summation of all forces of single point constraint with respect to a reference point specificated. The SPCFORCE card, shown in the following table, can be found in the .f06 output listing. A useful equilibrium check can be made by summing the SPCFORCE resultant and the OLOAD resultant.

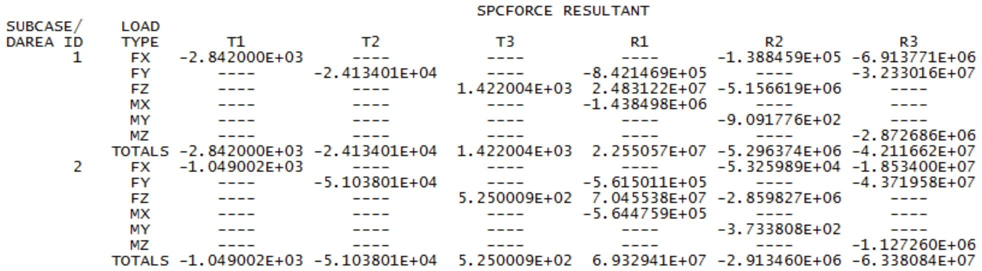

```
                                                      SPCFORCE RESULTANT
SUBCASE/      LOAD
DAREA ID      TYPE        T1            T2            T3            R1            R2            R3
       1       FX   -2.842000E+03      ----          ----          ----     -1.388459E+05 -6.913771E+06
               FY        ----     -2.413401E+04      ----     -8.421469E+05      ----     -3.233016E+07
               FZ        ----          ----      1.422004E+03  2.483122E+07 -5.156619E+06      ----
               MX        ----          ----          ----     -1.438498E+06      ----          ----
               MY        ----          ----          ----          ----     -9.091776E+02      ----
               MZ        ----          ----          ----          ----          ----     -2.872686E+06
             TOTALS -2.842000E+03 -2.413401E+04  1.422004E+03  2.255057E+07 -5.296374E+06 -4.211662E+07
       2       FX   -1.049002E+03      ----          ----          ----     -5.325989E+04 -1.853400E+07
               FY        ----     -5.103801E+04      ----     -5.615011E+05      ----     -4.371958E+07
               FZ        ----          ----      5.250009E+02  7.045538E+07 -2.859827E+06      ----
               MX        ----          ----          ----     -5.644759E+05      ----          ----
               MY        ----          ----          ----          ----     -3.733808E+02      ----
               MZ        ----          ----          ----          ----          ----     -1.127260E+06
             TOTALS -1.049002E+03 -5.103801E+04  5.250009E+02  6.932941E+07 -2.913460E+06 -6.338084E+07
```

Table 30: SPCFORCE card

Reaction Load Verification This control is used to verify that the reaction forces are those expected; if that were, it would mean that the constraint has been modeled correctly. Using the command Freebody implemented in Patran is possible to observe the forces that pass through an element and the force exchanged with the constraints.

The fin is connected to the rear fuselage by means of 10 bolts. The loads have been extracted from the FEM as freebody loads with respect to the coordinate system 360008. In Table 31 have been reported the applied load for each bolt of the root rib of the current configuration.

Ultimate Loads		**Test LC**		
Root Rib Fittings		F_x [N]	F_z [N]	F_y [N]
1	Forward RHS	33646	-543	69276
2	Forward LHS	-34457	-843	-71060
3	Center RHS (fwd)	6149	0	83271
4	Center LHS (fwd)	-6179	0	-83685
5	Center RHS (rear)	44973	-11461	75334
6	Center LHS (rear)	-45339	-11362	-75321
7	Rear RHS (fwd)	7138	0	96665
8	Rear LHS (fwd)	-7053	0	-95515
9	Rear RHS (rear)	3437	-15815	61424
10	Rear LHS (rear)	-3451	-15350	-59820
SPCFORCE resultant		-1049	-51038	525

Table 31: Current model: bolt applied load

A first check is the summation of all forces of single point constraint. The resultant in the three direction are the same reported in Table 30. In Figure 63 are reported the applied load at the interface of the fuselage of the spar model. The values are quite similar to the previous ones.

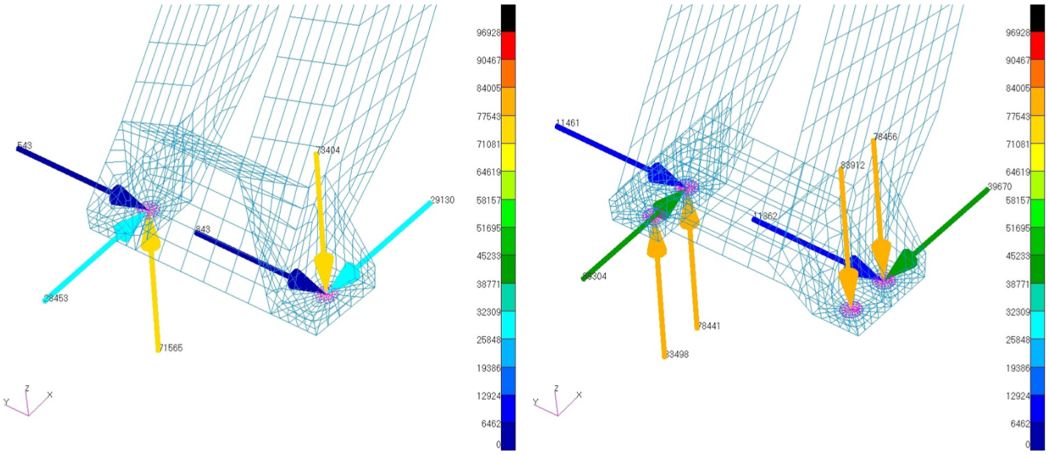
543
73404
29130
843
28453
71565
11461
78456
83912
39670
11362
39304
78441
33498
96928
90467
84005
77543
71081
64619
58157
51695
45233
38771
32309
25848
19386
12924
6462
0
Z
Y
X

Forward Center

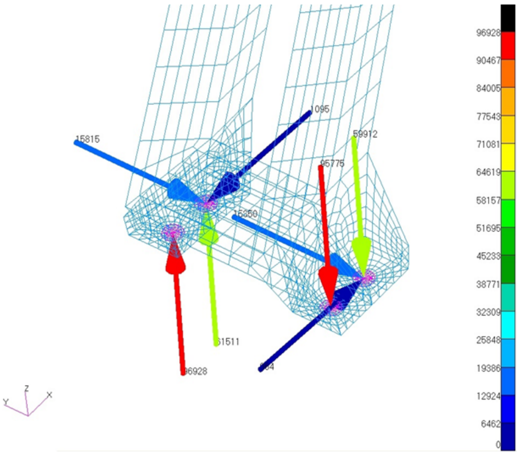
1095
15815
59912
95775
15350
61511
96928
604
96928
90467
84005
77543
71081
64619
58157
51695
45233
38771
32309
25848
19386
12924
6462
0
Z
Y
X

Rear

Figure 63: Spar model: bolt applied load

Rigid Body Check and Normal Modes For a general, unconstrained 3D structure without mechanisms, there are six rigid-body modes.
A mechanism mode occurs when a portion of the structure can displace as a rigid body, which can occur when there is an internal hinge in the structure. A mechanism mode can also occur when two parts of a structure are improperly joined. The presence of a rigid body and/or mechanism modes is indicated by zero frequency eigenvalues.
The deformed shape of a structure at a specific natural frequency of vibration is termed as normal mode of vibration.
Each mode shape is associated with a specific natural frequency. Natural frequencies and mode shapes are functions of the structural properties and boundary conditions.
In summary, a normal mode analysis (SOL 103) performed on an unconstrained model should indicate, for the first six mode, zero frequency eigenvalues (values up to 1.0^{-3} [Hz] are accepted), then frequencies and mode shapes that are function of the structural properties. The 7th frequency is expected to be different from zero, indicating that are no mechanism in the model.
Result from the analysis are presented in Table 32 and show that the model has passed the check.

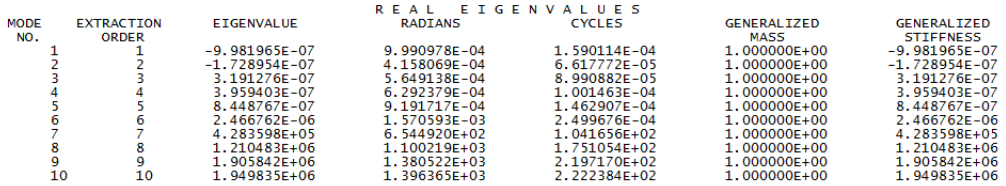

```
                                          R E A L   E I G E N V A L U E S
 MODE    EXTRACTION      EIGENVALUE            RADIANS             CYCLES            GENERALIZED         GENERALIZED
  NO.       ORDER                                                                       MASS              STIFFNESS
      1         1        -9.981965E-07        9.990978E-04        1.590114E-04        1.000000E+00       -9.981965E-07
      2         2        -1.728954E-07        4.158069E-04        6.617772E-05        1.000000E+00       -1.728954E-07
      3         3         3.191276E-07        5.649138E-04        8.990882E-05        1.000000E+00        3.191276E-07
      4         4         3.959403E-07        6.292379E-04        1.001463E-04        1.000000E+00        3.959403E-07
      5         5         8.448767E-07        9.191717E-04        1.462907E-04        1.000000E+00        8.448767E-07
      6         6         2.466762E-06        1.570593E-03        2.499676E-04        1.000000E+00        2.466762E-06
      7         7         4.283598E+05        6.544920E+02        1.041656E+02        1.000000E+00        4.283598E+05
      8         8         1.210483E+06        1.100219E+03        1.751054E+02        1.000000E+00        1.210483E+06
      9         9         1.905842E+06        1.380522E+03        2.197170E+02        1.000000E+00        1.905842E+06
     10        10         1.949835E+06        1.396365E+03        2.222384E+02        1.000000E+00        1.949835E+06
```

Table 32: First 10 eigenvalues and relevant cycles

In addition to this control, it is possible to observe the deformation modes of the constrained model to check if there are any strange and unexpected behaviors. Usually, for structures of this kind, the first two not rigid modes met are the flexural and torsional modes. By controlling the deformed is obtained confirmation of this, as can be seen in Figure 64.

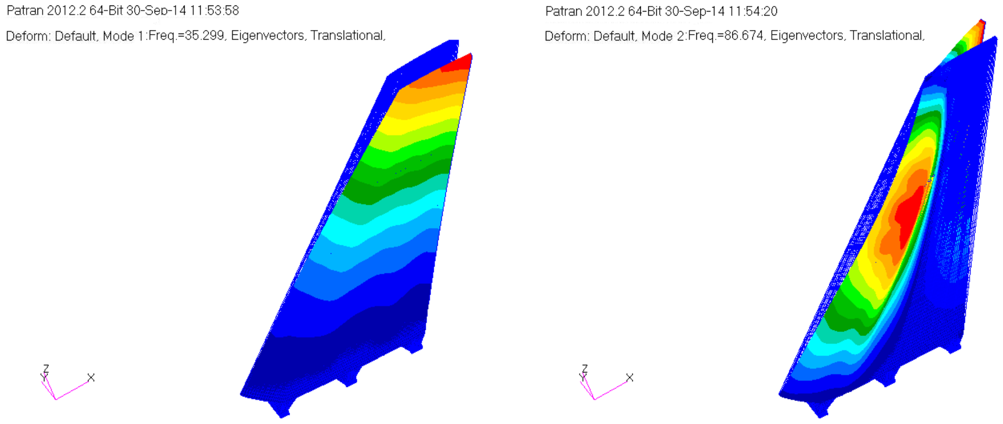
Patran 2012.2 64-Bit 30-Sep-14 11:53:58
Deform: Default, Mode 1:Freq.=35.299, Eigenvectors, Translational,
Z
Y
X
Patran 2012.2 64-Bit 30-Sep-14 11:54:20
Deform: Default, Mode 2:Freq.=86.674, Eigenvectors, Translational,
Z
Y
X

Figure 64: Deformation modes

Figure 65 show the first six rigid body modes of the spar model.

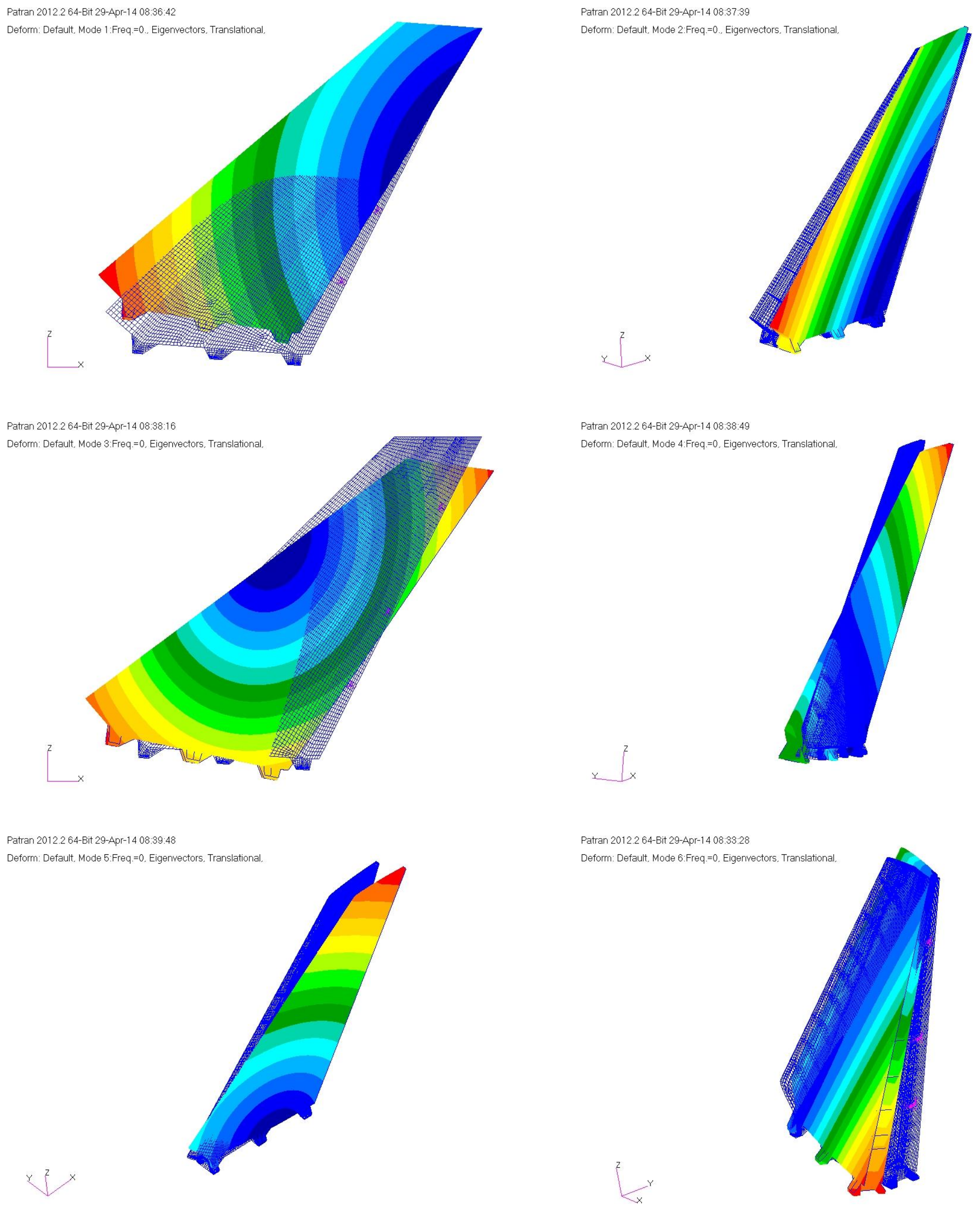
Patran 2012.2 64-Bit 29-Apr-14 08:36:42
Deform: Default, Mode 1:Freq.=0., Eigenvectors, Translational,
Z
X
Patran 2012.2 64-Bit 29-Apr-14 08:37:39
Deform: Default, Mode 2:Freq.=0., Eigenvectors, Translational,
Z
Y
X
Patran 2012.2 64-Bit 29-Apr-14 08:38:16
Deform: Default, Mode 3:Freq.=0., Eigenvectors, Translational,
Z
X
Patran 2012.2 64-Bit 29-Apr-14 08:38:49
Deform: Default, Mode 4:Freq.=0., Eigenvectors, Translational,
Z
Y
X
Patran 2012.2 64-Bit 29-Apr-14 08:39:48
Deform: Default, Mode 5:Freq.=0., Eigenvectors, Translational,
Y
Z
X
Patran 2012.2 64-Bit 29-Apr-14 08:33:28
Deform: Default, Mode 6:Freq.=0., Eigenvectors, Translational,
Z
Y
X

Figure 65: Rigid body modes

10.4 Static Analysis

Completed all the checks for validating the model it is possible to start with static analysis. A dimensioning of this type involves an iterative procedure in which the model is continually updated to satisfy all the requirements.
Before arriving to the configuration presented here there have been different intermediate configurations, starting from the preliminary one presented in the previous chapter.
For each new configuration was performed a static analysis, were checked the failure indices and, where these exceeded unity, displayed the stress tensor to see which ply failed and consequently change the lamination sequence.
In addition, for each step was performed a buckling analysis.
For sake of simplicity will be reported directly the final configuration used for the application of the Progressive Failure Analysis.

10.4.1 Thickness Distribution

The thickness distribution of the final configuration is shown in the following figures. As can be seen in Figure 66 the thickness of the skins has a longitudinal extension so that to increase the overall stiffness of the structure.
The caps of the three main spars are integrated into the skin while the intermediate spars, required to reduce the instability of panels, will require only small caps for the bonding. The caps of the rear spar are more extensive in order to: ensure a good resistance to the loads from the rudder, form the torsion box with the second spar and raise the limit of instability of the free edge, particularly sensitive to the buckling.
Also the interfaces with the constraint have a greater thickness to ensure adequate strength. The thickening of the leading edge serves to further stiffen the structure as well as guaranteeing a certain margin for the phenomenon of bird strikes.

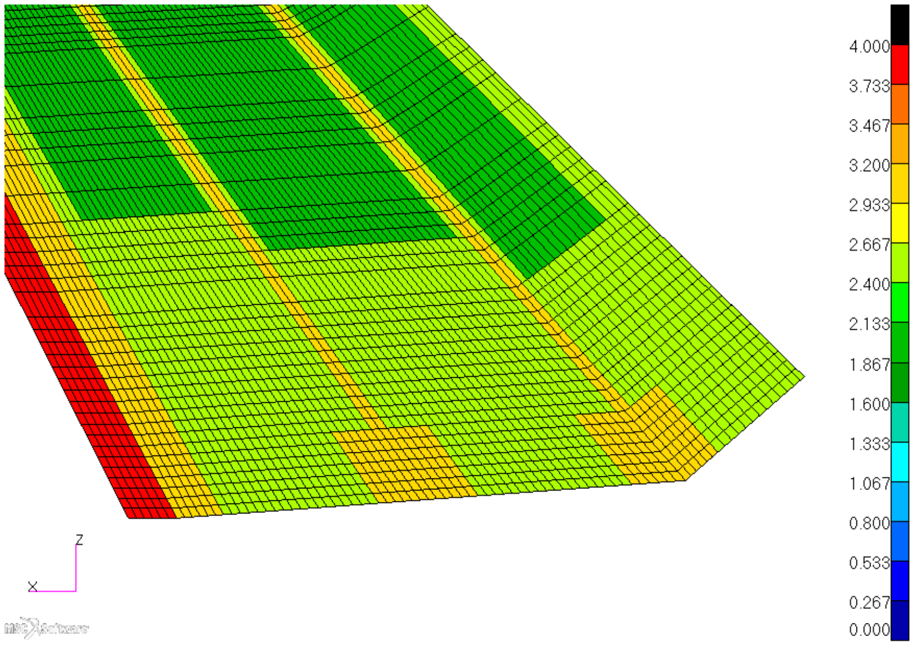

Figure 66: Spar model FPF thickness distribution: skin

Figure 67 show the thickness distribution of ribs and spars. These have a lamination with predominance of fibers oriented in the directions of 45 ° (see sub. 9.2.4). The thickening of the front spar is mainly due to shear buckling phenomenon that develop in that area.

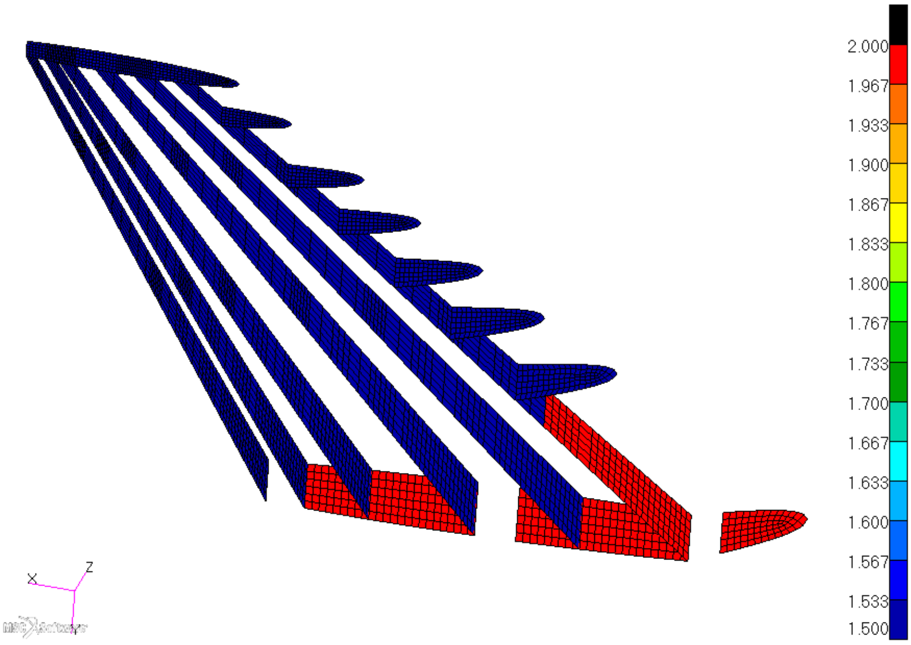

Figure 67: Spar model FPF thickness distribution: ribs and spars

The stringers of Figure 68 present thickenings near the root since the panels of that area are particularly sensitive to the effects of instability, so require additional stiffness.
The lamination is the same of the skin with a prevalence of fibers in the load direction in order to contribute to global stiffness.

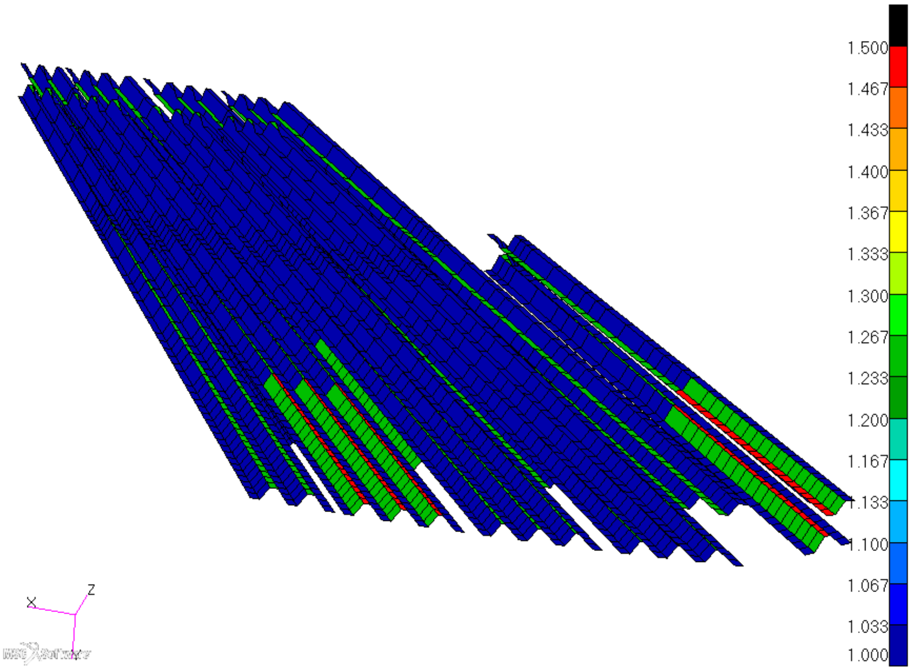

Figure 68: Spar model FPF thickness distribution: stringers

When changing the thickness has always been maintained a balanced symmetric laminate, according to the rules of thickness variation as described in sub. 9.2.3.

As regards the metallic components have been maintained, as far as possible, the same distributions of thickness of the original model.

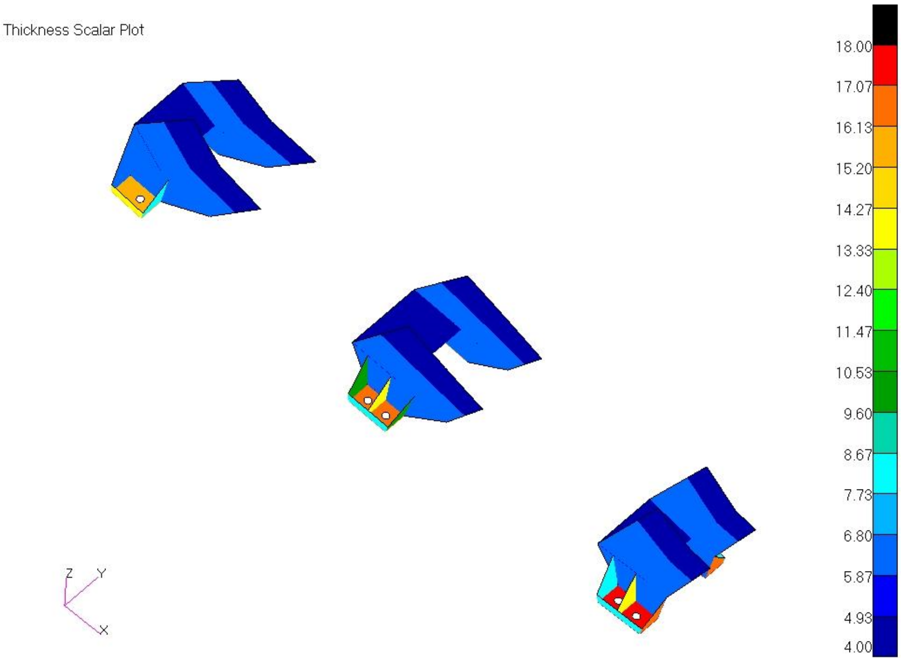
Thickness Scalar Plot
18.00
17.07
16.13
15.20
14.27
13.33
12.40
11.47
10.53
9.60
8.67
7.73
6.80
5.87
4.93
4.00
Z
Y
X

Figure 69: Root machined parts: thickness distribution

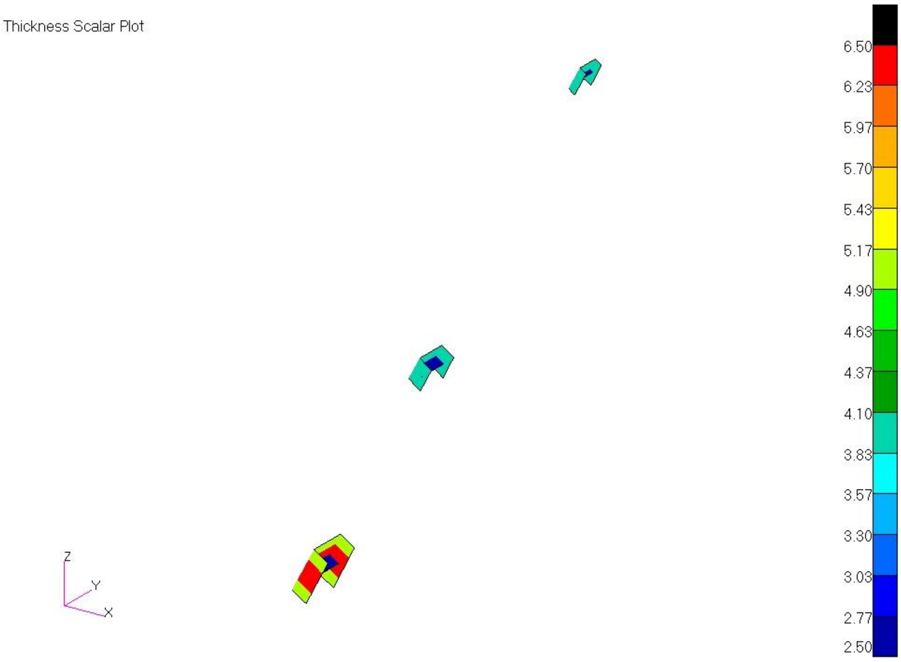
Thickness Scalar Plot
6.50
6.23
5.97
5.70
5.43
5.17
4.90
4.63
4.37
4.10
3.83
3.57
3.30
3.03
2.77
2.50
Z
Y
X

Figure 70: Hinges: thickness distribution

10.4.2 Composite Components Verification

To verify that the composite components are dimensioned correctly it is necessary to check if all the values of the FI, on the elements that compose them, are less than 1.
The more are the elements with FI slightly less than unity, the better will be the model.
Figure 71 shows the trend of the failure index obtained from a non-linear static analysis (SOL 106) up to ultimate load.

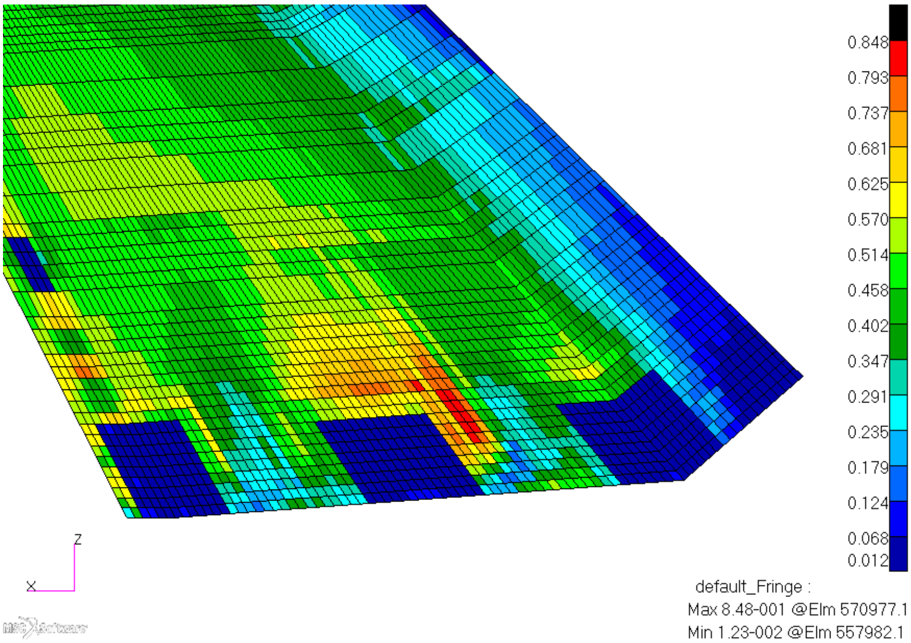

Figure 71: Spar model FPF skin: max FI (SOL 106)

Can be seen areas where the FI is almost zero. This condition was obtained by forcing, to the material, increased allowable values[4] with the following purposes:

- exclude the joint areas because not correctly modeled
- prevent the PFA from triggering in those areas, for the reason mentioned above

This choice is legitimate because normally the joints are analyzed separately with other specific programs and, because of their criticality, it would be preferred a dimensioning criteria such as the FPF, more consolidated, instead of the PFA.
Furthermore, the design of the joints is beyond the scope of this thesis. They should be dimensioned in the future with well established business methods.

The most stressed area of the entire VT is located on the skin, on the compressed side, three elements away from the junction, at the interface between the skin and the dummy strip (see sub. 10.2.2). Its extension is limited, with a values of FI around 0.848 (red zone), whereas the majority of the structure presents a very lower value of FI, below 0.570 (green zones). The load factor at which begin the FPF can be approximately calculated as:

$$n_{FPF} = \frac{1.5}{0.848} = 1.769$$

---

[4] In particular were imposed values ten times higher

As regards the internal elements, the distribution of FI is the following.

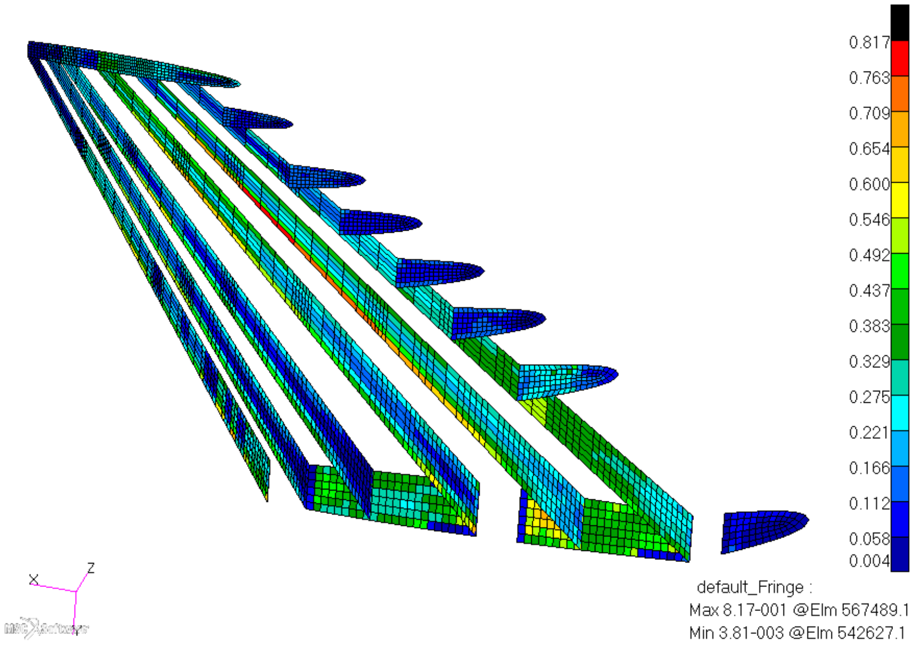
0.817
0.763
0.709
0.654
0.600
0.546
0.492
0.437
0.383
0.329
0.275
0.221
0.166
0.112
0.058
0.004
X
Z
default_Fringe :
Max 8.17-001 @Elm 567489.1
Min 3.81-003 @Elm 542627.1

Figure 72: Spar model FPF ribs and spars: max FI (SOL 106)

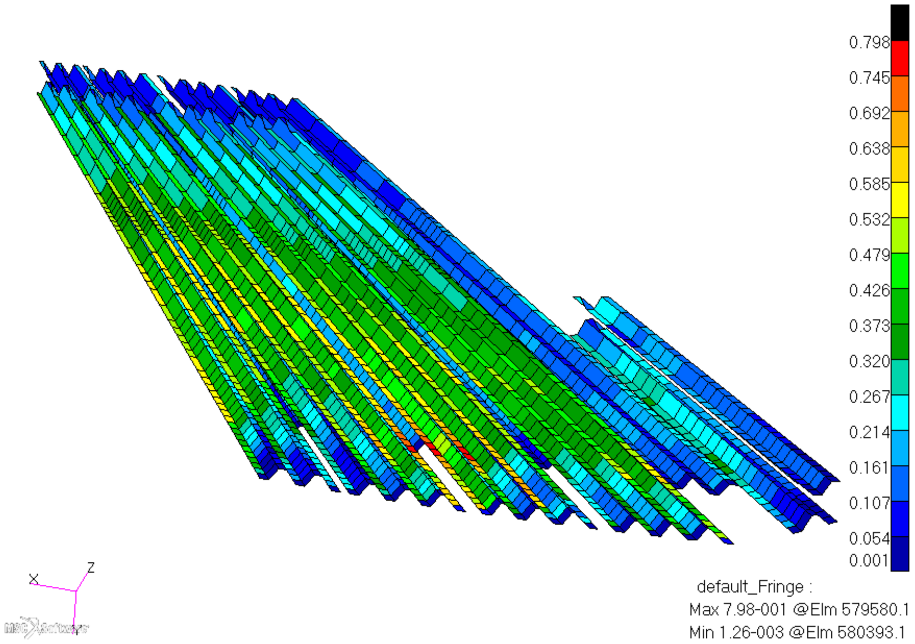
0.798
0.745
0.692
0.638
0.585
0.532
0.479
0.426
0.373
0.320
0.267
0.214
0.161
0.107
0.054
0.001
X
Z
default_Fringe :
Max 7.98-001 @Elm 579580.1
Min 1.26-003 @Elm 580393.1

Figure 73: Spar model FPF stringers: max FI (SOL 106)

As already mentioned these elements are less stressed than the skin. The critical area for the spars webs is at the point of interruption of the stringers, where there is a jump in stiffness, and has a value of FI equal to 0.817. The ribs are slightly stressed and show no particular problems. The stringers present concentrations of stress at the upper interface of the central constraint but still with a maximum value of FI equal to 0.798.
Both in the ribs that in the stringers, to avoid incorrect indexes, the first row of elements, directly linked to the machined through the merge, presents increased allowable values.

10.4.3 Metallic Components Verification

To verify that the metallic components are dimensioned correctly is necessary to calculate the margin of safety. Comparing the Von Mises stress with the allowable material it will be possible to extract the MS and assess the positive value.
The constraint of the root, made of aluminum alloy Al 7050 T7451 has the following values for the Von Mises stress.

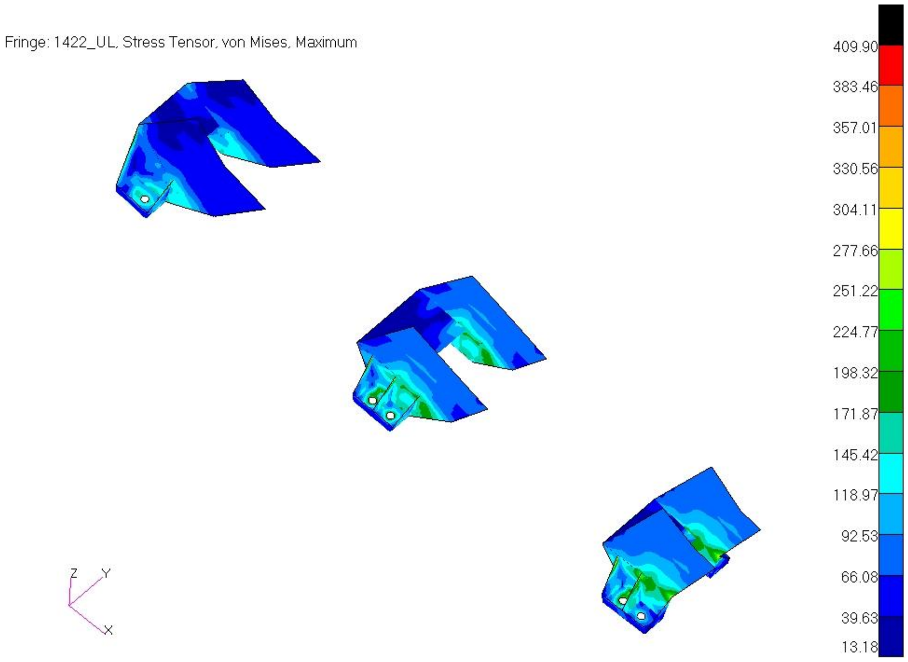
Fringe: 1422_UL, Stress Tensor, von Mises, Maximum
409.90
383.46
357.01
330.56
304.11
277.66
251.22
224.77
198.32
171.87
145.42
118.97
92.53
66.08
39.63
13.18
Z
Y
X

Figure 74: Root machined parts: Von Mises Stress (SOL 101)

As can be noted from the full scale, it has a maximum value of 409.9 MPa.
Comparing this value with Ultimate Tensile Strength reported in Table 24 is obtained a safety margin equal to:

$$MS_{UL} = \frac{\sigma^{U}}{\sigma_{VM}^{max}} - 1 = \frac{410}{409.9} - 1 = 0.0002$$

It is also necessary to verify that stress does not exceed the Yield Tensile Strength at Limit Load. Because of the linearity of the solution, we have:

$$MS_{LL} = \frac{\sigma^{Y}}{\frac{\sigma_{VM}^{max}}{1.5}} - 1 = \frac{386}{273.3} - 1 = 0.41$$

The margins of safety are positive, then the constraints of the root have been dimensioned correctly. Although the margins are minimal, it must be considered that the constraints have been modeled in a simple way, without taking into account any fittings that tend to limit the stress concentrations and thus to increase the MS.

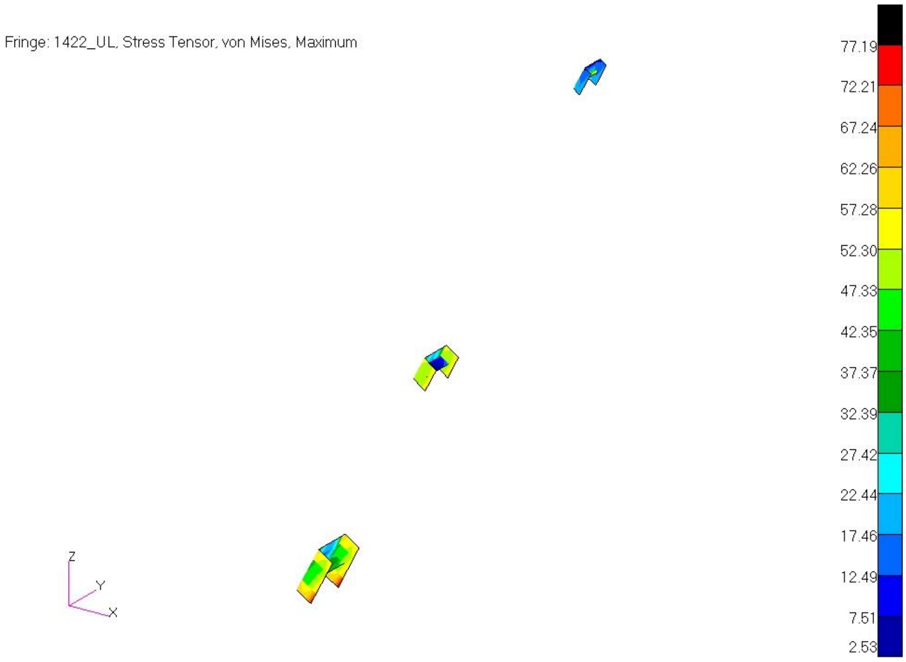

Figure 75: Hinges: Von Mises Stress (SOL 101)

As for the hinges, also made of aluminum alloy, have been obtained the following MS (see Tab. 23):

$$MS_{UL} = \frac{\sigma^U}{\sigma_{VM}} - 1 = \frac{433}{71.19} - 1 = 5.08$$

$$MS_{LL} = \frac{\sigma^Y}{\frac{\sigma_{VM}}{1.5}} - 1 = \frac{411}{47.46} - 1 = 7.66$$

Even if the margins obtained are very wide, the thicknesses will be maintained similar to those used on the current model.

10.5 Buckling Analysis

10.5.1 General Description

In practice, buckling is characterized by a sudden failure of a structural member subjected to high compressive stress, where the actual compressive stress at the point of failure is less than the ultimate compressive stresses that the material is capable of withstanding. Usually an axial load eccentricity introduces a secondary bending moment, which is not a part of the primary applied forces to which the element is subjected. As the applied load is increased, it will ultimately become large enough to cause the element to become unstable and is said to have buckled.

Further load will cause significant and somewhat unpredictable deformations, possibly leading to complete loss of the element's load-carrying capacity. If the deformations that follow buckling are not catastrophic it will continue to carry the load that caused it to buckle. If the buckled element is part of a larger assemblage of components, any load applied to the structure beyond that which caused the member to buckle will be redistributed within the structure.

In aeronautics is allowed the onset of buckling under certain conditions or maneuvers as long as, removing the load, the buckled components return to their original configuration, therefore remain in the elastic field.

Nowadays, for metallic structures, this phenomenon is easily predictable and analyzable. On the other hand, for composite structures, all the internal mechanisms are not yet know so it is preferred, conservatively, to avoid the buckling. This means having the critical load greater than the maximum applied load.

The determination of the critical load can be performed by means of the code NASTRAN (SOL 105). The result provides an eigenvalue λ, which, multiplied by the applied load P_a, indicates that the panel will go to buckling for a critical load equal to:

$$P_{cr_i} = \lambda_i P_a$$

The project specifications require that there is no phenomenon of instability up to ultimate load. This condition is respected if the buckling analysis provides a minimum eigenvalue greater than unity.

Several studies, such as the COCOMAT are studying the behavior of the post-buckled panel in order to admit instability also below the limit load.

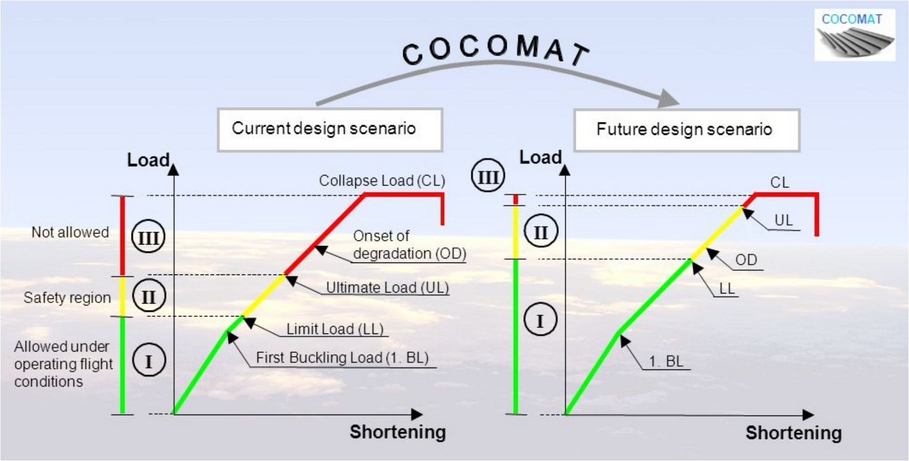
COCOMAT
COCOMAT
Current design scenario
Future design scenario
Load
Collapse Load (CL)
Not allowed
III
Onset of degradation (OD)
Safety region
II
Ultimate Load (UL)
Limit Load (LL)
Allowed under operating flight conditions
I
First Buckling Load (1. BL)
Shortening
III
Load
CL
II
UL
OD
LL
I
1. BL
Shortening

Figure 76: COCOMAT

In view of this we reserve the right to reduce the limit of instability up to the limit load.

10.5.2 Buckling of the Panels

The structure is composed mostly of panels therefore is shown the equation which describes the critical load of a panel subjected to compression:

$$\sigma_{cr} = K_c E_c \left(\frac{t}{b}\right)^2$$

where E_c is the equivalent elastic modulus, t is the thickness, b is the loaded side of the panel and K_c is a constant that depends on the type of constraint and the length of the panel sides, as shown in the following figure. The curves to be considered are the number 6, for the central panels, and the number 10 for the rear free edge.

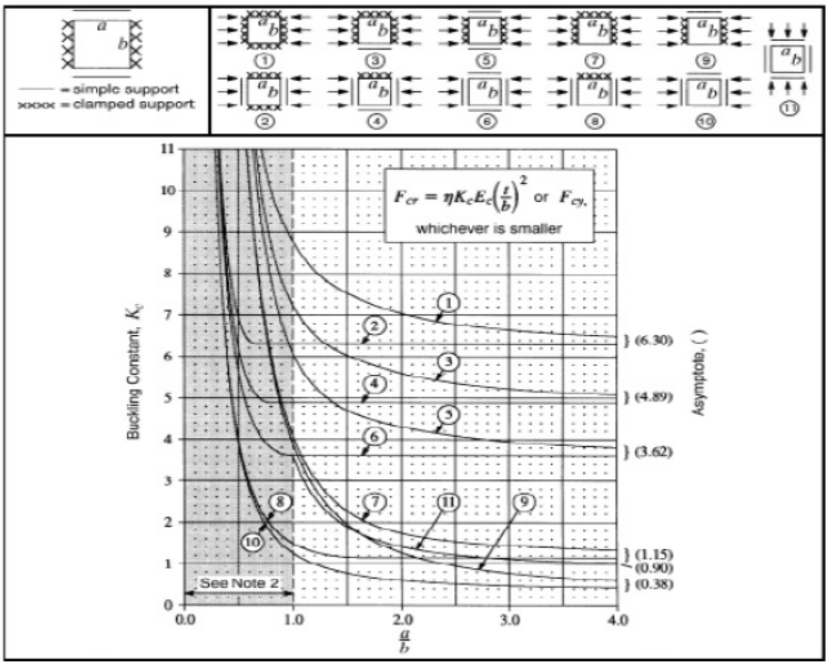

Figure 77: Buckling constant K_c

As can be noted the rear free edge is particularly susceptible to the phenomenon of instability, as also demonstrated by the successive analysis.
To increase the critical load is possible to act in three ways:

- increase the value of K_c by acting on the ratio $\frac{a}{b}$
- increase the ratio $\frac{t}{b}$ by increasing the thickness or reducing b
- increase the stiffness of the panel

The best choice would be to modify b, which affects both K_c and $\frac{b}{t}$. This can be done by introducing ribs. The second option is to increase the thickness t, however, for wide panels, this leads to an excessive increase in weight. A more effective alternative solution may be addition of stringers, which also contribute to the global stiffness.

10.5.3 Improvement of the Model

The initial configuration did not include the stringers. Despite the static test had been passed, the verification of instability led to a minimal eigenvalue equal to 0.3 in the middle panels. Being much less than unity, the increase in skin thickness would have led to excessive increase of weight.
The best solution was the introduction of the stringers to stiffen the panels (see Figure 60). Another area that was particularly susceptible to instability was the rear free edge, with an eigenvalues of 0.7. To resolve this problem has been increased the thickness and reduced the buckling length through diaphragms, as shown in Figure 78.

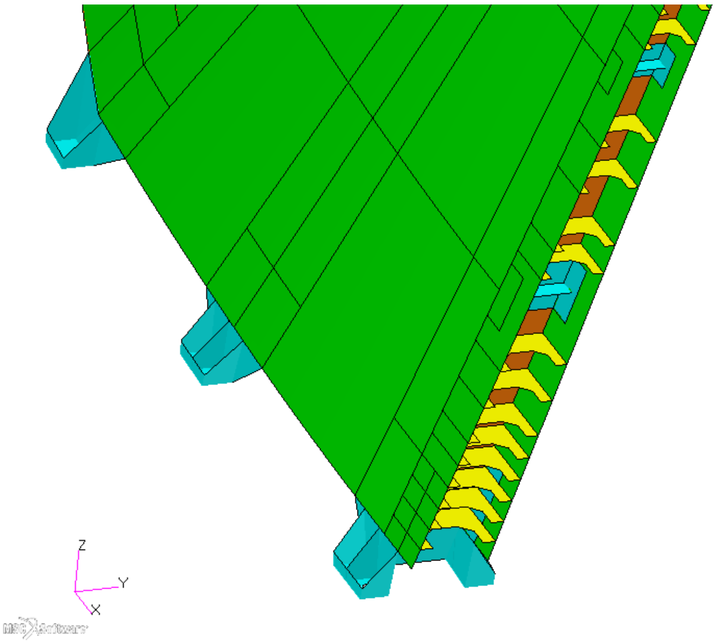

Figure 78: Stiffening of the rear free edges

After applying the changes described, the buckling analysis has led to the following results. As can be noted from the first figure the rear free edge is the first subject to instability. The eigenvalue of the First Buckling (FB) is equal to 1.1168, meaning that the critical load is about the 11% greater than the ultimate load ($n_{FB} = 1.66$).
The panels are the second components which go in buckling, in the area where there are no longer the stringers. The circular shape of the waves indicates that the panels are subjected to compression instability.
Finally, the spars webs and the ribs are the last which buckled and they are subjected to shear instability since the waves are elliptical and inclined at 45°.

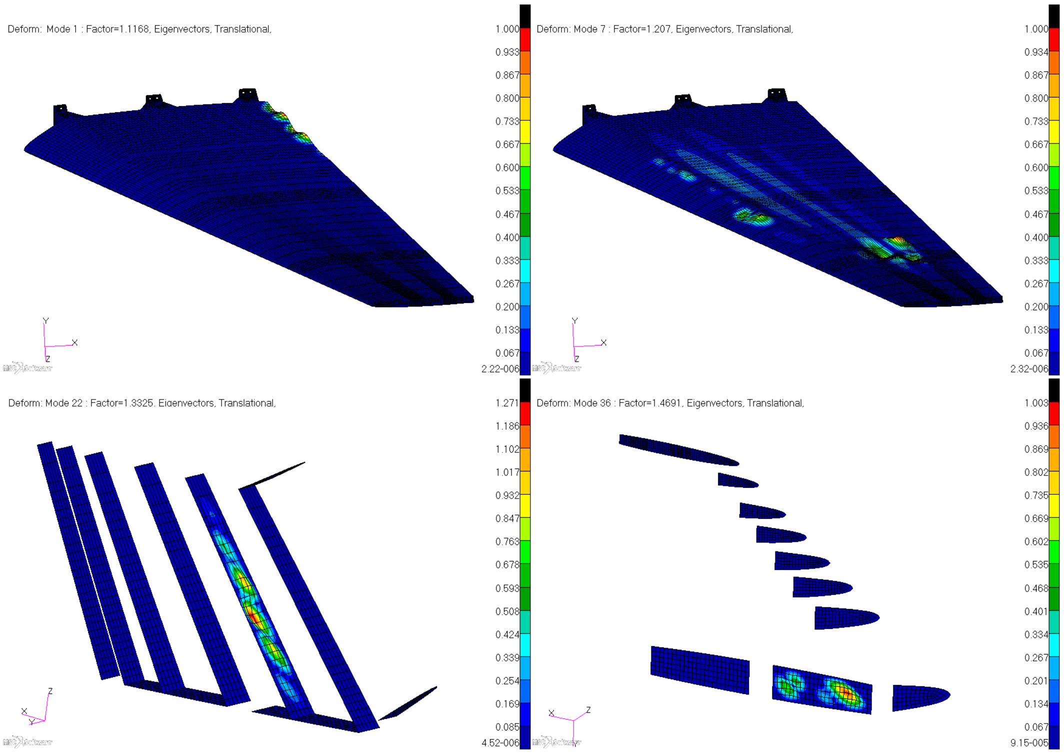
Deform: Mode 1 : Factor=1.1168, Eigenvectors, Translational,
1.000
0.933
0.867
0.800
0.733
0.667
0.600
0.533
0.467
0.400
0.333
0.267
0.200
0.133
0.067
2.22-006
Deform: Mode 7 : Factor=1.207, Eigenvectors, Translational,
1.000
0.934
0.867
0.800
0.733
0.667
0.600
0.533
0.467
0.400
0.333
0.267
0.200
0.133
0.067
2.32-006
Deform: Mode 22 : Factor=1.3325, Eigenvectors, Translational,
1.271
1.186
1.102
1.017
0.932
0.847
0.763
0.678
0.593
0.508
0.424
0.339
0.254
0.169
0.085
4.52-006
Deform: Mode 36 : Factor=1.4691, Eigenvectors, Translational,
1.003
0.936
0.869
0.802
0.735
0.669
0.602
0.535
0.468
0.401
0.334
0.267
0.201
0.134
0.067
9.15-005

Figure 79: Spar model FPF: buckling

10.6 SOL 400

According to what has been presented in section 2, is now possible to perform the Progressive Failure analysis in order to evaluate the margin available between FPF and the FC, which will be used for new static analysis to lighten the structure. This latter will be checked again with the PFA so as to comply with the following requirements:

- FPF between the LL and the UL ($1.0 < n_{FPF} < 1.5$)
- FC above the UL ($n_{FC} > 1.5$)
- FB above the UL ($n_{FB} > 1.5$)
- weight less than the current configuration and the FPF configuration
- maximum deflection not exceeding the 70% of the current configuration
- all the margin of safety positive ($MS > 0$)

The PFAs that will be performed, from now on, will use the Newton-Raphson method up to the FC and subsequently the Arc-Length method (see sub. 4.5). The number of step will be 100 and the RSF will be set equal to 0.05.

10.6.1 FPF Check

The first thing to check in a PFA is the correspondence of the results, up to the FPF, with the static solution. The following figures shows the trends of the failure index obtained from the PFA (SOL 400) up to ultimate load.

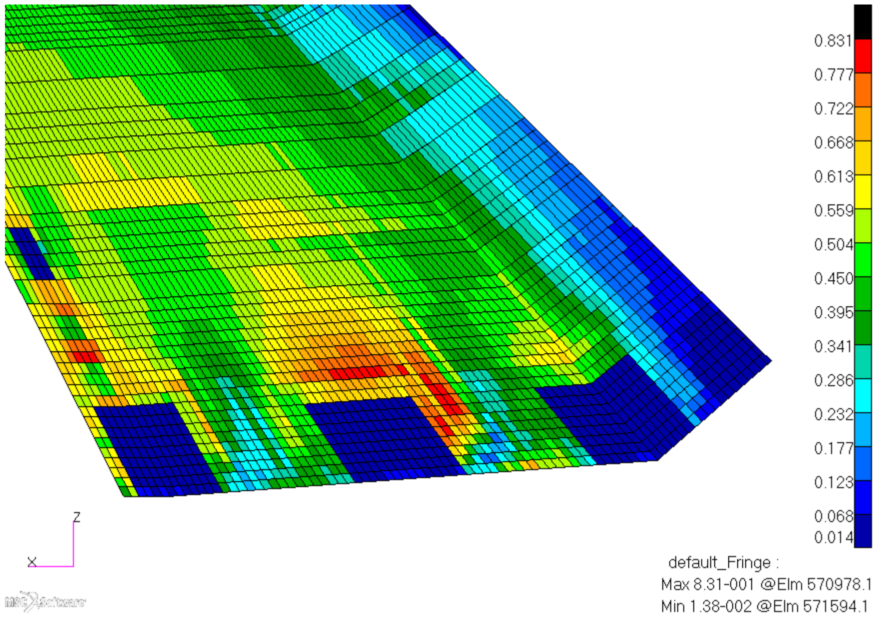

Figure 80: Spar model FPF skin: max FI (SOL 400)

Comparing Figure 80 with the results showed in Figure 71 it can be seen that the distribution of the FI at the UL is quite similar. The maximum FI of the skin is lower compared to SOL 106 but there are more element in the red zone and yellow zone.

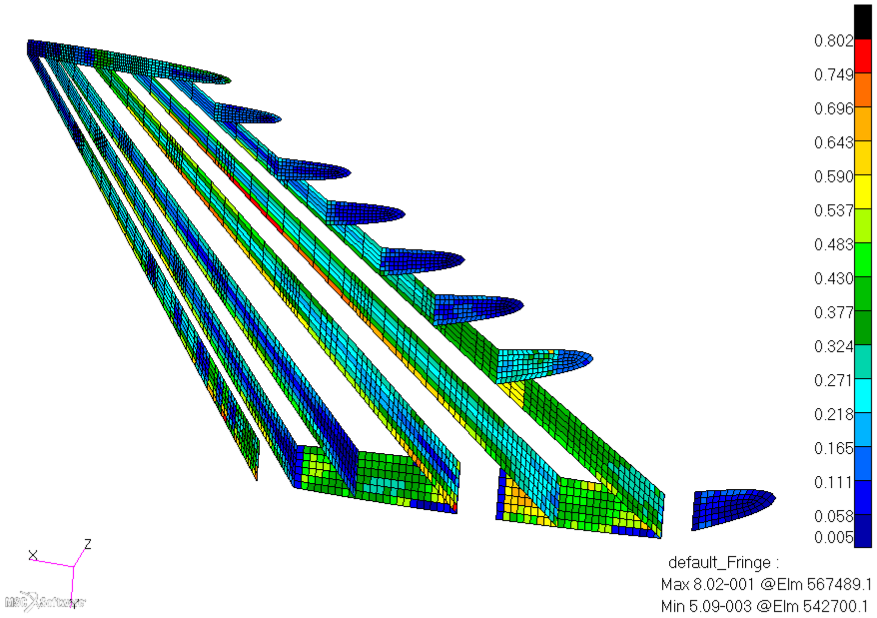

Figure 81: Spar model FPF ribs and spars: max FI (SOL 400)

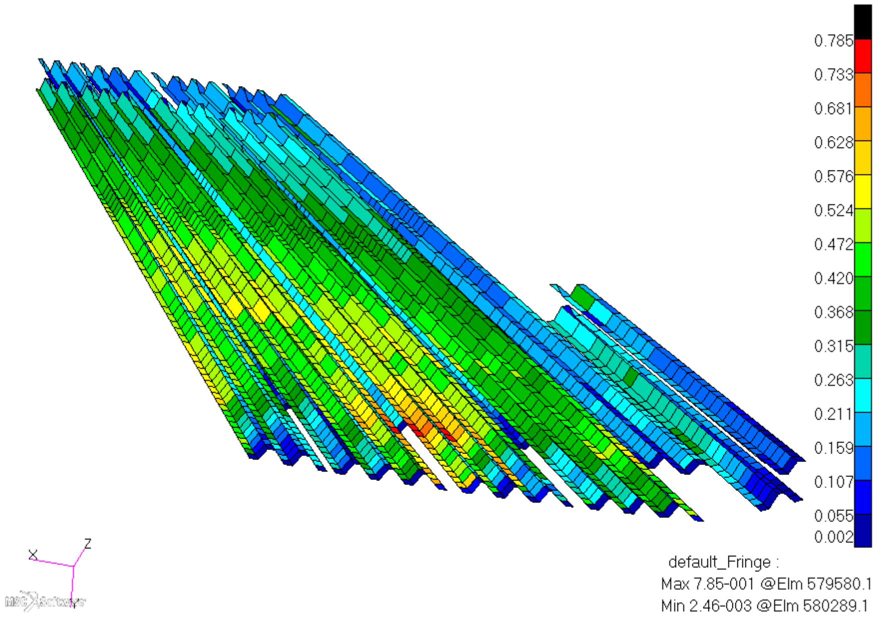

Figure 82: Spar model FPF stringers: max FI (SOL 400)

Because of the strong non-linearity, the load at which begin the FPF can not be obtained by dividing the load factor for the FI. The only way is to search the load step at which the FI is as close as possible to the unit, that is corresponding to a load factor equal to:

$$n_{FPF} = 1.78$$

As regards the internal elements are valid the consideration made previously.

UL FI max	**SOL 106**	**SOL 400**	Δ%
Skin	0.848	0.831	2.0%
Ribs and spars	0.817	0.802	1.8%
Stringers	0.798	0.785	1.6%

Table 33: FPF: differences between SOL 106 and SOL 400

10.6.2 Evaluation of the Margin from the FC

Further increasing the load, we come to the birth of the first crack at a load factor:

$$n_{FC} = 3.32$$

There is a wide margin between the FPF and FC ($n_{FC} - n_{FPF} = 1.54$) with which is possible to reduce substantially the weight. Probably, in order to reduce the thickness of the laminates, will be necessary to admit the buckling below the UL (see sub. 10.5).

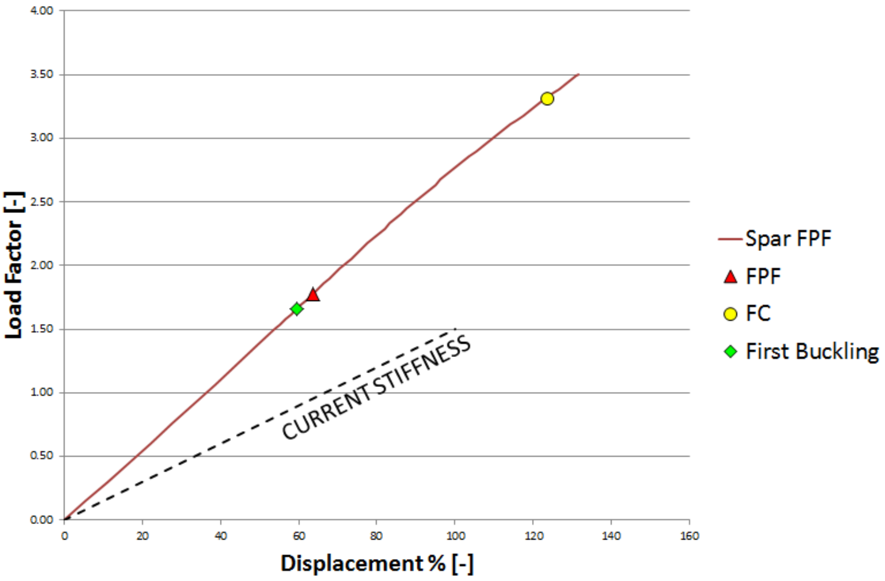

Figure 83: Spar model FPF: load displacement curve

First crack takes place simultaneously on the skin and on the rear spar web near the lower hinge, and on the central spar web and on the stringers near the central root constrain.

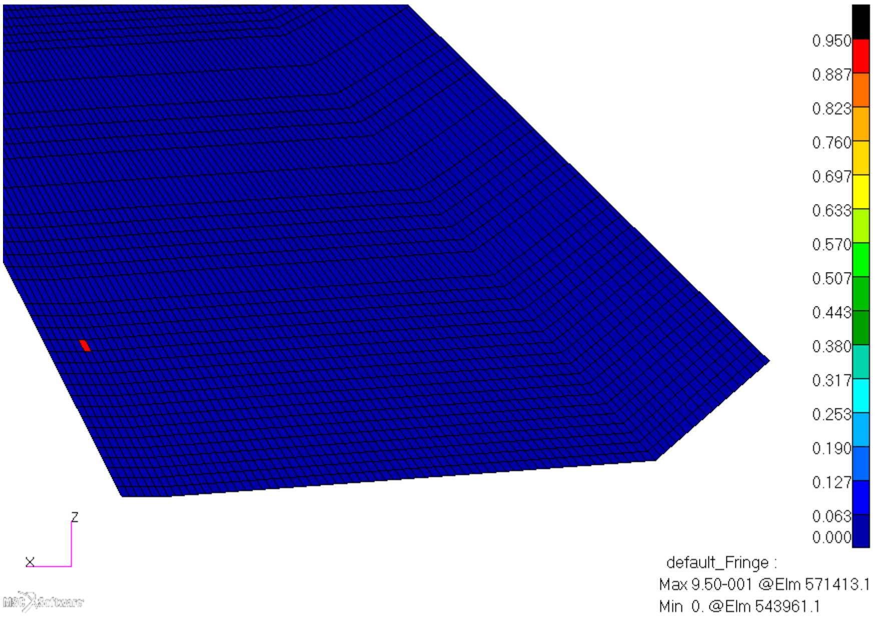
0.950
0.887
0.823
0.760
0.697
0.633
0.570
0.507
0.443
0.380
0.317
0.253
0.190
0.127
0.063
0.000
Z
X
default_Fringe :
Max 9.50-001 @Elm 571413.1
Min 0. @Elm 543961.1

Figure 84: Spar model FPF skin: TD min

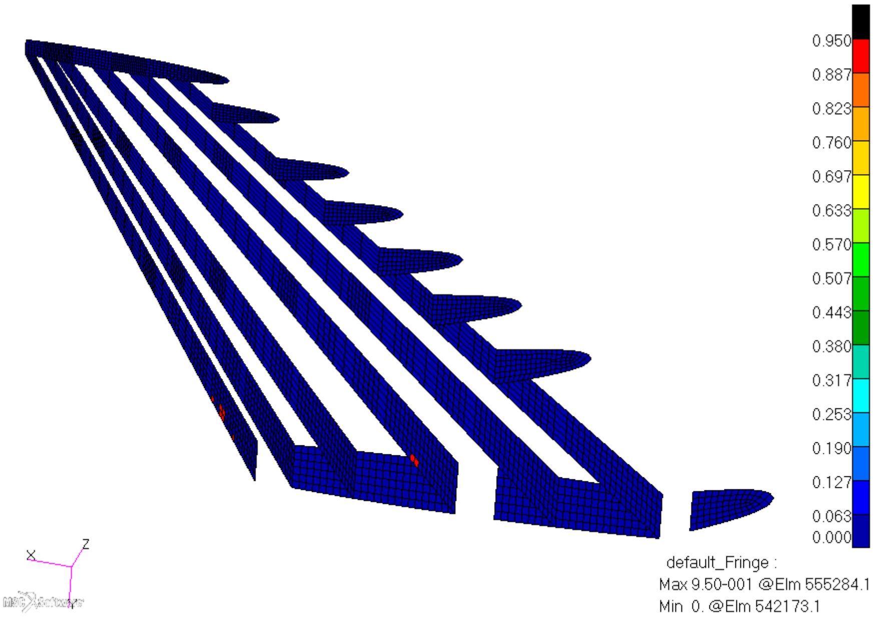
0.950
0.887
0.823
0.760
0.697
0.633
0.570
0.507
0.443
0.380
0.317
0.253
0.190
0.127
0.063
0.000
default_Fringe :
Max 9.50-001 @Elm 555284.1
Min 0. @Elm 542173.1
X
Z

Figure 85: Spar model FPF ribs and spars: TD min

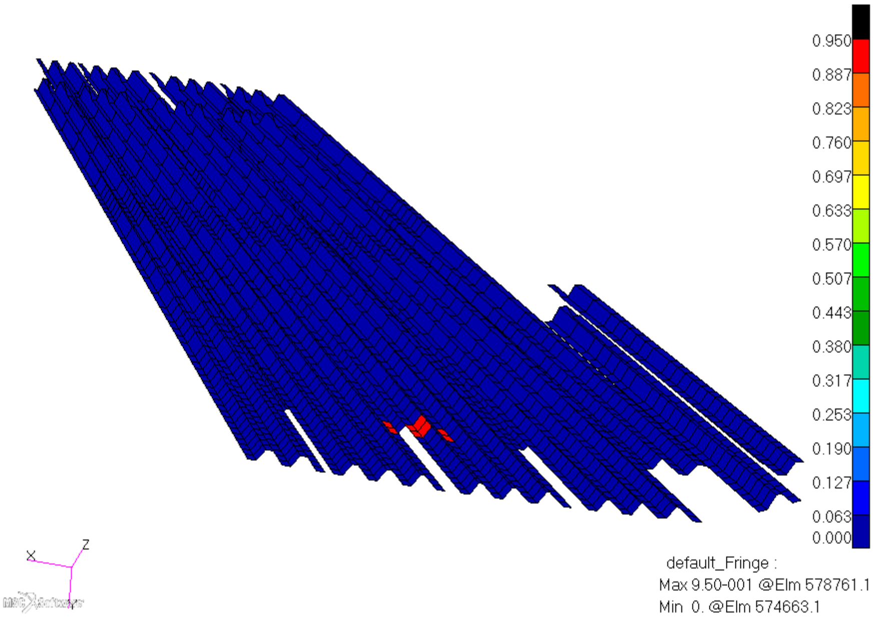
0.950
0.887
0.823
0.760
0.697
0.633
0.570
0.507
0.443
0.380
0.317
0.253
0.190
0.127
0.063
0.000
default_Fringe :
Max 9.50-001 @Elm 578761.1
Min 0. @Elm 574663.1
X
Z

Figure 86: Spar model FPF stringers: TD min

Another interesting result, that can be plotted, is the propagation of the damage in the laminate. This can be shown by mean of the maximum total damage or through the failure index with a proper reference scale.

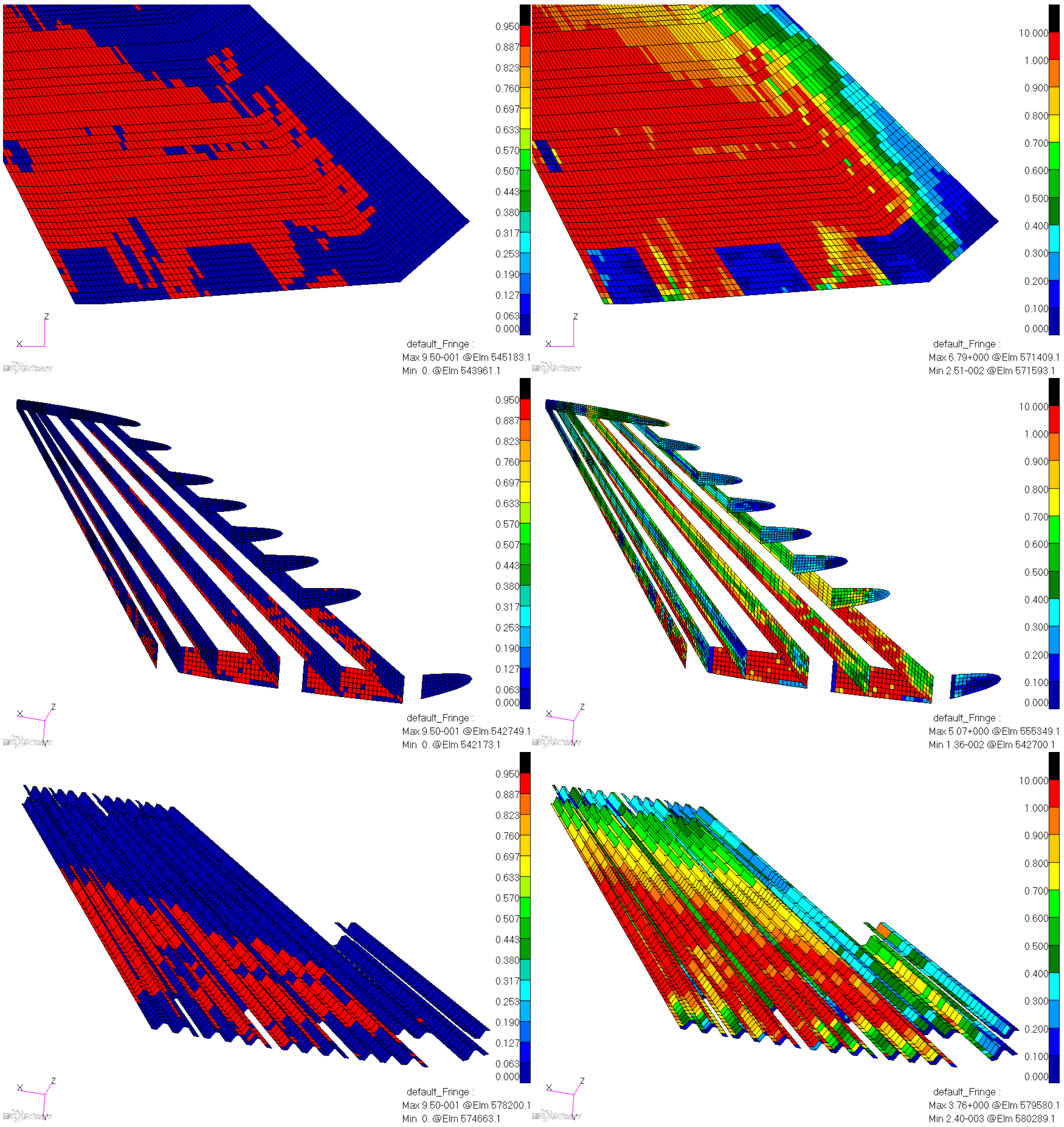

Figure 87: Spar model FPF: propagation of damage

As can be seen, by setting the FC as a criterion for sizing, is possible to bring the material to the limit of its possibilities on a much wider area, while ensuring the integrity of the structure up to the ultimate load as required by regulations.

10.7 Conclusions

Once completed all the controls, the verified model presents the following specifications.

Specification	**Spar Model FPF**	**Current**
FEM Weight	75.7%	100%
Maximum Deflection	57.1%	100%

Table 34: Spar model FPF vs. current model specifications

As expected the transition from metallic material to composite material has brought positive results.

The stiffness is greatly increased, in particular of about 42.9%, well above the design specification, which provided for an increase in stiffness of 30%.

Also the reduction of weight, in terms of the FEM model, is considerable, with a saving which is around 24.3%.

The deformed of the model is reported in Figure 60. Despite the trend of displacements is not perfectly linear the result is acceptable.

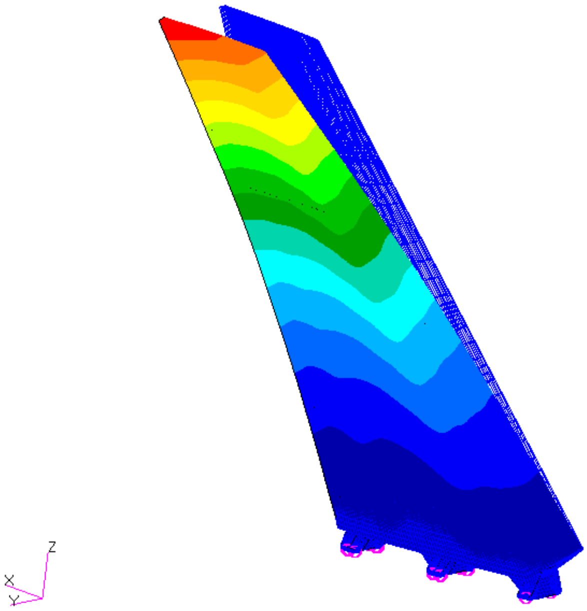

Figure 88: Spar model FPF deformed: maximum deflection 57.1%

The displacements of the whole structure are reported in the following tables at the nodes described in sub. 6.4.

Nodes		Δy
Leading Edge	1	0.0%
	3	4.4%
	5	11.9%
	7	22.1%
	9	34.6%
	11	49.5%
Trailing Edge	2	0.1%
	4	4.5%
	6	11.5%
	8	22.2%
	10	36.9%
	12	54.1%

Table 35: Spar model FPF: nodes displacement

These values will be successfully compared in a summary section to evaluate the results achieved.

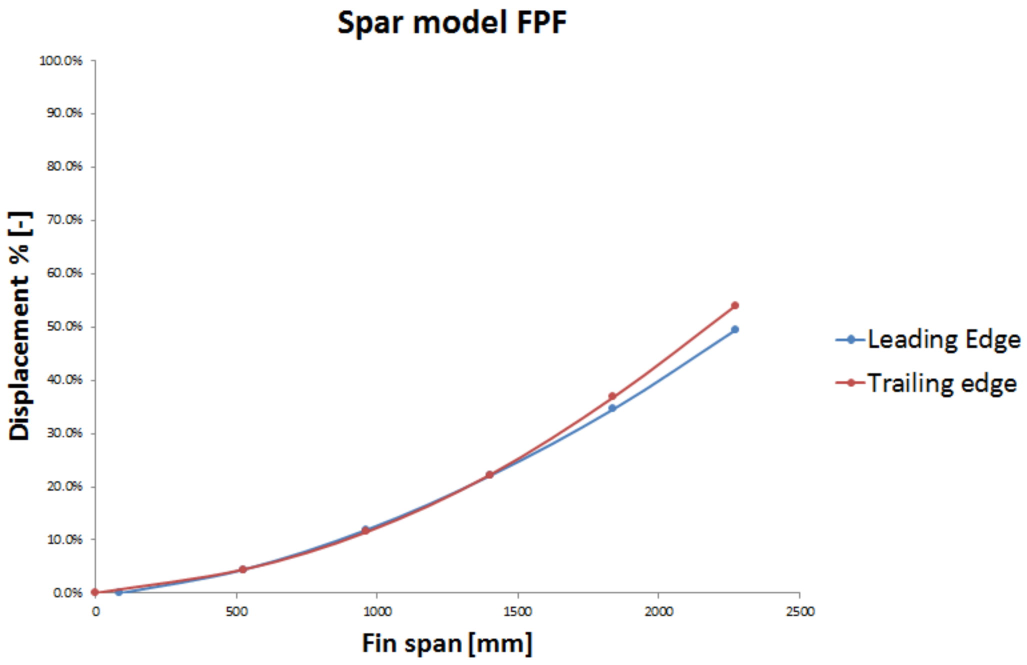

Figure 89: Spar model FPF: nodes displacement

11 Spar Model PFA

The passage from the FPF configuration to the PFA configuration requires an iterative procedure with a considerable expenditure of time and resources.
For simplicity, only the final configuration will be reported, without mentioning all the validation checks thus far described. Even static analysis on the metallic components will not be shown[5] in order to focus only on those parts affected by progressive failure.

11.1 General Description

The final configuration has been obtained by removing more than half of the stringers[6] and by reducing the thickness of the skin. Ribs and spars webs have remained unchanged.

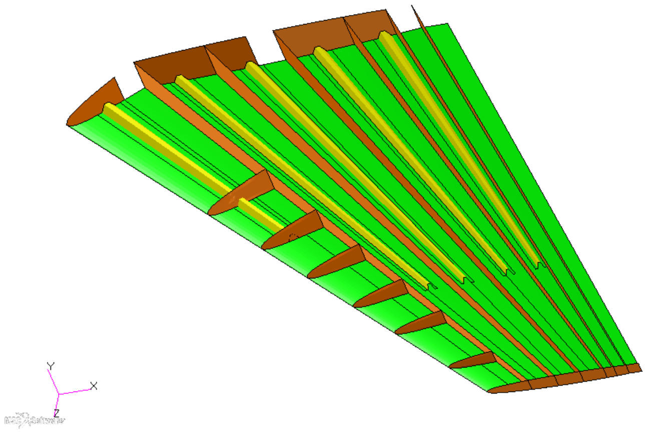

Figure 90: Spar model FPF vs. spar model PFA: cutaways

Spar Model FPF

Components	FEM Weight
Ribs	1.4%
Stringers	12.9%
Spars webs	6.8%
Skins	37.9%
Machined Parts	16.7%
Total	75.7%

Spar Model PFA

Components	FEM Weight
Ribs	1.4%
Stringers	5.7%
Spars webs	6.8%
Skins	36.8%
Machined Parts	16.7%
Total	67.4%

Table 36: Spar model FPF vs. spar model PFA: weight

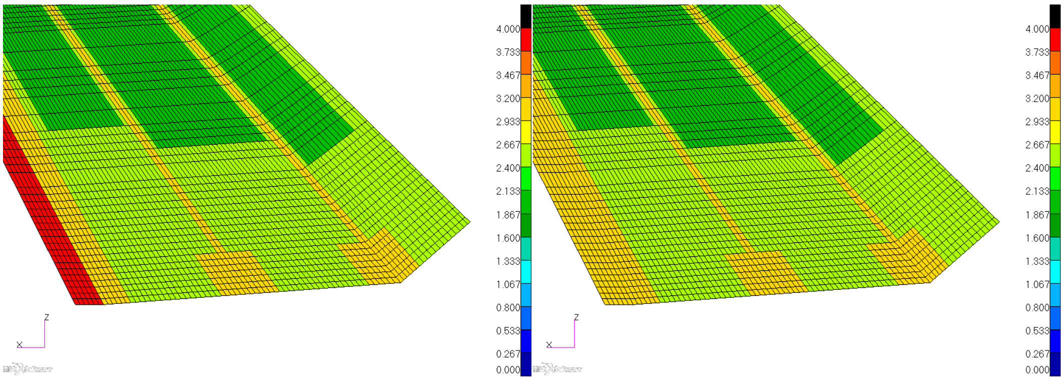

Figure 91: Spar model FPF vs. spar model PFA: thickness

---

[5] In all the model presented have been obtained $MS > 0$

[6] From the initial 24 to 10 stringers

11.2 Static Analysis and SOL 400

11.2.1 FI Verification

Once again, to verify that the composite components are dimensioned correctly it is necessary to check if all the values of the FI, on the elements that compose them, are less than 1, but this time calculated at the limit load. As done previously is necessary to look for the load step in which the FI is close to unity, which correspond to a load factor equal to:

$$n_{FPF} = 1.30$$

This mean that the FPF will take place in a range between LL and UL, as required by the specification. Figure 92 shows the comparison of the trend of the failure index obtained from a non-linear static analysis and a progressive failure analysis, at ultimate load.

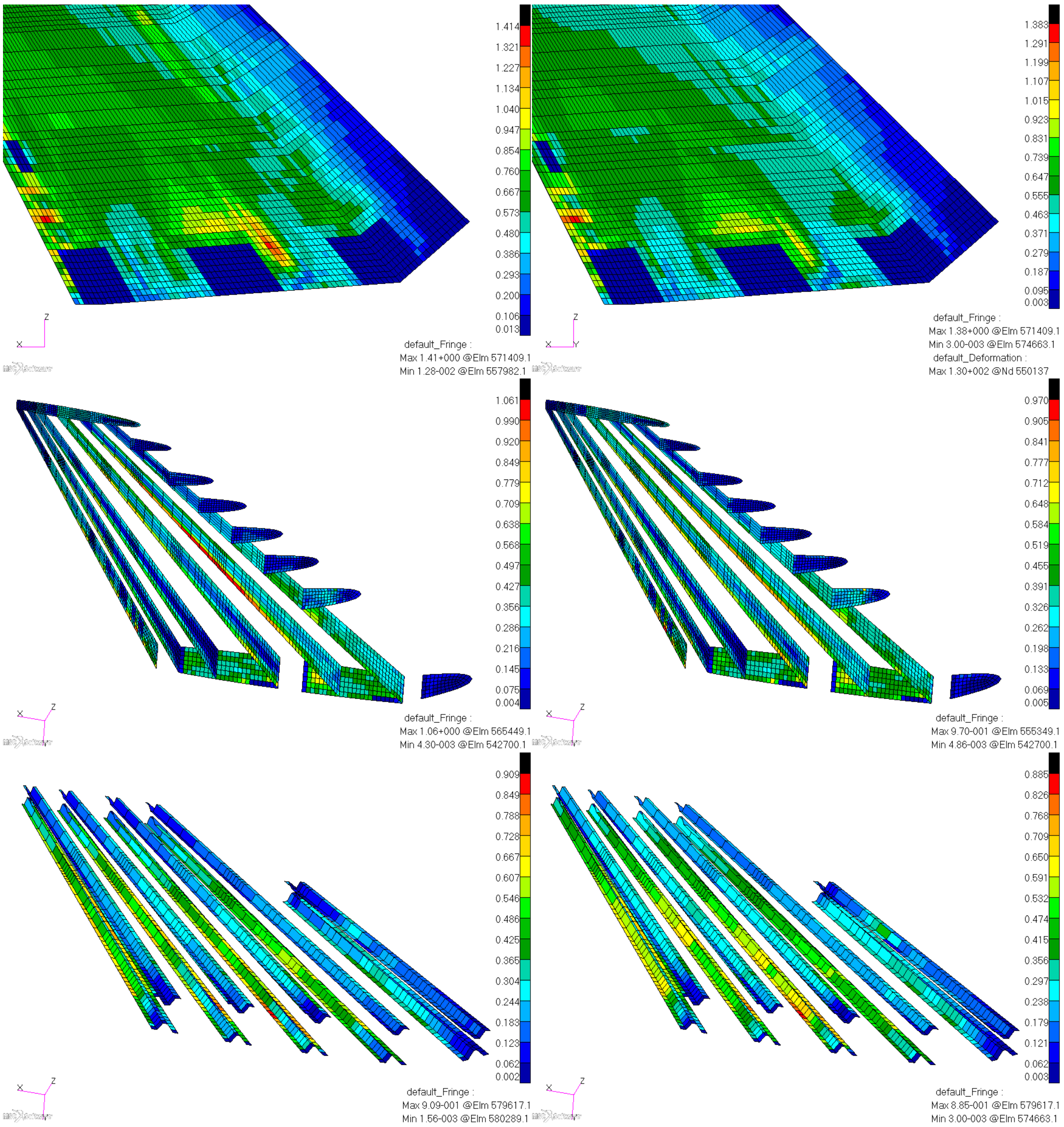
1.414
1.321
1.227
1.134
1.040
0.947
0.854
0.760
0.667
0.573
0.480
0.386
0.293
0.200
0.106
0.013
default_Fringe :
Max 1.41+000 @Elm 571409.1
Min 1.28-002 @Elm 557982.1
1.383
1.291
1.199
1.107
1.015
0.923
0.831
0.739
0.647
0.555
0.463
0.371
0.279
0.187
0.095
0.003
default_Fringe :
Max 1.38+000 @Elm 571409.1
Min 3.00-003 @Elm 574663.1
default_Deformation :
Max 1.30+002 @Nd 550137
1.061
0.990
0.920
0.849
0.779
0.709
0.638
0.568
0.497
0.427
0.356
0.286
0.216
0.145
0.075
0.004
default_Fringe :
Max 1.06+000 @Elm 565449.1
Min 4.30-003 @Elm 542700.1
0.970
0.905
0.841
0.777
0.712
0.648
0.584
0.519
0.455
0.391
0.326
0.262
0.198
0.133
0.069
0.005
default_Fringe :
Max 9.70-001 @Elm 555349.1
Min 4.86-003 @Elm 542700.1
0.909
0.849
0.788
0.728
0.667
0.607
0.546
0.486
0.425
0.365
0.304
0.244
0.183
0.123
0.062
0.002
default_Fringe :
Max 9.09-001 @Elm 579617.1
Min 1.56-003 @Elm 580289.1
0.885
0.826
0.768
0.709
0.650
0.591
0.532
0.474
0.415
0.356
0.297
0.238
0.179
0.121
0.062
0.003
default_Fringe :
Max 8.85-001 @Elm 579617.1
Min 3.00-003 @Elm 574663.1
X
Y
Z

Figure 92: Spar model PFA: max FI (SOL 106 vs. SOL 400)

As before, the difference between the two solutions is such as to be able to consider the two analysis equivalent until the FPF. The most stressed area is still located on the compressed side of the skin but this time is more concentrated in the rear area due to thinning of the thickness. The critical area for the spars webs has shifted down, compared to the previous condition, due to the change of the load path, after the removal of the stringers. The ribs still show no particular problems and the stringers present the same concentrations of stress at the upper interface of the central constraint.

11.2.2 FC Verification

The birth of the first crack is very similar to that occurred in the previous model, but at a lower load corresponding to a load factor of:

$$n_{FC} = 2.77$$

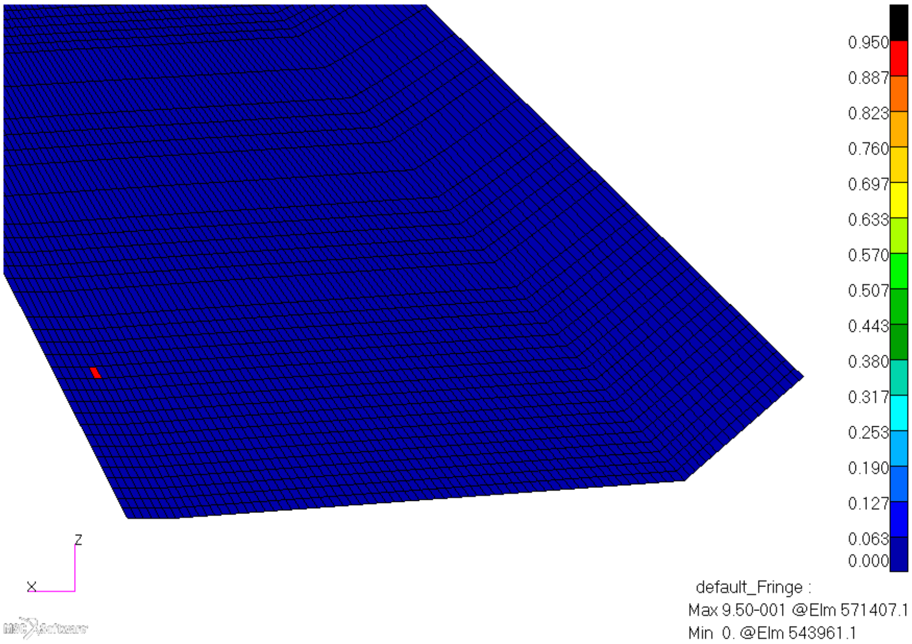
0.950
0.887
0.823
0.760
0.697
0.633
0.570
0.507
0.443
0.380
0.317
0.253
0.190
0.127
0.063
0.000
Z
X
default_Fringe :
Max 9.50-001 @Elm 571407.1
Min 0. @Elm 543961.1

Figure 93: Spar model PFA skin: TD min

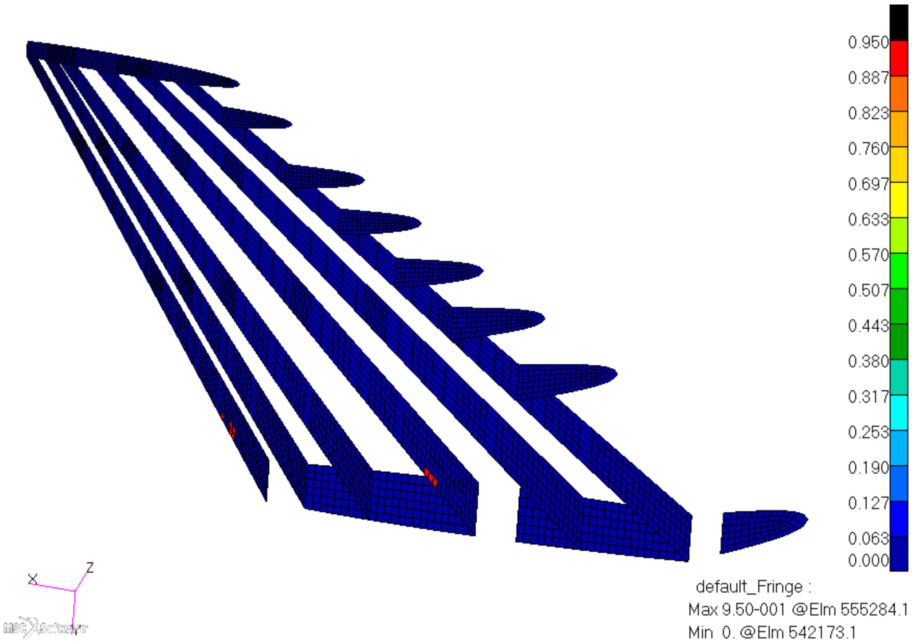
0.950
0.887
0.823
0.760
0.697
0.633
0.570
0.507
0.443
0.380
0.317
0.253
0.190
0.127
0.063
0.000
X
Z
default_Fringe :
Max 9.50-001 @Elm 555284.1
Min 0. @Elm 542173.1

Figure 94: Spar model PFA ribs and spars: TD min

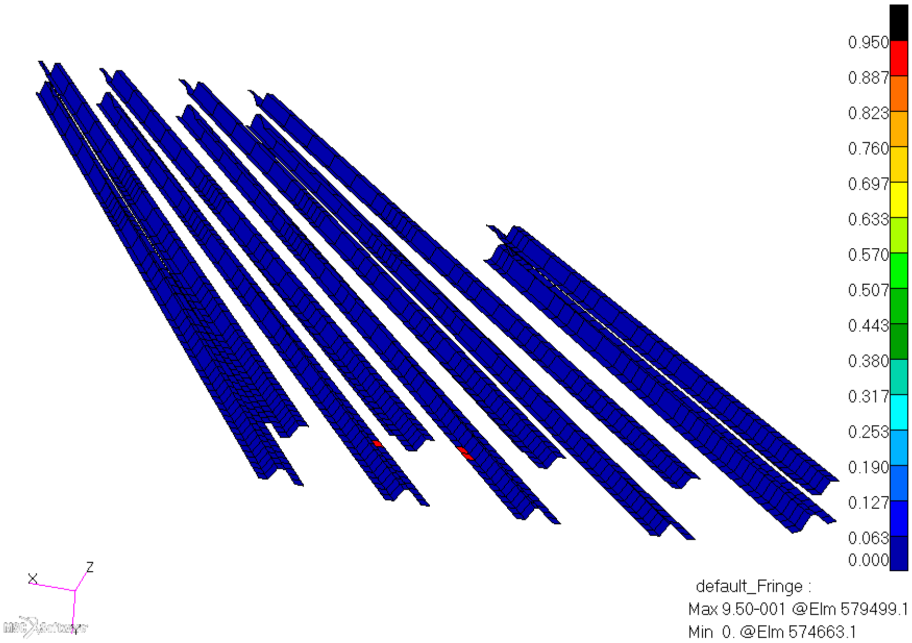

Figure 95: Spar model PFA stringers: TD min

Also the propagation of the damage is quite similar. There was to be expected, since most of the load is supported by the skin that has been modified slightly from the previous model.

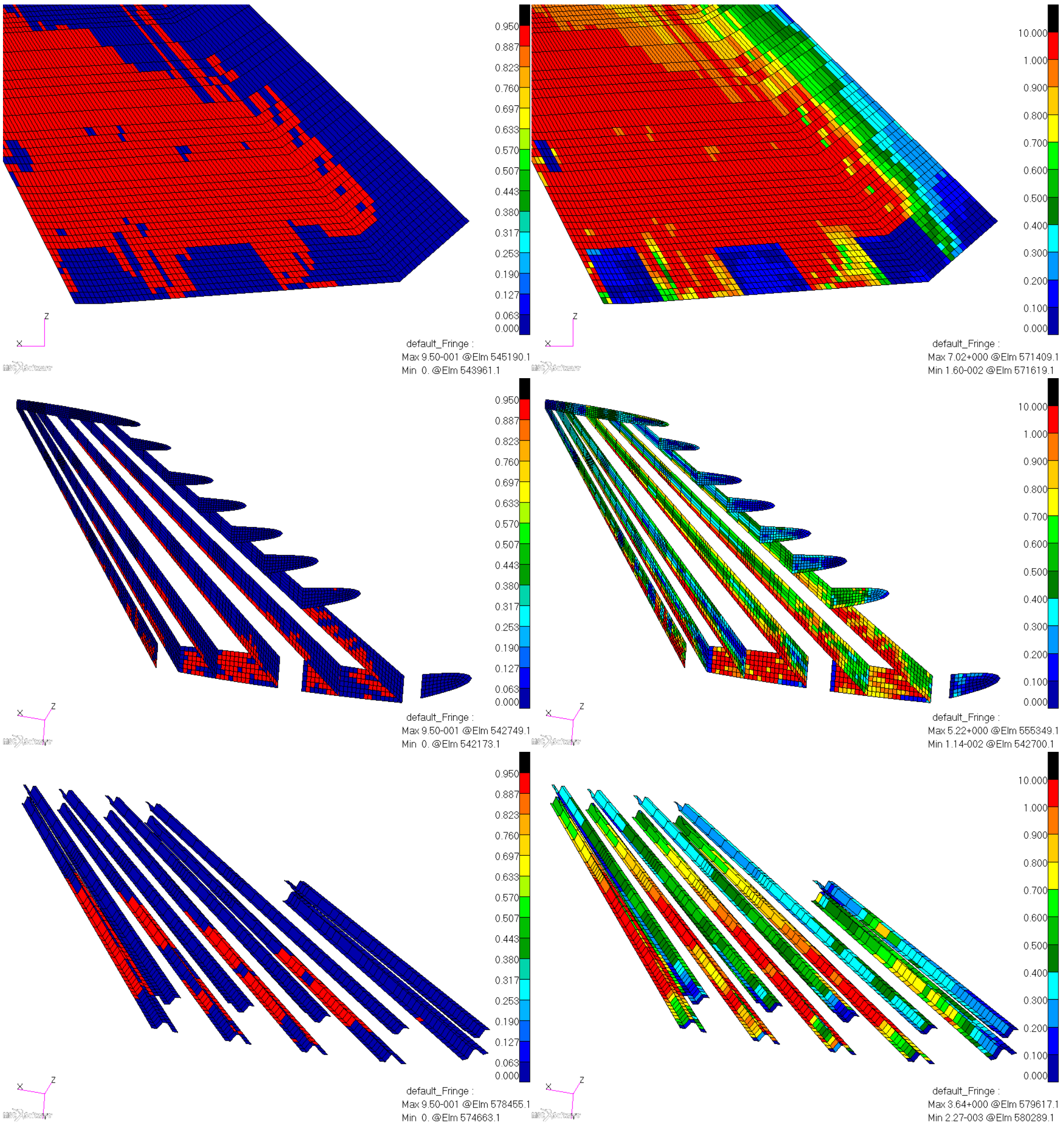
0.950
0.887
0.823
0.760
0.697
0.633
0.570
0.507
0.443
0.380
0.317
0.253
0.190
0.127
0.063
0.000
Z
X
default_Fringe :
Max 9.50-001 @Elm 545190.1
Min 0. @Elm 543961.1
10.000
1.000
0.900
0.800
0.700
0.600
0.500
0.400
0.300
0.200
0.100
0.000
Z
X
default_Fringe :
Max 7.02+000 @Elm 571409.1
Min 1.60-002 @Elm 571619.1
0.950
0.887
0.823
0.760
0.697
0.633
0.570
0.507
0.443
0.380
0.317
0.253
0.190
0.127
0.063
0.000
X
Z
default_Fringe :
Max 9.50-001 @Elm 542749.1
Min 0. @Elm 542173.1
10.000
1.000
0.900
0.800
0.700
0.600
0.500
0.400
0.300
0.200
0.100
0.000
X
Z
default_Fringe :
Max 5.22+000 @Elm 555349.1
Min 1.14-002 @Elm 542700.1
0.950
0.887
0.823
0.760
0.697
0.633
0.570
0.507
0.443
0.380
0.317
0.253
0.190
0.127
0.063
0.000
X
Z
default_Fringe :
Max 9.50-001 @Elm 578455.1
Min 0. @Elm 574663.1
10.000
1.000
0.900
0.800
0.700
0.600
0.500
0.400
0.300
0.200
0.100
0.000
X
Z
default_Fringe :
Max 3.64+000 @Elm 579617.1
Min 2.27-003 @Elm 580289.1

Figure 96: Spar model PFA: propagation of damage

Once again it is emphasized that the composite material is not exploited to its full capacity with the criterion of the FPF, contrary to what happens with the criterion of PFA.

11.3 Buckling Analysis

The thinning of the rear spar caps and the removal of the stringers have considerably reduced the stiffness of the panels and also the global stiffness of the structure. This has accentuated the problem of instability, greatly reducing the critical load.
In order to demonstrate the potential of the PFA criterion, has been decided to lower the threshold of instability, up to the limit load.
The buckling analysis, performed at the LL, has led to the following results.

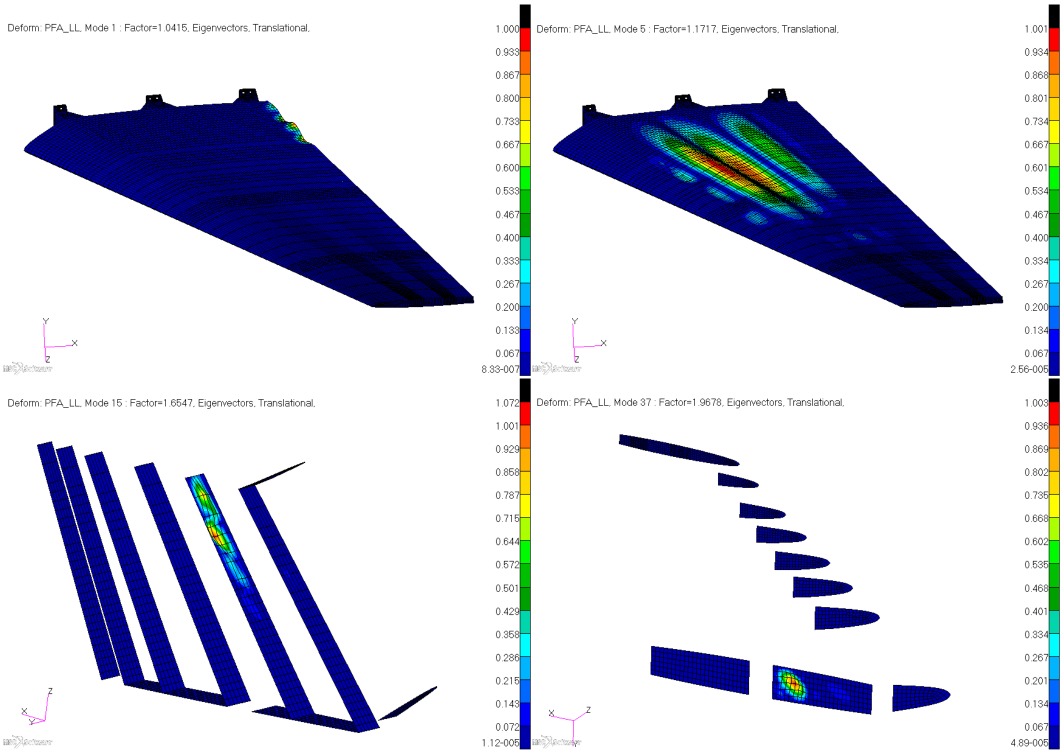
Deform: PFA_LL, Mode 1 : Factor=1.0415, Eigenvectors, Translational.
1.000
0.933
0.867
0.800
0.733
0.667
0.600
0.533
0.467
0.400
0.333
0.267
0.200
0.133
0.067
8.33-007
Deform: PFA_LL, Mode 5 : Factor=1.1717, Eigenvectors, Translational.
1.001
0.934
0.868
0.801
0.734
0.667
0.601
0.534
0.467
0.400
0.334
0.267
0.200
0.134
0.067
2.56-005
Deform: PFA_LL, Mode 15 : Factor=1.6547, Eigenvectors, Translational.
1.072
1.001
0.929
0.858
0.787
0.715
0.644
0.572
0.501
0.429
0.358
0.286
0.215
0.143
0.072
1.12-005
Deform: PFA_LL, Mode 37 : Factor=1.9678, Eigenvectors, Translational.
1.003
0.936
0.869
0.802
0.735
0.668
0.602
0.535
0.468
0.401
0.334
0.267
0.201
0.134
0.067
4.89-005

Figure 97: Spar model PFA: buckling

As before the rear free edge is the first subject to instability. The eigenvalue of the First Buckling (FB) is equal to 1.0415, meaning that the critical load is almost equal to the Limit Load. The panels are the second components which go in buckling, but unlike before it is no longer a local buckling but a global buckling. Once again the spars webs and the ribs are the last which buckled due to shear instability.

11.4 Conclusion

The modification of the model has led to the curve shown in Figure 98. As can be seen the margin between the FPF and the FC is still considerable. Despite this, it was not possible to further reduce the weight of the structure, both to ensure the stiffness requirement, and to avoid the phenomenon of instability below the limit load.

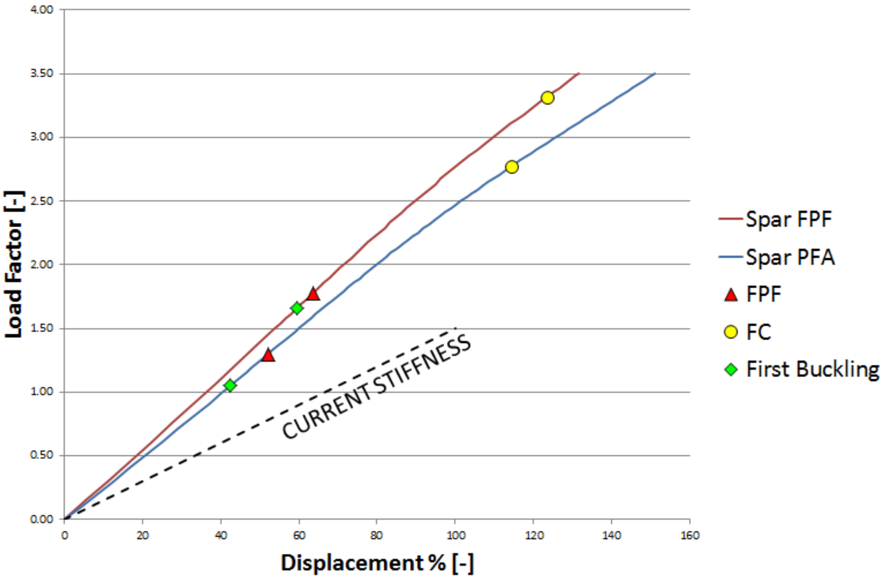

Figure 98: Spar models: load displacement curves

Table 37 summarize the specifications of this model:

Specification	**Spar Model PFA**	**Spar Model FPF**	**Current**
FEM Weight	67.4%	75.7%	100%
Maximum Deflection	64.1%	57.1%	100%

Table 37: Spar model PFA vs. current model specifications

In comparison to the current model the stiffness is increased, in particular of about 35.9%, enough to meet the design specification (increase in stiffness of 30%). Compared with the FPF criterion, the weight is further reduced by a quantity not negligible passing from a weight saving of 24.3% to 32.6%.
The deformed of the model is reported in the following figure.

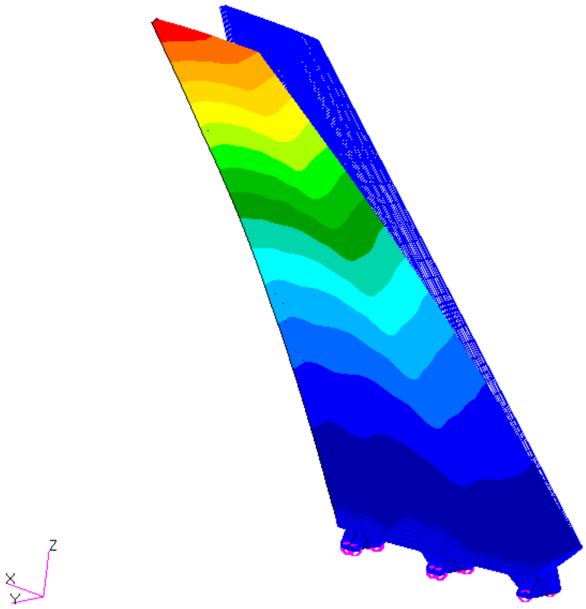

Figure 99: Spar model PFA deformed: maximum deflection 64.1%

The displacements of the whole structure are reported in the following table and figure.

Nodes		Δy
Leading Edge	1	0.0%
	3	4.5%
	5	12.6%
	7	24.1%
	9	38.4%
	11	55.0%
Trailing Edge	2	0.0%
	4	4.8%
	6	12.8%
	8	24.9%
	10	41.5%
	12	60.7%

Table 38: Spar model PFA: nodes displacement

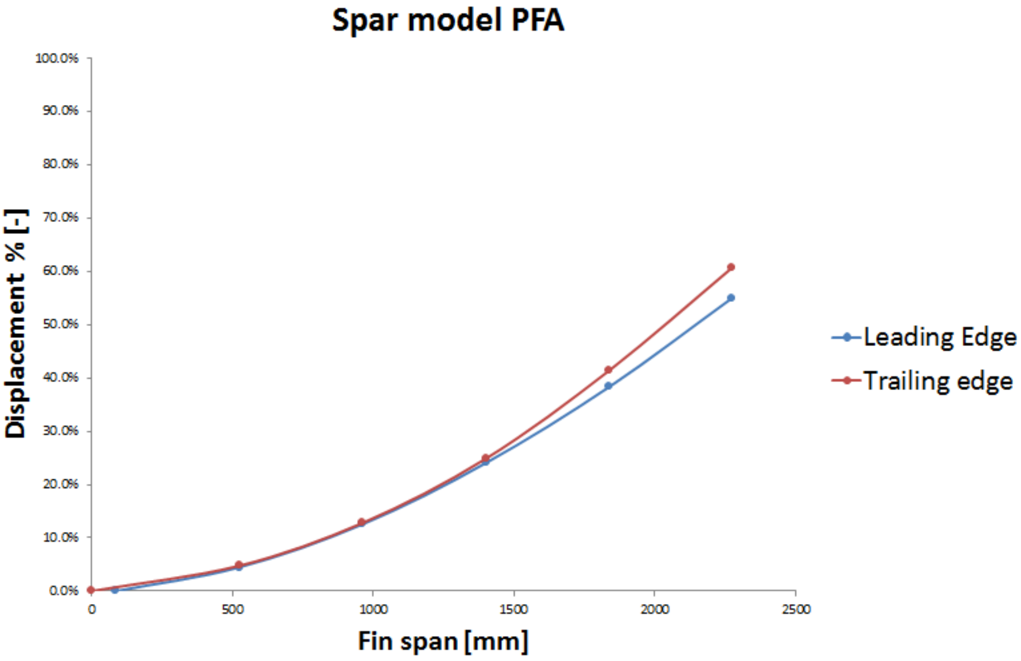

Figure 100: Spar model PFA: nodes displacement

12 Sandwich Model FPF

12.1 General Description

The sandwich model, mainly consists of full depth sandwich panels, divided by 5 ribs and 4 spars. In addition to the root and the end ribs, there are three central ribs suitable for transmitting the load from the three hinges to the fin box, and, like the previous model, there are the shape ribs of the leading edge. The sandwich panels of the root are shaped to not interfere with the junctions. The aerodynamic surfaces and the machined parts have remained unchanged.

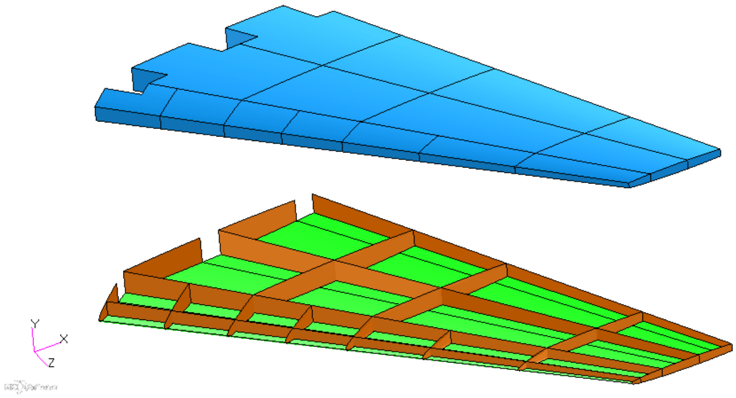

Figure 101: Sandwich model FPF cutaways

The starting model has been derived from the previous one by replacing the longitudinal elements, with ribs and sandwiches. After a certain number of iterations has been obtained the final model, for the criterion of FPF, with the following thickness distribution.

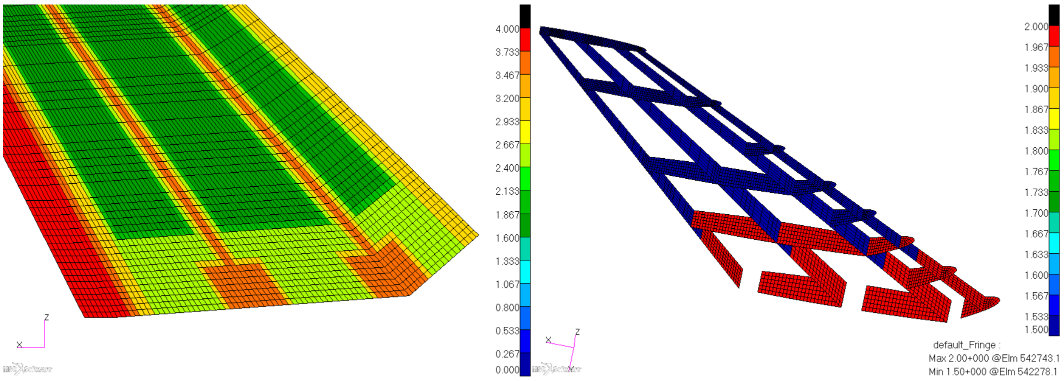
4.000
3.733
3.467
3.200
2.933
2.667
2.400
2.133
1.867
1.600
1.333
1.067
0.800
0.533
0.267
0.000
Z
X
2.000
1.967
1.933
1.900
1.867
1.833
1.800
1.767
1.733
1.700
1.667
1.633
1.600
1.567
1.533
1.500
Z
X
default_Fringe :
Max 2.00+000 @Elm 542743.1
Min 1.50+000 @Elm 542278.1

Figure 102: Sandwich model FPF thickness distribution

The lamination is the same used as far (see sub. 9.2.4).

12.2 Static Analysis and SOL 400

12.2.1 FI Verification

Figure 103 shows the comparison of the trend of the failure index obtained from a nonlinear static analysis and a progressive failure analysis, at ultimate load.
As can be seen the FI is close to unity, which means that the FPF load correspond to the UL with a load factor equal to:

$$n_{FPF} = 1.50$$

Unlike before, to speed up the analysis, it was decided to exclude the joint areas while performing the PFA. This is the reason why these zones are displayed in black.

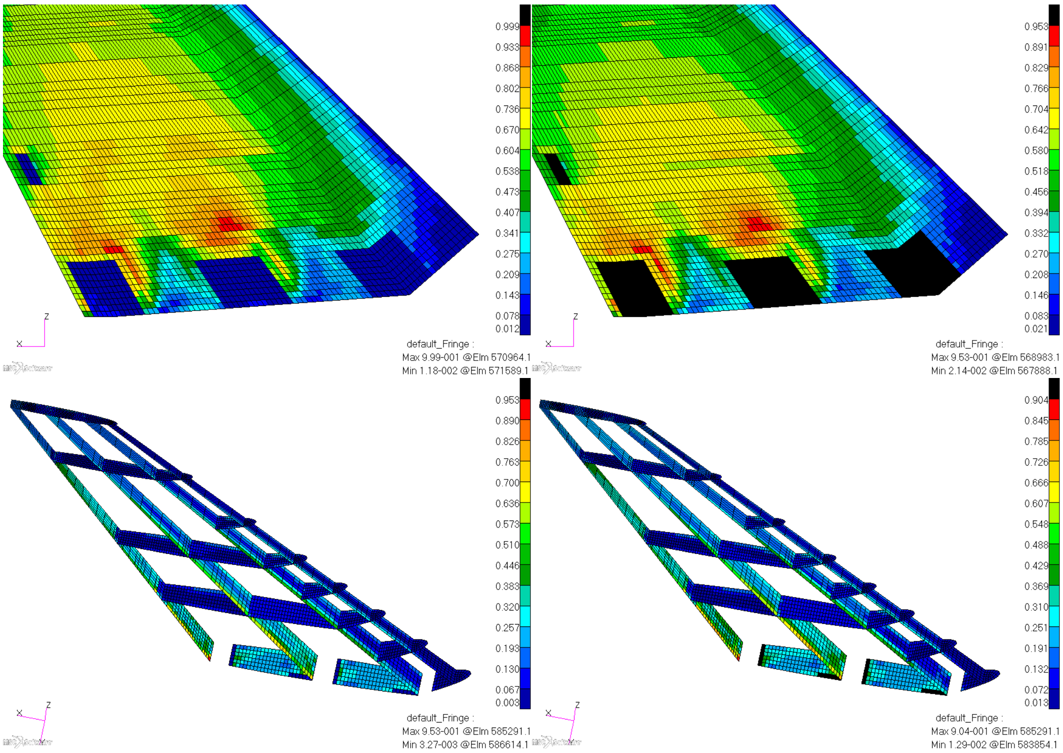
0.999
0.933
0.868
0.802
0.736
0.670
0.604
0.538
0.473
0.407
0.341
0.275
0.209
0.143
0.078
0.012
default_Fringe :
Max 9.99-001 @Elm 570964.1
Min 1.18-002 @Elm 571589.1
0.953
0.891
0.829
0.766
0.704
0.642
0.580
0.518
0.456
0.394
0.332
0.270
0.208
0.146
0.083
0.021
default_Fringe :
Max 9.53-001 @Elm 568983.1
Min 2.14-002 @Elm 567888.1
0.953
0.890
0.826
0.763
0.700
0.636
0.573
0.510
0.446
0.383
0.320
0.257
0.193
0.130
0.067
0.003
default_Fringe :
Max 9.53-001 @Elm 585291.1
Min 3.27-003 @Elm 586614.1
0.904
0.845
0.785
0.726
0.666
0.607
0.548
0.488
0.429
0.369
0.310
0.251
0.191
0.132
0.072
0.013
default_Fringe :
Max 9.04-001 @Elm 585291.1
Min 1.29-002 @Elm 583854.1
x
z

Figure 103: Sandwich model FPF: max FI (SOL 106 vs. SOL 400)

Right away it can be seen that, thanks to the addition of the sandwich, the distribution of FI has changed, becoming much more uniform than that obtained so far. The most stressed area is still located on the compressed side of the skin near the central root constraint where there is a change in thickness. Spars webs and ribs show no particular problems except for an element, connected to the root by the merge, with an high concentrations of stress.

12.2.2 FC Verification

Figure 104 show a drop in the curve just after the FC.

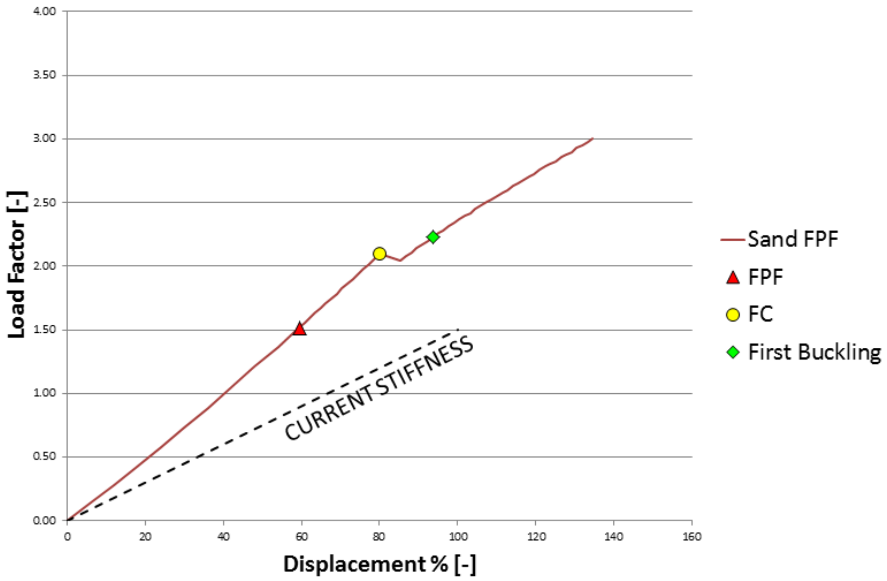

Figure 104: Sandwich model FPF: load displacement curve

This is because the birth of the crack is not progressive and primarly relates to a quite extended area of the skin and of the central spar web, where there is a thinning of the skin, at a load factor of:

$$n_{FC} = 2.10$$

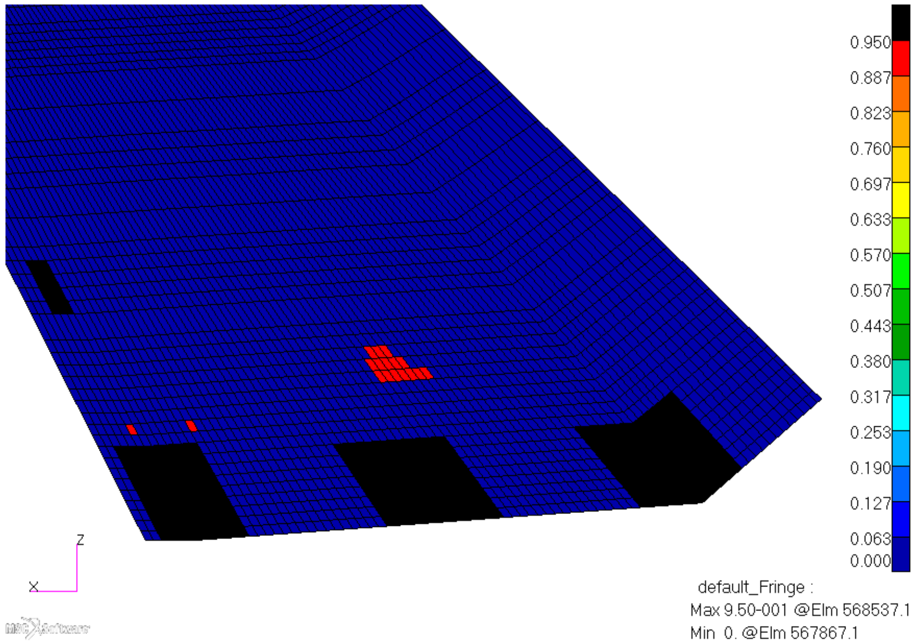
0.950
0.887
0.823
0.760
0.697
0.633
0.570
0.507
0.443
0.380
0.317
0.253
0.190
0.127
0.063
0.000
Z
X
default_Fringe :
Max 9.50-001 @Elm 568537.1
Min 0. @Elm 567867.1

Figure 105: Sandwich model FPF skin: TD min

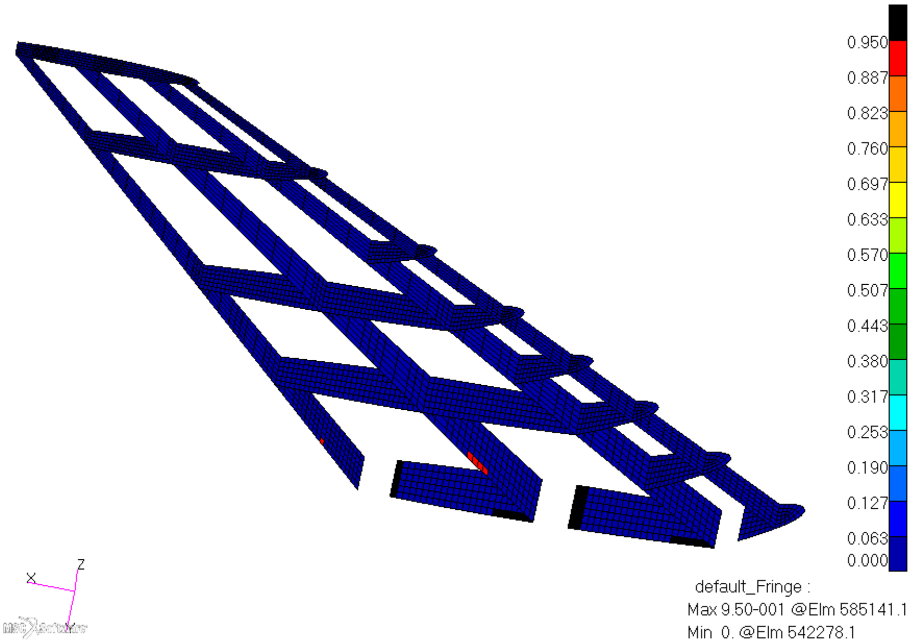
0.950
0.887
0.823
0.760
0.697
0.633
0.570
0.507
0.443
0.380
0.317
0.253
0.190
0.127
0.063
0.000
default_Fringe :
Max 9.50-001 @Elm 585141.1
Min 0. @Elm 542278.1
Z
X

Figure 106: Sandwich model FPF ribs and spars: TD min

As can be seen from the following figure the propagation of the damage is not as extensive as has happened in the spar model because the distance between FPF and FC, in terms of load factor, is much lower (margin between the FPF and FC of $n_{FC} - n_{FPF} = 0.6$).

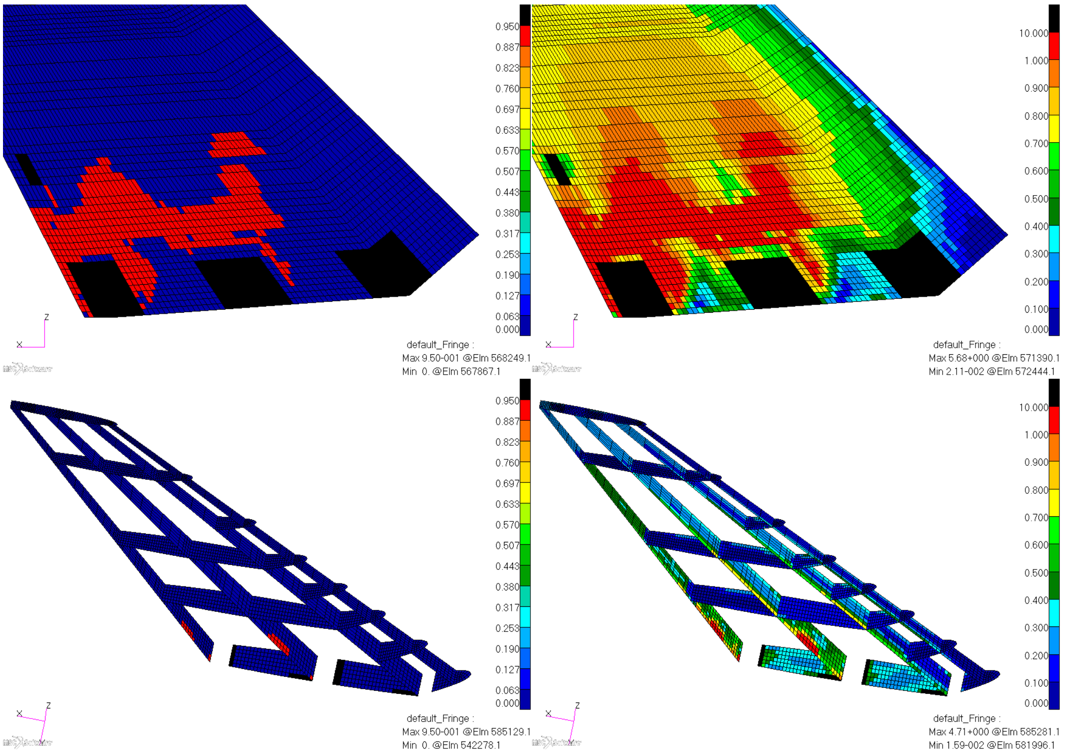
default_Fringe :
Max 9.50-001 @Elm 568249.1
Min 0. @Elm 567867.1
default_Fringe :
Max 5.68+000 @Elm 571390.1
Min 2.11-002 @Elm 572444.1
default_Fringe :
Max 9.50-001 @Elm 585129.1
Min 0. @Elm 542278.1
default_Fringe :
Max 4.71+000 @Elm 585281.1
Min 1.59-002 @Elm 581996.1
10.000
1.000
0.900
0.800
0.700
0.600
0.500
0.400
0.300
0.200
0.100
0.000

Figure 107: Sandwich model FPF: propagation of damage

12.2.3 Honeycomb Verification

In reference to what is explained in the subsection 9.3 we are going to check the honeycomb.

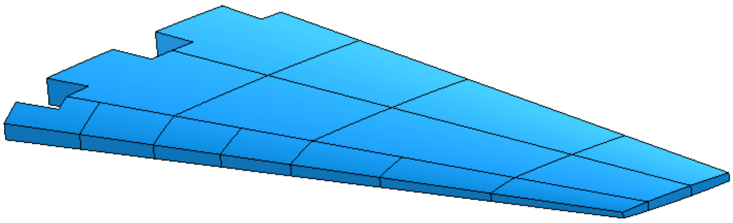

Figure 108: Sandwich model FPF: full depth honeycomb

Referring now to the Table 26 and making the proper conversions for density ρ in kg/mm^3, and elastic modulus E and allowable values σ, τ in MPa is obtained:

	ρ	E_T	E_L	E_W	σ_T	τ_L	τ_W
HRH-10-1/8-1.8	2.9e-8	55.16	26.20	10.34	0.79	0.62	0.34
HRH-10-1/8-3.0	4.8e-8	137.89	44.82	24.13	2.24	1.21	0.69

Table 39: Honeycomb: elastic modulus and allowable values

By applying the correction factors with respect to temperature and thickness[7], the values given above become

	KDF_t	KDF_T	σ_T^{kd}	τ_L^{kd}	τ_W^{kd}
HRH-10-1/8-1.8	0.700	0.913	0.72	0.42	0.23
HRH-10-1/8-3.0	0.700	0.913	2.04	0.77	0.44

Table 40: Honeycomb: knock down allowable values

For this first configuration it was decided to use only one type of honeycomb, particularly the HRH-10-1/8-3.0.
Knowing the allowable values it is possible to collect the stresses acting on the honeycomb and calculate margins of safety. The following figures show only the section near the root, being the most stressed.

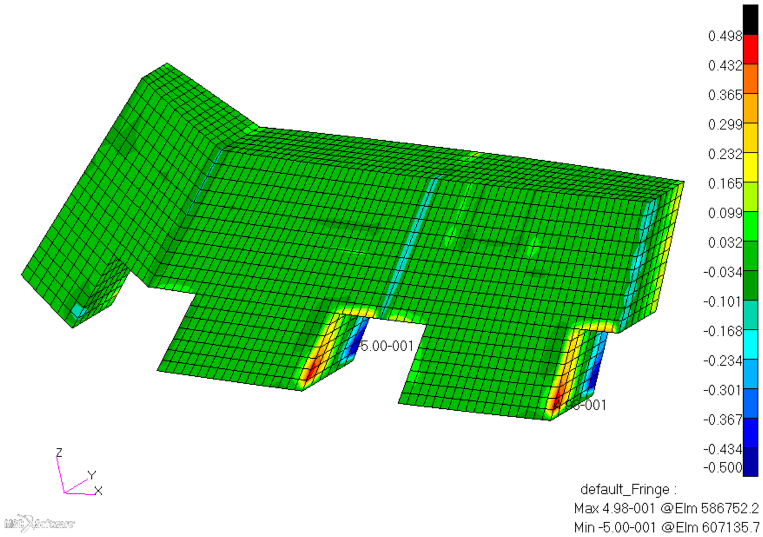
0.498
0.432
0.365
0.299
0.232
0.165
0.099
0.032
-0.034
-0.101
-0.168
-0.234
-0.301
-0.367
-0.434
-0.500
-5.00-001
4.98-001
Z
Y
X
default_Fringe :
Max 4.98-001 @Elm 586752.2
Min -5.00-001 @Elm 607135.7

Figure 109: Sandwich model FPF: stress in T-direction

---

[7] For simplicity, it was considered the maximum distance between the skins

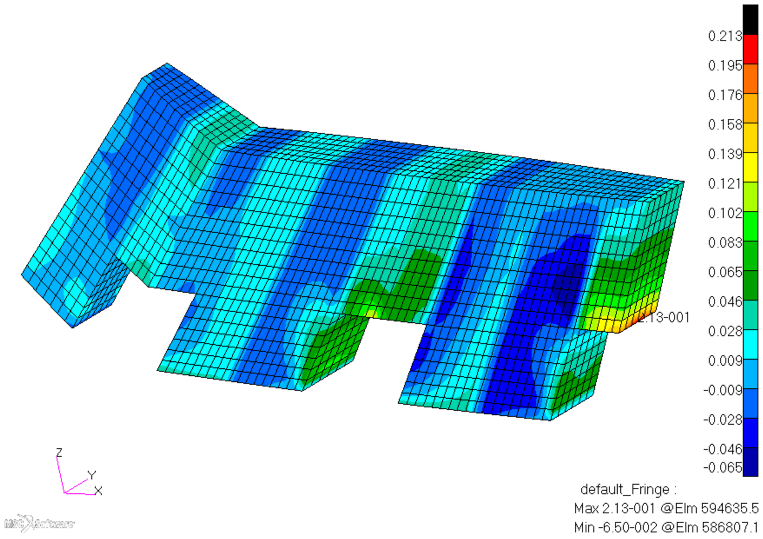
0.213
0.195
0.176
0.158
0.139
0.121
0.102
0.083
0.065
0.046
0.028
0.009
-0.009
-0.028
-0.046
-0.065
2.13-001
Z
Y
X
default_Fringe :
Max 2.13-001 @Elm 594635.5
Min -6.50-002 @Elm 586807.1

Figure 110: Sandwich model FPF: stress in L-direction

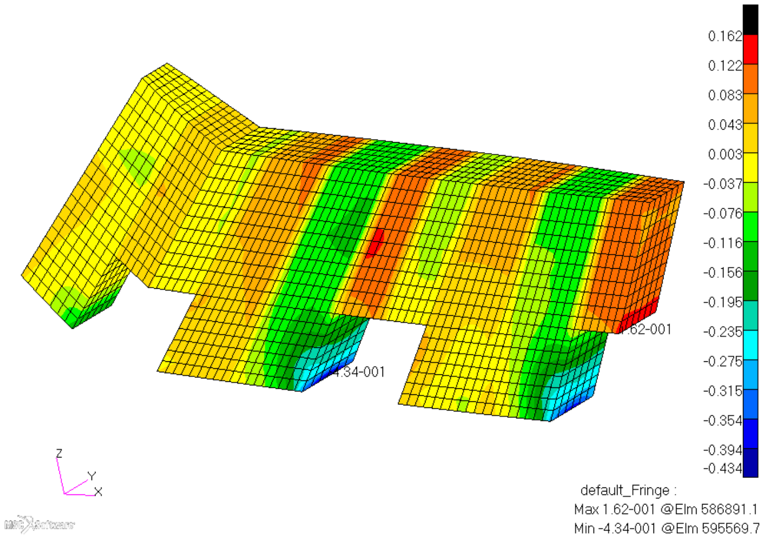
0.162
0.122
0.083
0.043
0.003
-0.037
-0.076
-0.116
-0.156
-0.195
-0.235
-0.275
-0.315
-0.354
-0.394
-0.434
1.62-001
-4.34-001
Z
Y
X
default_Fringe :
Max 1.62-001 @Elm 586891.1
Min -4.34-001 @Elm 595569.7

Figure 111: Sandwich model FPF: stress in W-direction

	σ_T^{max}	σ_T^{min}	σ_L^{max}	σ_L^{min}	σ_W^{max}	σ_W^{min}
HRH-10-1/8-3.0	0.498	-0.500	0.213	-0.065	0.162	-0.434

Table 41: Sandwich model FPF: stresses acting on the honeycomb

By comparing these values with the allowable in Table 40 it is possible to calculate the margins of safety:

	σ_T^{max}	σ_T^{min}	σ_L^{max}	σ_L^{min}	σ_W^{max}	σ_W^{min}
HRH-10-1/8-3.0	3.10	3.09	2.63	10.89	1.72	0.02

Table 42: Sandwich model FPF: margin of safety

As can be seen there is a MS very close to zero. This is due to a stress concentration, in the area of contact between the honeycomb and the central constraint (see. Figure 111), caused by the type of modeling. Given that, the result is totally acceptable.

12.3 Buckling Analysis

The buckling analysis, performed at the UL, has led to the following results.

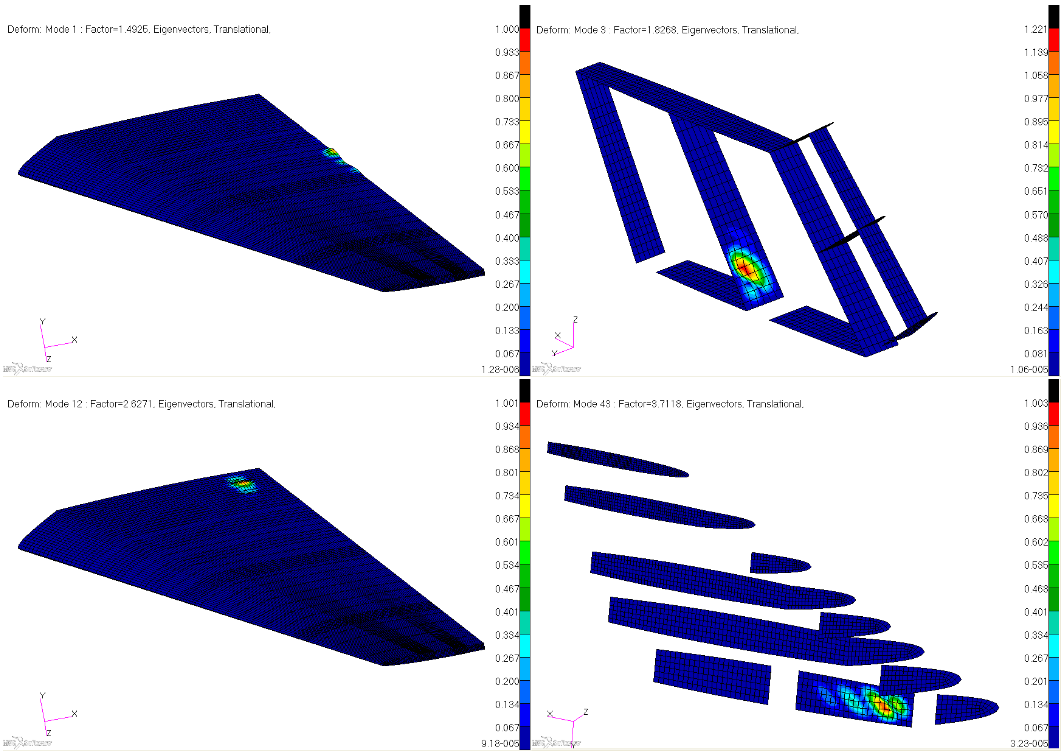
Deform: Mode 1 : Factor=1.4925, Eigenvectors, Translational.
1.000
0.933
0.867
0.800
0.733
0.667
0.600
0.533
0.467
0.400
0.333
0.267
0.200
0.133
0.067
1.28-006
Deform: Mode 3 : Factor=1.8268, Eigenvectors, Translational.
1.221
1.139
1.058
0.977
0.895
0.814
0.732
0.651
0.570
0.488
0.407
0.326
0.244
0.163
0.081
1.06-005
Deform: Mode 12 : Factor=2.6271, Eigenvectors, Translational.
1.001
0.934
0.868
0.801
0.734
0.667
0.601
0.534
0.467
0.401
0.334
0.267
0.200
0.134
0.067
9.18-005
Deform: Mode 43 : Factor=3.7118, Eigenvectors, Translational.
1.003
0.936
0.869
0.802
0.735
0.668
0.602
0.535
0.468
0.401
0.334
0.267
0.201
0.134
0.067
3.23-005
X
Y
Z

Figure 112: Sandwich model FPF: buckling

The rear free edge is the first subject to instability. The eigenvalue of the First Buckling (FB) is equal to 1.4925, meaning that the critical load is about the 49% greater than the ultimate load ($n_{FB} = 2.23$).
The spars are the second components which go in buckling, subjected to shear instability since the waves are elliptical and inclined at 45°.
The third components subjected to compression instability, are the panels of the junction, not sustained by the sandwich, and finally the root rib subjected to shear instability.

12.4 Conclusion

Once completed all the controls, the verified model presents the following specifications.

Specification	**Sandwich Model FPF**	**Current**
FEM Weight	81.1%	100%
Maximum Deflection	65.2%	100%

Table 43: Sandwich model FPF vs. current model specifications

As expected the transition to the sandwich configuration has led to an increase in weight compared to the spar configuration. This, however, has brought the advantage of increasing the threshold of instability.
Also the stiffness has decreased as the contribution of the sandwich does not have the same effect of the addition of the stringers. Compared to the current configuration the stiffness is increased, in particular of about 34.8%, above the design specification, which provided for an increase in stiffness of 30%.
The reduction of weight, in terms of the FEM model, is considerable, with a saving which is around 18.9%.
The deformed of the model is reported in Figure 113. The trend of displacements is more regular than the spar model.

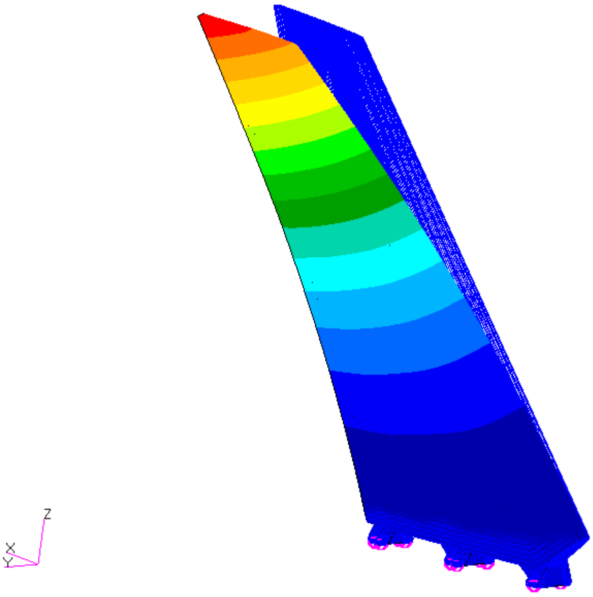

Figure 113: Sandwich model FPF deformed: maximum deflection 65.2%

The displacements of the whole structure are reported in the following table and figure.

Nodes		Δy
Leading Edge	1	0.0%
	3	2.5%
	5	8.6%
	7	19.5%
	9	35.2%
	11	54.9%
Trailing Edge	2	0.0%
	4	5.5%
	6	14.4%
	8	27.4%
	10	43.9%
	12	62.3%

Table 44: Sandwich model FPF: nodes displacement

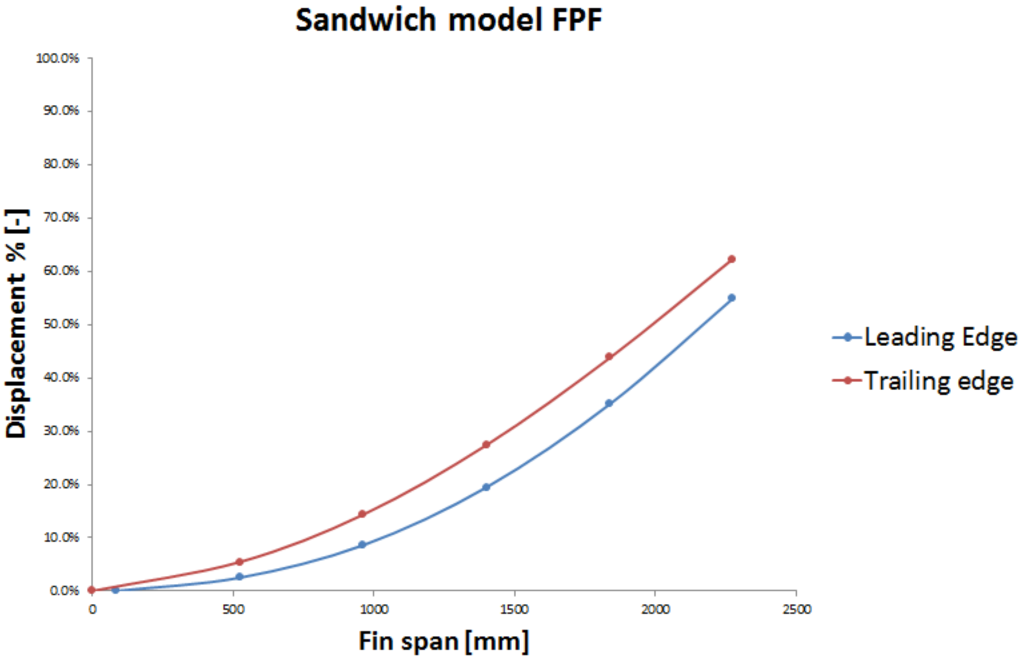

Figure 114: Sandwich model FPF: nodes displacement

13 Sandwich Model PFA

13.1 General Description

The final configuration has been obtained by replacing part of the honeycomb with one of lower density and by reducing the thickness of the skin. Ribs, Spars webs and machined parts have remained unchanged.

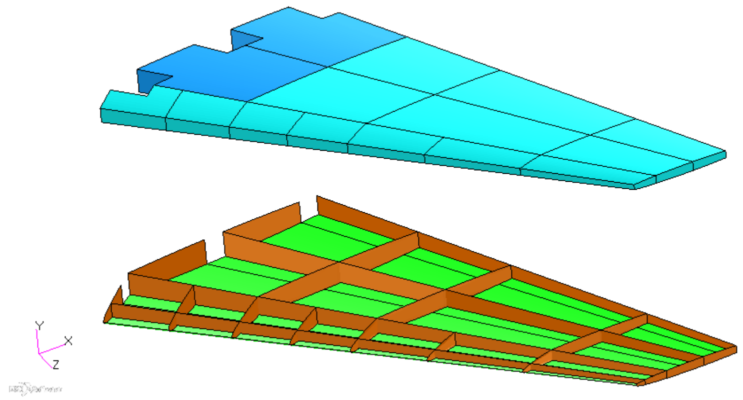

Figure 115: Sandwich model PFA cutaways

Sandwich Model FPF

Components	**FEM Weight**
Ribs	2.8%
Honeycomb	18.8%
Spars webs	4.4%
Skins	38.4%
Machined Parts	16.7%
Total	81.1%

Sandwich Model PFA

Components	**FEM Weight**
Ribs	2.8%
Honeycomb	11.3%
Spars webs	4.4%
Skins	30.9%
Machined Parts	16.7%
Total	66.1%

Table 45: Sandwich model FPF vs. sandwich model PFA: weight

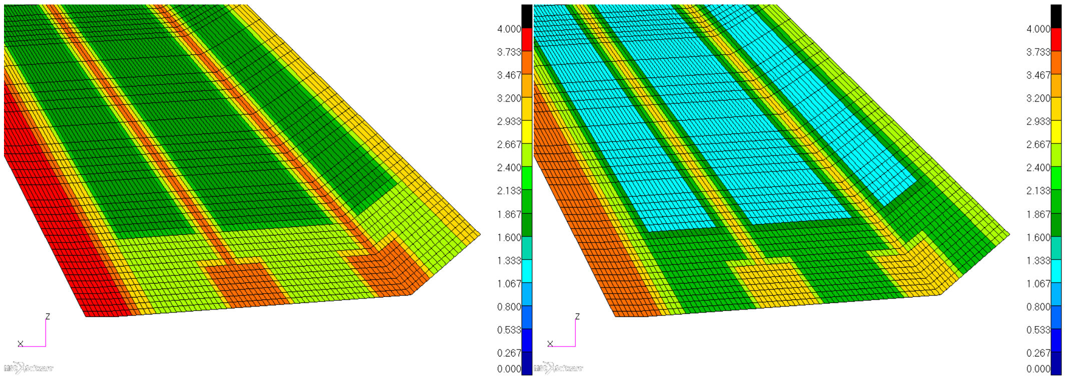

Figure 116: Sandwich model FPF vs. sandwich model PFA: thickness

13.2 Static Analysis and SOL 400

13.2.1 FI Verification

Once again, to verify that the composite components are dimensioned correctly it is necessary to check if all the values of the FI are less than 1 at the limit load. As done previously is necessary to look for the load step in which the FI is close to unity, which correspond to a load factor equal to:

$$n_{FPF} = 1.26$$

This mean that the FPF will take place in a range between LL and UL, as required by the specification. Figure 117 shows the comparison of the trend of the failure index obtained from a nonlinear static analysis and a progressive failure analysis, at ultimate load.

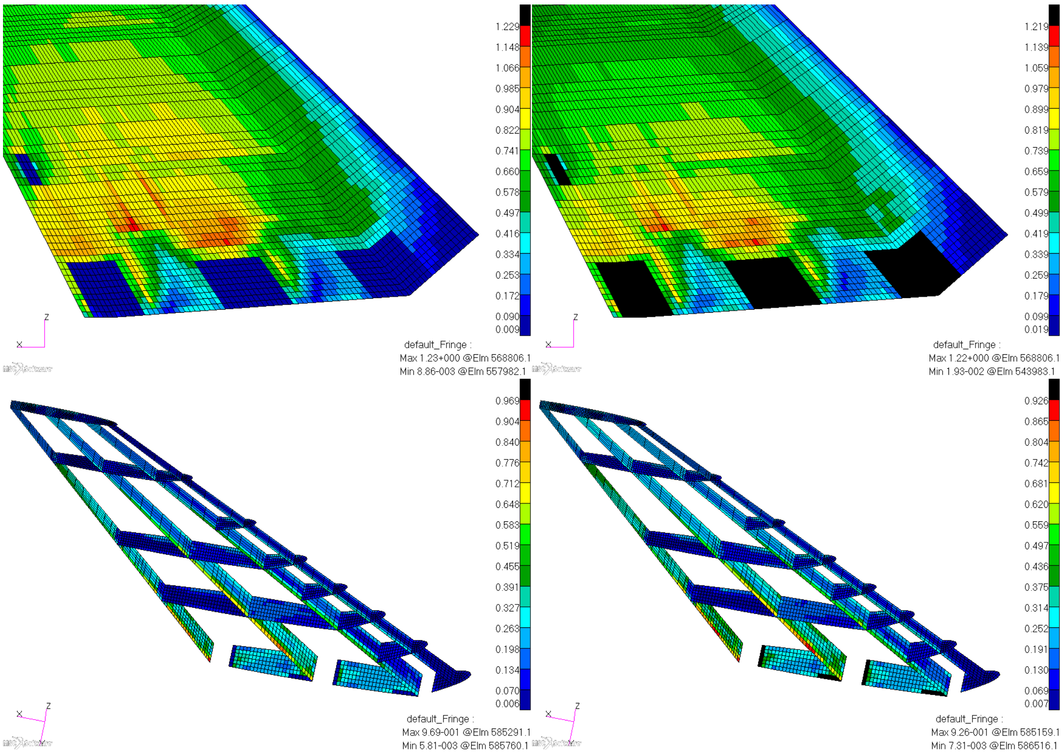
1.229
1.148
1.066
0.985
0.904
0.822
0.741
0.660
0.578
0.497
0.416
0.334
0.253
0.172
0.090
0.009
default_Fringe :
Max 1.23+000 @Elm 568806.1
Min 8.86-003 @Elm 557982.1
1.219
1.139
1.059
0.979
0.899
0.819
0.739
0.659
0.579
0.499
0.419
0.339
0.259
0.179
0.099
0.019
default_Fringe :
Max 1.22+000 @Elm 568806.1
Min 1.93-002 @Elm 543983.1
0.969
0.904
0.840
0.776
0.712
0.648
0.583
0.519
0.455
0.391
0.327
0.263
0.198
0.134
0.070
0.006
default_Fringe :
Max 9.69-001 @Elm 585291.1
Min 5.81-003 @Elm 585760.1
0.926
0.865
0.804
0.742
0.681
0.620
0.559
0.497
0.436
0.375
0.314
0.252
0.191
0.130
0.069
0.007
default_Fringe :
Max 9.26-001 @Elm 585159.1
Min 7.31-003 @Elm 586516.1
x
z

Figure 117: Sandwich model PFA: max FI (SOL 106 vs. SOL 400)

The most stressed area is still located on the compressed side of the skin but this time near the rear root constraint where there is a change in thickness. Also the spars webs show an high concentrations of stress above the constraint. Ribs show no particular problems.

13.2.2 FC Verification

The birth of the crack, in the lightened model, is located at a load factor greater than the previous configuration, due to the new load path on the skin.
The new distribution of thicknesses has moved most of the load on the spar's cap which has a greater thickness than the skin of the previous model where the crack was born.

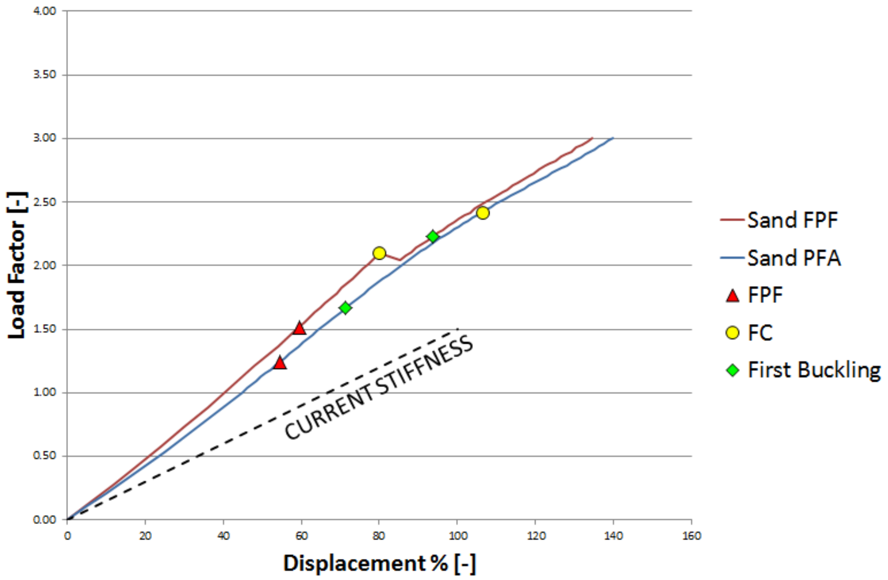

Figure 118: Sandwich models: load displacement curves

The First Crack occurs at a load factor of:

$$n_{FC} = 2.42$$

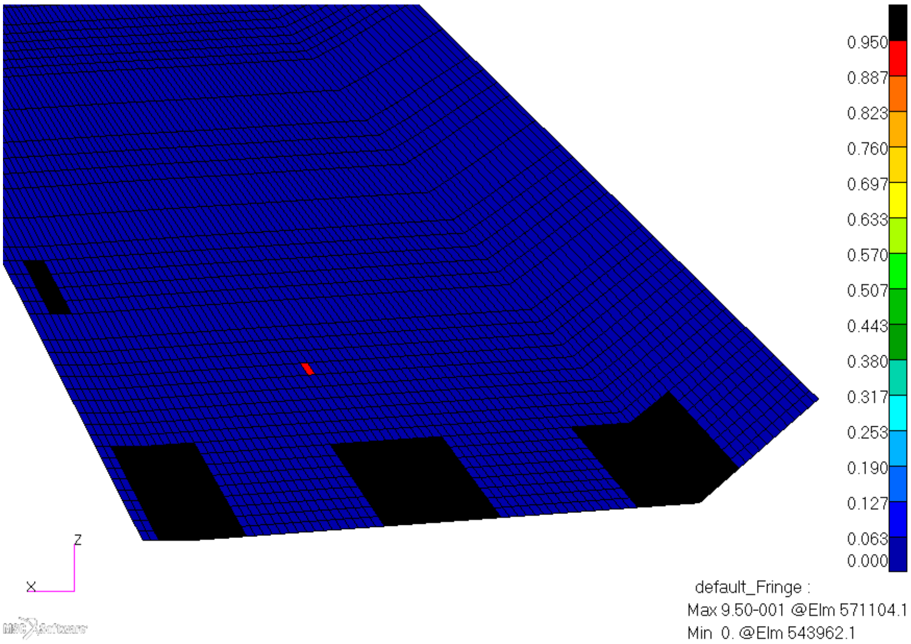
0.950
0.887
0.823
0.760
0.697
0.633
0.570
0.507
0.443
0.380
0.317
0.253
0.190
0.127
0.063
0.000
Z
X
default_Fringe :
Max 9.50-001 @Elm 571104.1
Min 0. @Elm 543962.1

Figure 119: Sandwich model PFA skin: TD min

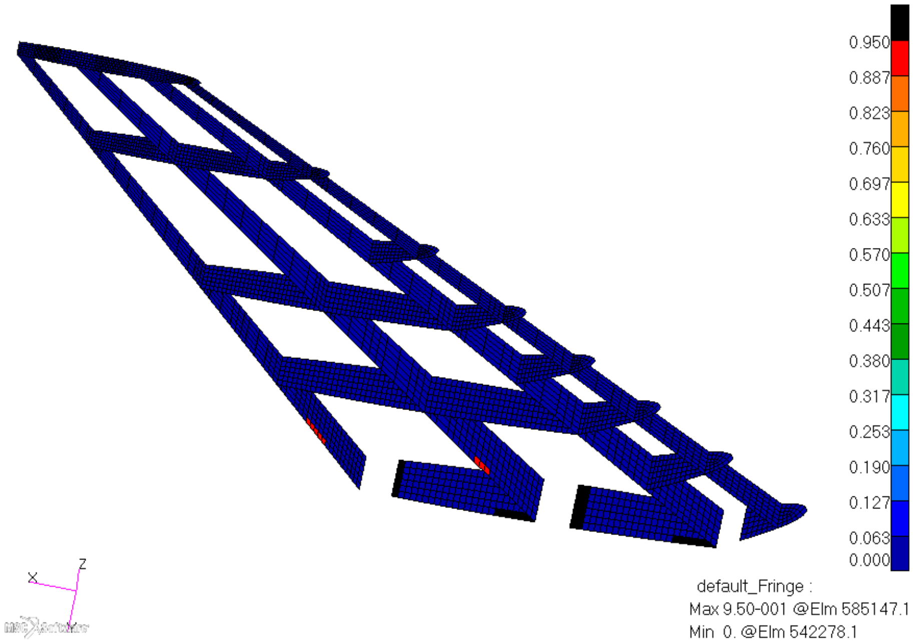
0.950
0.887
0.823
0.760
0.697
0.633
0.570
0.507
0.443
0.380
0.317
0.253
0.190
0.127
0.063
0.000
default_Fringe :
Max 9.50-001 @Elm 585147.1
Min 0. @Elm 542278.1
X
Z

Figure 120: Sandwich model PFA ribs and spars: TD min

Unlike before the propagation of the damage is more extensive than the FPF model because the distance between FPF and FC, in terms of load factor, has increased (margin between the FPF and FC of $n_{FC} - n_{FPF} = 1.16$).

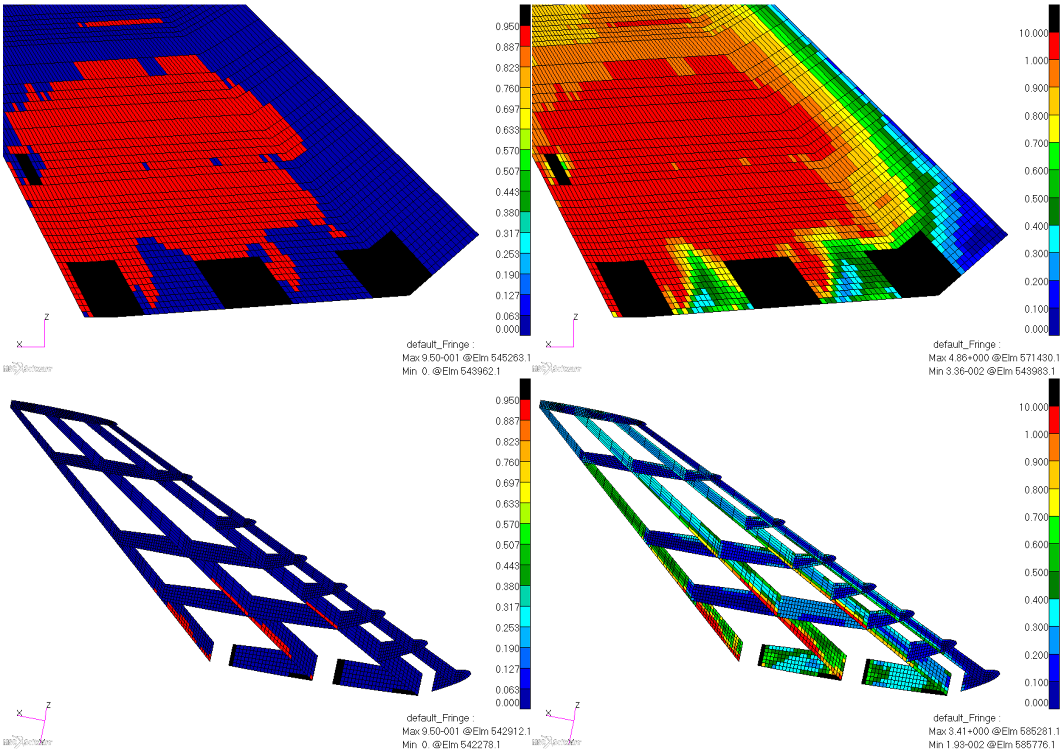
default_Fringe :
Max 9.50-001 @Elm 545263.1
Min 0. @Elm 543962.1
default_Fringe :
Max 4.86+000 @Elm 571430.1
Min 3.36-002 @Elm 543983.1
default_Fringe :
Max 9.50-001 @Elm 542912.1
Min 0. @Elm 542278.1
default_Fringe :
Max 3.41+000 @Elm 585281.1
Min 1.93-002 @Elm 585776.1

Figure 121: Sandwich model PFA: propagation of damage

13.2.3 Honeycomb Verification

For this configuration, it was decided to use two types of honeycomb. In the most stressed area of the root has been maintained that used previously (HRH-10-1/8-3.0), while in the remaining area has been used the one with lower density, particularly the HRH-10-1/8-1.8.

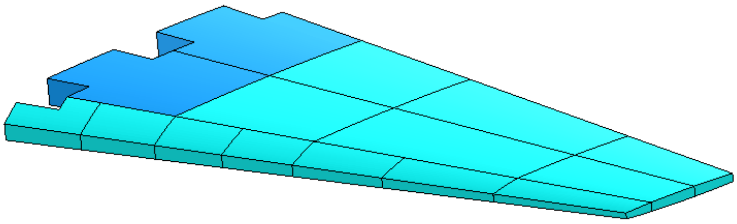

Figure 122: Sandwich model PFA: full depth honeycomb

As done previously in the subsection 12.2.3 we are going to check the honeycomb. The following figures show only the section near the root and the interface between the two types of honeycomb, being the most stressed zones.

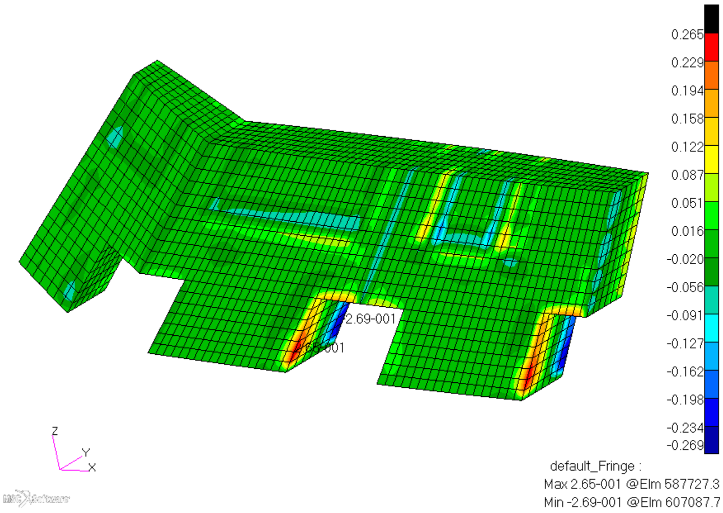

Figure 123: Sandwich model PFA: stress in T-direction

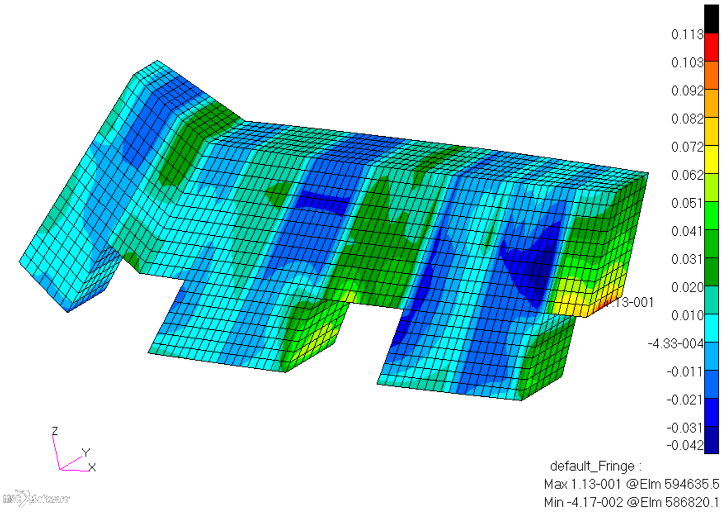

Figure 124: Sandwich model PFA: stress in L-direction

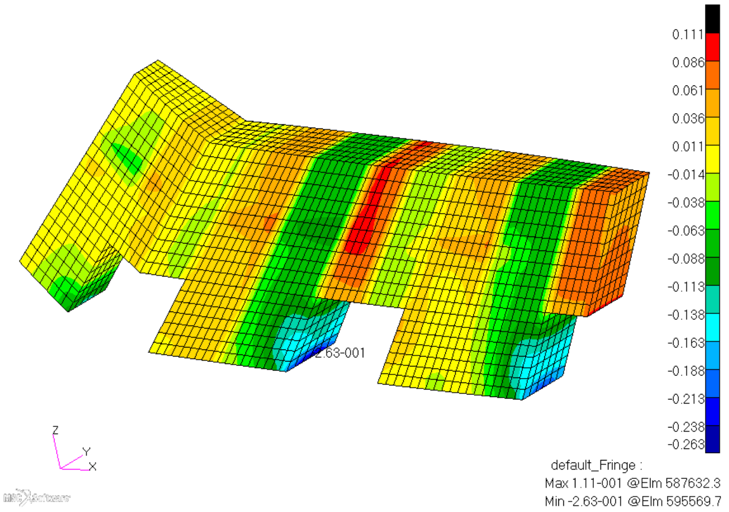

Figure 125: Sandwich model PFA: stress in W-direction

	σ_T^{max}	σ_T^{min}	σ_L^{max}	σ_L^{min}	σ_W^{max}	σ_W^{min}
HRH-10-1/8-1.8	0.120	-0.165	0.041	-0.031	0.111	-0.087
HRH-10-1/8-3.0	0.265	-0.269	0.113	-0.041	0.053	-0.263

Table 46: Sandwich model PFA: stresses acting on the honeycomb

By comparing these values with the allowable in Table 40 it is possible to calculate the margins of safety:

	σ_T^{max}	σ_T^{min}	σ_L^{max}	σ_L^{min}	σ_W^{max}	σ_W^{min}
HRH-10-1/8-1.8	5.01	3.37	8.66	11.77	0.96	1.50
HRH-10-1/8-3.0	6.71	6.60	5.84	17.85	7.32	0.68

Table 47: Sandwich model PFA: margin of safety

This time all the margin are well above the zero so the honeycomb has passed the check.

13.3 Buckling Analysis

The buckling analysis, performed at the UL, has led to the following results.

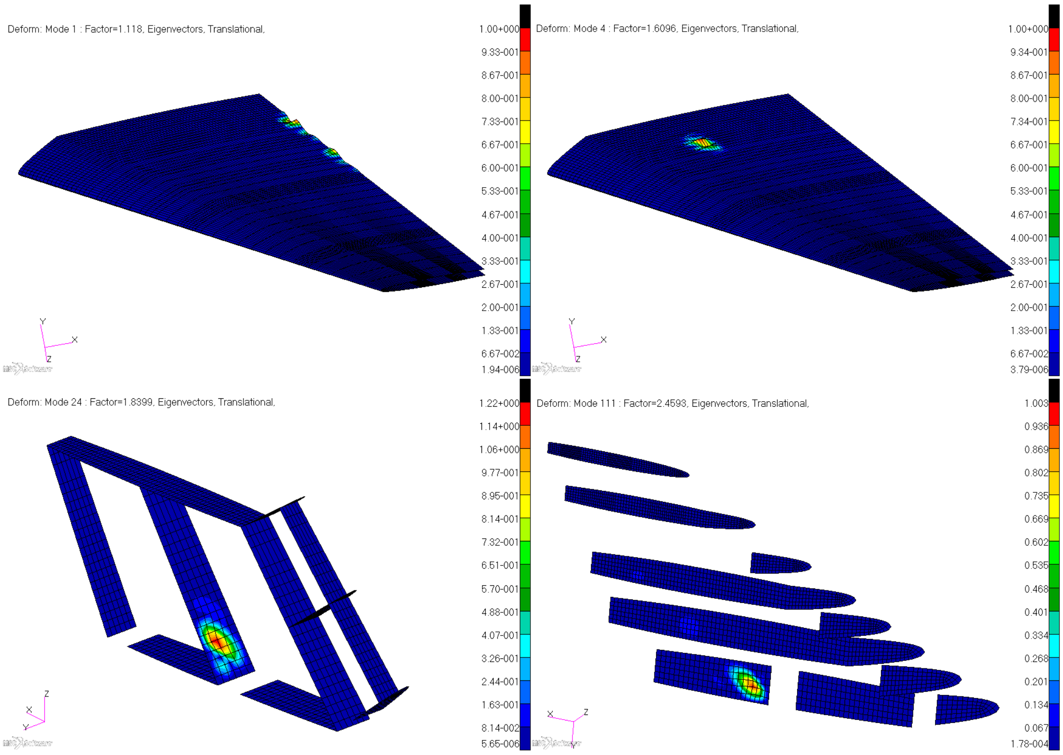
Deform: Mode 1 : Factor=1.118, Eigenvectors, Translational,
1.00+000
9.33-001
8.67-001
8.00-001
7.33-001
6.67-001
6.00-001
5.33-001
4.67-001
4.00-001
3.33-001
2.67-001
2.00-001
1.33-001
6.67-002
1.94-006
Deform: Mode 4 : Factor=1.6096, Eigenvectors, Translational,
1.00+000
9.34-001
8.67-001
8.00-001
7.34-001
6.67-001
6.00-001
5.33-001
4.67-001
4.00-001
3.33-001
2.67-001
2.00-001
1.33-001
6.67-002
3.79-006
Deform: Mode 24 : Factor=1.8399, Eigenvectors, Translational,
1.22+000
1.14+000
1.06+000
9.77-001
8.95-001
8.14-001
7.32-001
6.51-001
5.70-001
4.88-001
4.07-001
3.26-001
2.44-001
1.63-001
8.14-002
5.65-006
Deform: Mode 111 : Factor=2.4593, Eigenvectors, Translational,
1.003
0.936
0.869
0.802
0.735
0.669
0.602
0.535
0.468
0.401
0.334
0.268
0.201
0.134
0.067
1.78-004

Figure 126: Spar model PFA: buckling

The thinning of the rear spar caps has lowered the critical load of instability but keeping it above the ultimate load. The eigenvalue of the First Buckling (FB) is equal to 1.118, meaning that the critical load is 11.8% higher than the UL. The panels are the second components which go in buckling. Once again the spars webs and the ribs are the last which buckled due to shear instability.

13.4 Conclusion

The following table summarize the specifications of this model:

Specification	**Sandwich Model PFA**	**Sandwich Model FPF**	**Current**
FEM Weight	66.1%	81.1%	100%
Maximum Deflection	73.2%	65.2%	100%

Table 48: Sandwich model PFA vs. current model specifications

In comparison to the current model the stiffness is increased, in particular of about 26.8%, not enough to meet the design specification (increase in stiffness of 30%) but, at this level of the design, acceptable and still easily adjustable having available large margins.
Compared with the FPF criterion, the weight is significantly reduced by a quantity not negligible passing from a weight saving of 18.9% to 33.9%.
The deformed of the model is reported in the following figure.

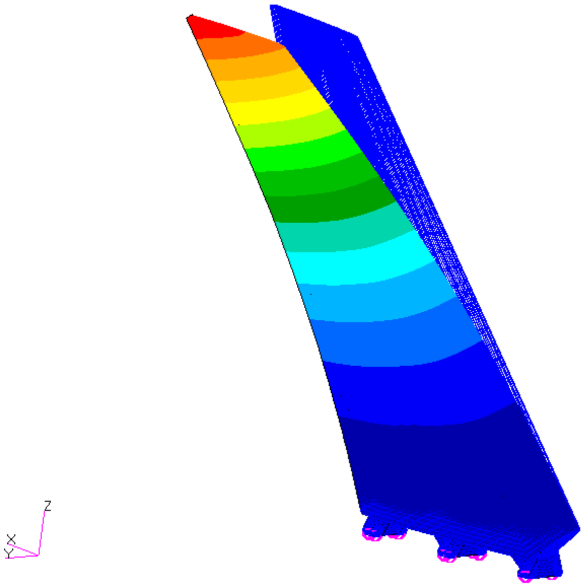

Figure 127: Sandwich model PFA deformed: maximum deflection 73.2%

The displacements of the whole structure are reported in the following table and figure.

Nodes		Δy
Leading Edge	1	0.0%
	3	2.8%
	5	9.9%
	7	22.3%
	9	40.2%
	11	62.6%
Trailing Edge	2	0.0%
	4	5.8%
	6	15.9%
	8	30.4%
	10	49.0%
	12	70.0%

Table 49: Sandwich model PFA: nodes displacement

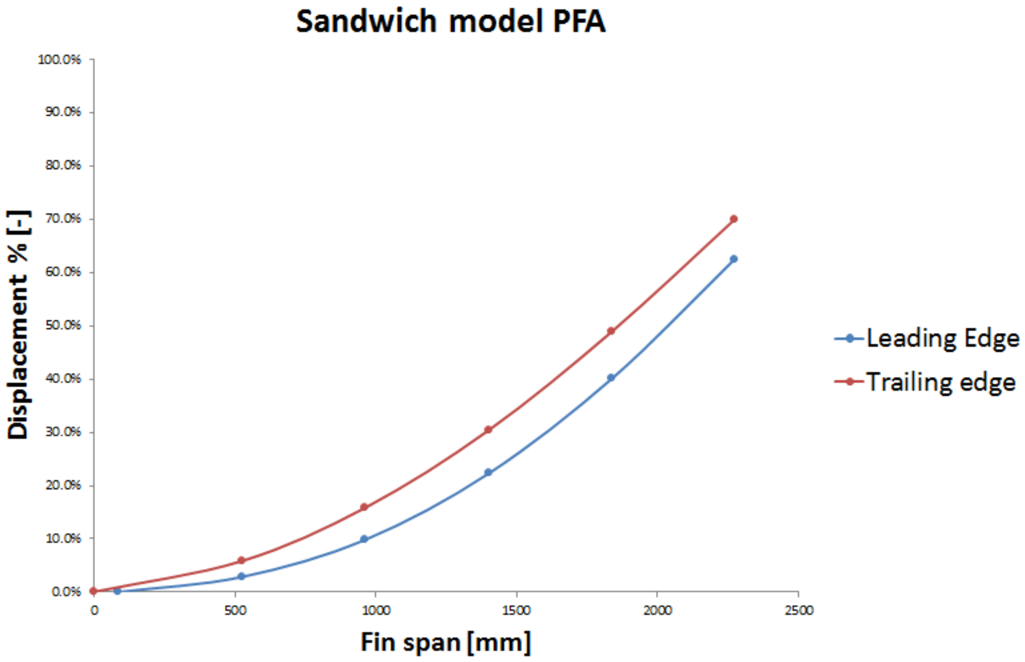

Figure 128: Sandwich model PFA: nodes displacement

14 Models Comparison

In this section are compared all the models analyzed so far to determine the advantages of each configuration. The following table shows the weights and maximum deflection, including the percentage variations from the current model.

Model	FEM Weight	$\Delta\%$	Maximum Deflection	$\Delta\%$
Current	100%	0%	100%	0%
Spar Model FPF	75.7%	24.3%	57.1%	42.9%
Spar Model PFA	67.4%	32.6%	64.1%	35.9%
Sandwich Model FPF	81.1%	18.9%	65.2%	34.8%
Sandwich Model PFA	66.1%	33.9%	73.2%	26.8%

Table 50: Comparison between all models specifications

Looking at the results you will immediately notice how all the new configurations have achieved significant benefits in terms of weight savings and increased stiffness.
Through the readings of the trasducers, and the corresponding nodes, is also possible to determine the punctual stiffness of the various models. For this purpose have been compared the displacements of the leading edges and trailing edges.
In Figure 130 and Figure 131 we can see how all the models realized present a regular trend similar to the current model. Obviously, in the PFA models, the removal of a certain amount of laminae has caused a decrease of the stiffness of the model, which, however, has always remained more stiff than the structure currently installed on the aircraft.
The following figure show the load displacement curves of the two configuration dimensioned by means of the Progressive Failure Analysis.

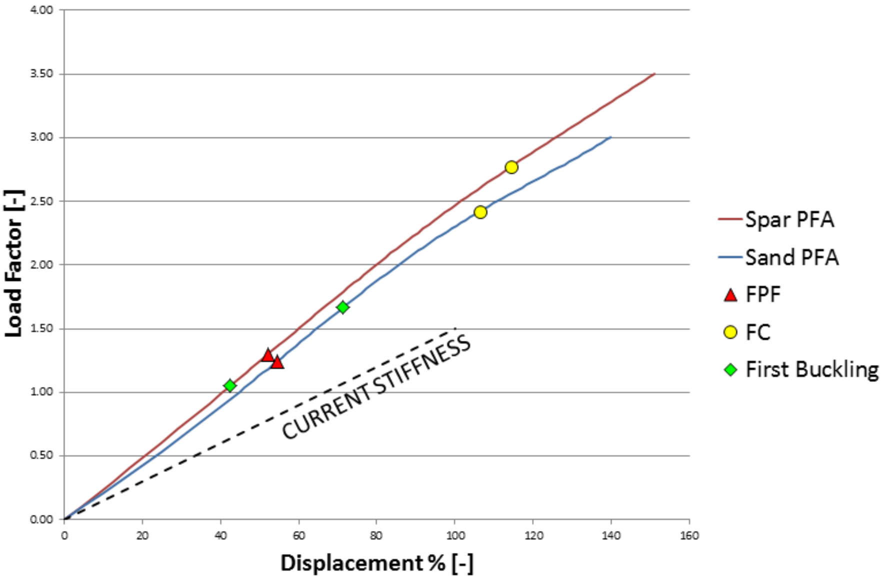

Figure 129: PFA models comparison: load displacement curves

Considering that the two models have a weight comparable it is clear that the spar model present a stiffness greater than the sandwich model. Although there is a wide margin between first crack and first ply failure is not possible to further optimize the model due to the limit of instability. Same thing can be said for the sandwich model because, in this case, has already exceeded the specification of stiffness

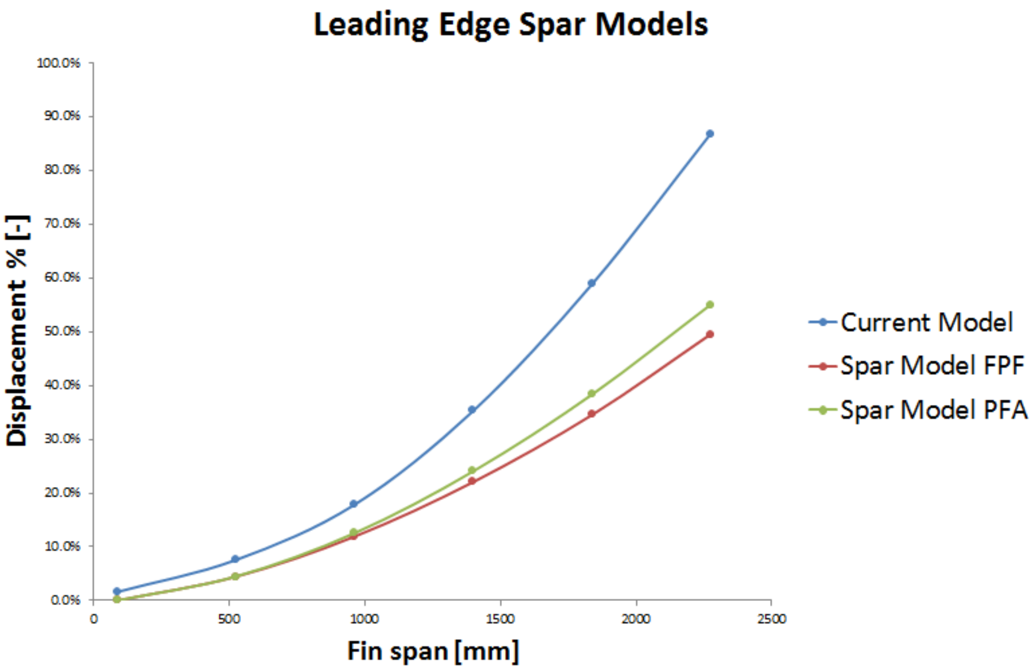

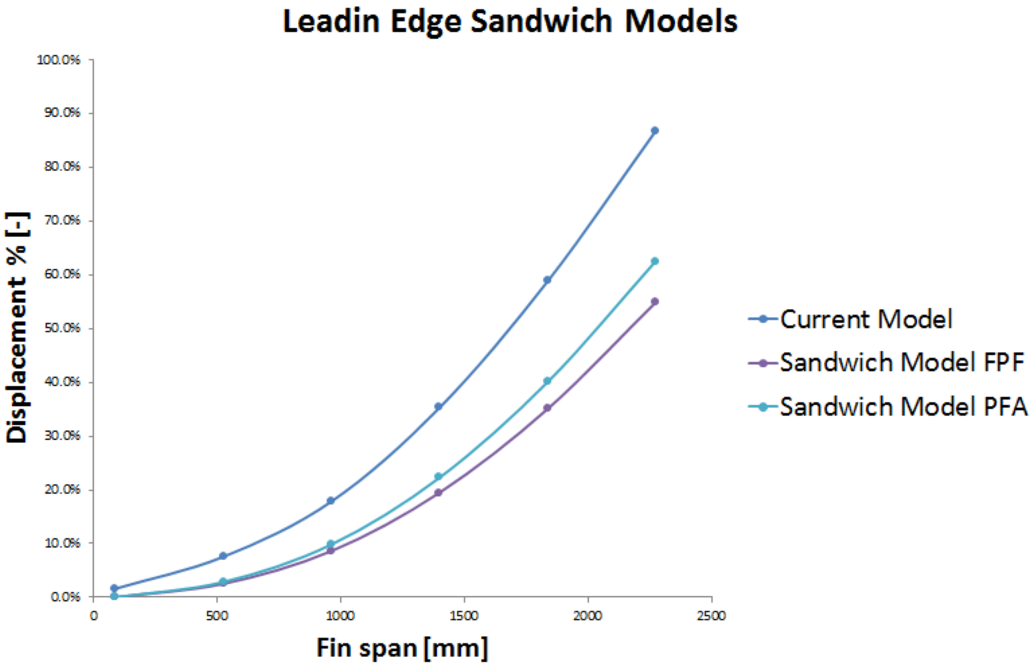

Figure 130: Leading edge comparison

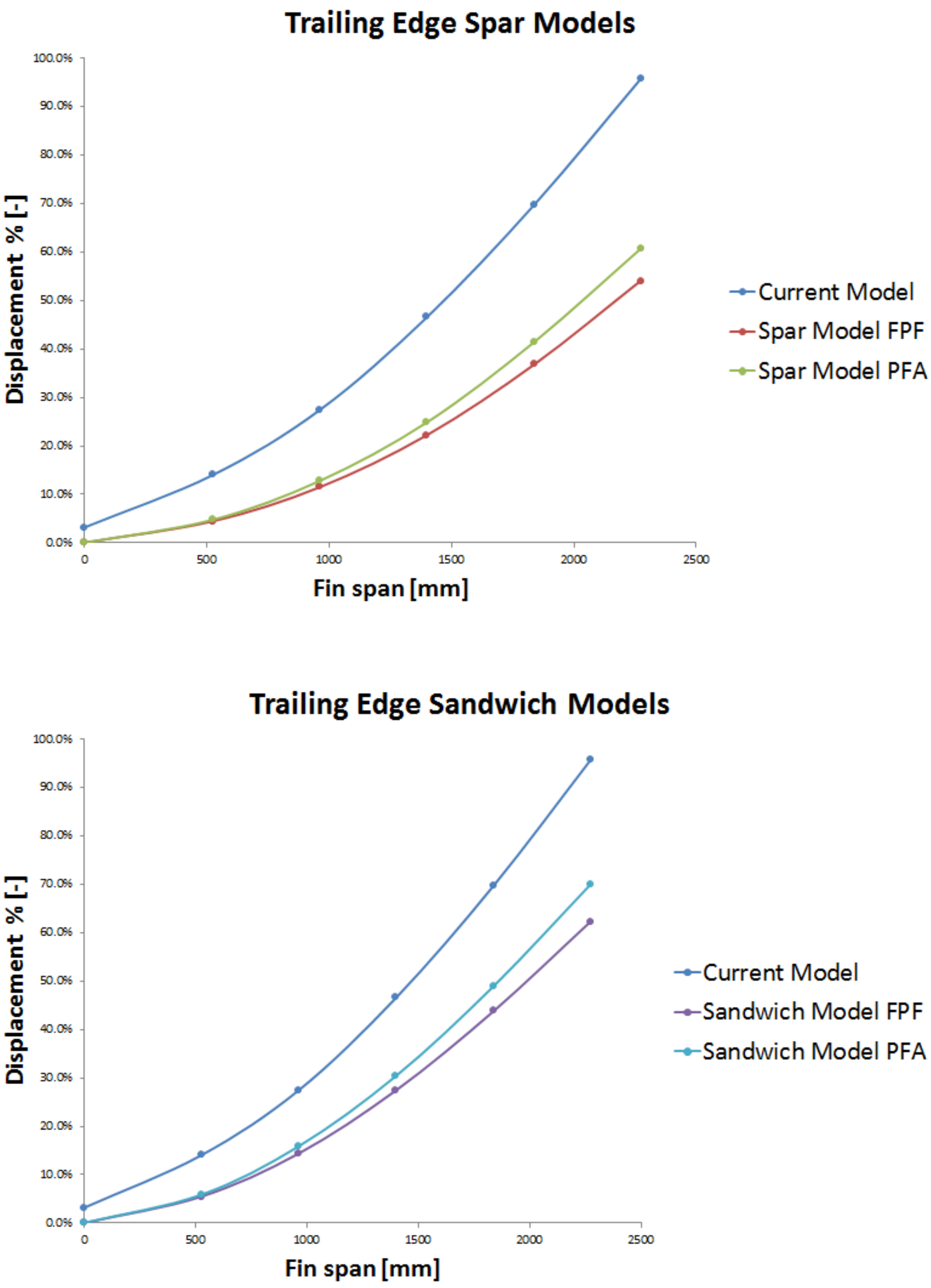

Figure 131: Trailing edge comparison

15 Conclusion

In this thesis, after understanding the underlying benefits and limits of the Progressive Failure Analysis, have been realized various configurations of Vertical Tail made of composite material and compared with the current configuration made primarily of aluminum alloy. Both First Ply Failure Analysis and Progressive Failure Anaysis, have led to an improvement in the performance of the structure. This is mainly due to the fact that the composite materials, thanks to their characteristic are suitable for this type of structures. It must be said, however, that the models built are simple and do not consider all phenomena, both positive and negative, to which this type of structure is subjected. In any case to take account of all these uncertainties have been used knock down allowable values and, to set the analysis of progressive failure, have always been chosen conservative parameters.

By applying a progressive failure analysis it has been found that “spar” structures have a higher stiffness than the “sandwich” structures. However, has been highlighted how the problem of buckling is limiting for this type of dimensioning, due to the reduction in thickness. For this reason, the sandwich structures are more suitable for supporting instability phenomena. Nevertheless, the tendency is to admit the buckling of the panels also below the limit load so, for this reason, the configuration with spars would be the best.
Another important result, obtained during the dimensioning of the sandwich model with the PFA, was the increase in the first crack load in comparision with the model dimensioned at FPF. This has highlighted how a good distribution of thicknesses can bring the crack to be born in areas much more resistant. In this sense, an analysis of progressive failure can also be used to better understand the propagation of the crack and consequently take countermeasures to inhibit this phenomenon as much as possible.

To confirm the results obtained so far is important to emphasize the need to have the experimental evidence, very expensive and difficult to obtain, to properly calibrate the analysis. Should also be said as this type of analysis have a high computational cost both in terms of time and memory.

In conclusion, the progressive failure analysis results to be a valid instrument to exploit the capabilities of composite materials, worthy of further studies.

16 Appendix

16.1 SOL 400 - NASTRAN Cards

The NASTRAN cards used to implement the SOL 400 for the Progressive Failure Analysis are essentially two: the card MATF and the card NLSTEP. Here will not be given the generic formatting but only partial ones, containing the parameters used for this specific analysis.

16.1.1 MATF

The Material Failure Model card specifies failure model properties for linear elastic materials to be used for static, quasi static or transient dynamic analysis in SOL 400. Up to three criteria may be specified for each material.
Failure occurs when any one of the specified failure criterion is satisfied; that is, the Failure Index exceed 1.0. Upon failure, the elastic moduli are reduced. This is done differently depending on failure criterion. The behavior up to the failure point is linear elastic. After failure the behavior is still elastic but with a different stiffness.
For progressive failure (ITYPE=2) only the first criterion will contribute to failure. The other two will only provide output of failure index.

MATF	MID	ITYPE						
	“CRI”	Criteria						
								W_1^1
	W_2^1	W_3^1	W_4^1	W_5^1	W_6^1	W_7^1	W_8^1	W_9^1
	“PF”	A1						

Table 51: MATF - format

MID	Identification number of MAT8 entry.
ITYPE	Flag to invoke progressive failure: 0 no progressive failure, compute failure indices only 2 gradual selective stiffness degradation 3 immediate selective stiffness degradation
“CRI”	Enter the character string “CRI” to start input data for failure criterion.
Criteria	Select an integer corresponding to the failure criterion to be applied, ie: 1 max stress 2 max strain etc...
W_i^j	Strain limit i for criterion j.
“PF”	Enter the character string “PF” to start progressive failure input data if ITYPE is 2 or 3.
A1	Residual stiffness fraction. For ITYPE=2, the stiffness is not reduced beyond this fraction of the initial stiffness. For ITYPE=3, this is the fraction of initial stiffness upon failure.

The card MATF used for the analysis carried out on the specimen looks like the following:

MATF	1	3						
	CRI	2						
								0.0178
	0.0097	0.0067	0.0187	0.0067	0.0187	0.0153	0.0153	0.0153
	PF	0.05						

Table 52: MATF - example

16.1.2 NLSTEP

This card specifies the convergence criteria, step size control and numerical procedure for time/load stepping. It is used for mechanical, thermal and coupled analysis in SOL 400 and for linear contact analysis in SOL 101.
There are three groups of data that can be entered through this option:

1. General data which defined parameters that may be used for a variety of simulations. This data is provided by the GENERAL keyword.
2. Selecting the type of procedure used to control the time/load stepping procedure. These procedures are activated by the keywords: LCNT, FIXED, ADAPT, or ARCLN (arc length or continuation method). Only one of the keywords may be chosen in a load case.
3. Data associated with the physics type that are activated by the keywords: MECH, HEAT, COUP, and RCHEAT. One can enter as many as necessary.

NLSTEP	ID	TOTTIME				
	“GENERAL”	MAXITER	MINITER	MAXBIS		
	“ADAPT”	DTINITF	DTMINF	DTMAXF	NDESIR	SFACT
	“MECH”	CONV				KMETHOD

Table 53: NLSTEP - format

ID	Identification number.
TOTTIME	Total time for the load case. (Default = 1.0)
“GENERAL”	Keyword for parameters used for overall analysis.
MAXITER	Maximum number of iterations allowed for each increment.
MINITER	Minimum number of iterations needed for each increment.
MAXBIS	Maximum number of bisections allowed in the current step.
“ADAPT”	Keyword to indicate that the adaptive load stepping procedure should be used.
DTINITF	Initial time step defined as fraction of total load step time (TOTTIM).
DTMINF	Minimum time step defined as fraction of total load step time (TOTTIM).
DTMAXF	Maximum time step defined as fraction of total load step time (TOTTIM).
NDESIR	Desired number of iterations per increment.
SFACT	Factor for increasing time steps due to number of iterations up to DTMAXF.
“MECH”	Keyword for parameters for mechanical analysis
CONV	Flags to select convergence criteria. (Character “U” = displacement error, “P” = load equilibrium error, “W” = work error, “V” = vector component method, “N” = length method, and “A” = auto switch or any combination)
KMETHOD	Method for controlling stiffness updates (default: modified Newton-Raphson procedure “PFNT”)

NLSTEP	1	1				
	“GENERAL”	10	1	5		
	“ADAPT”	0.01	1e-5	0.5	4	1.2
	“MECH”	PV				PFNT

Table 54: NLSTEP - default

References

[1] American Institute of Aeronautics an Astronautics - Norman F. Knight, Jr. - *Factor Influencing Progressive Failure Analysis Predictions for Laminated Composite Structures*

[2] NASA - David W. Sleight - *Progressive Failure Analysis Methodology for Laminated Composite Structures*

[3] Politecnico di Milano - Chiara Bisagni - *Non Linear Analysis of Aerospace Structure*

[4] MSC^{TM} - *Nastran 2001 Linear Static User's Guide*

[5] MSC^{TM} - *Nastran 2004 Reference Manual*

[6] MSC^{TM} - *Nastran 2012 - Quick Reference Guide*

[7] NASA - Contractor Report 4675 - *A Verification Procedure for MSC/NASTRAN Finite Element Models*

[8] Report aziendale: *Guidelines for Finite Elements Models*

[9] Report aziendale: *Composites Analysis Method*

[10] Report aziendale: *Structural Static Analysis and Strength Justification Documentation Guidelines*

[11] Report aziendale: *Vertical Tail Stress Report*

[12] Michael C.Y. Niu - COMPOSITE AIRFRAME STRUCTURES - *Pratical Design Information and Data*

[13] *Military Handbook MIL-HDBK-5H*

[14] HexWeb^{TM} - *Honeycomb Attributes and Properties*

Ringraziamenti

Ringrazio Gianluca Ghiringhelli per la sua pazienza ed i consigli utili per procedere con il lavoro di tesi
Camillo Pedetti per aver reso possibile questa esperienza
Veronica Ielmini per la sua cortesia e disponibilità
Guido Mario per averci fornito i disegni base per la modellazione
Andrea Russo per averci aiutato nei momenti di “panico” e aver contribuito al miglioraremento della tesi
Gianluca Bottini per avermi insegnato ad “amare” i pasti della mensa
Maurizio Ghioldi per aver riempito le nostre giornate con le sue frasi celebri tra cui: “ottimo ed abbondante”, “molto bene” e “timbraxio maxima”
Claudio Bossi per averci rifornito di MOMENT ACT quando la testa non reggeva più
Paolo Roi per avermi fatto capire, prima del tempo, cosa significhi essere stressati dal lavoro
Maurizio Galli per aver fornito supporto informatico ed avermi allietato la giornata con il suo linguaggio “colorito”
Andrea Piccoli per averci insegnato ad usare il supercomputer
Elisabetta Guffanti per come guardava Ghioldi quando si padellava la camicia in mensa
Battista Simonelli per averci portato nelle clean room e averci fatto conoscere i colleghi delle tecnologie NDT
Mauro Linari della MSC SOFTWARE, gentilmente presentatoci da Gianluca, per averci dato delle dritte su come indagare un’analisi di PFA
Raimondo Scala per avermi insegnato il termine pseudo-napoletano *staifté*.

Un ringraziamento dovuto va al *Ficus Benjamin* di Bottini per aver rifornito di ossigeno l’ufficio (nel limite delle sue ormai non più 60 foglie).

Ringrazio i miei compagni di università Raoul, Andrea, Jan, Alessandra, Daniele, Silvia e Stefano per aver condiviso con me gioie e dolori in tutti questi lunghi anni di studio. Infine, ringrazio il mio “collega di tesi” Fabio Ceriotti senza il quale questo lavoro sarebbe stato il doppio difficile e la metà divertente.

“The last but not the least”
Ringrazio i miei genitori per avermi cresciuto ed accompagnato fino a questo importantissimo traguardo, per avermi rimproverato quando serviva e per avermi compreso quando ne avevo bisogno. Spero in futuro di continuare a rendervi orgogliosi di me.